UNIVERSITY OF CALIFORNIA, MERCED

Optical Trapping, Parametric Oscillations, and Active Learning

A Dissertation submitted in partial fulfillment of the
requirements for the degree of
Doctor of Philosophy
in

Physics

by

Alison Aiko Huff

June 2018

The dissertation of Alison Aiko Huff, titled Optical Trapping, Parametric Oscillations, and Active Learning, is approved, and it is acceptable in quality and form for publication.

(Professor Jay E. Sharping) Principal Adviser	Date
(Professor Linda Hirst) Committee Chair	Date
(Professor Kara McCloskey) Committee Member	Date

University of California, Merced
2018

This dissertation is dedicated to my parents, Robert and Kumiko Huff, for always pushing me to achieve more than what I thought I could obtain, and never giving up on me, even when I had my doubts.

Acknowledgments

My accomplishments would have never occurred without the support of multiple people and groups. First and foremost, there are not enough words I can use to thank my adviser, Dr. Jay Sharping, for his tremendous guidance during my time at the University of California, Merced. Without his mentorship and humor, I would have never finished my doctorate.

I thank the support and comedic relief from my labmates, both current and past: Dr. Tessa Piñon, Dr. Leily Kiani, Alessandro Castelli, Rodolfo Lopez, Jacob Pate, Johnathon Thompson, Deepak Sapkota, Jeffery Miller, and Nabin Raut. I also extend my thanks to Dr. David Quint and Dr. Makiko Quint, for their support and friendship. Without their presence, graduate school would have been extremely difficult to complete.

I thank my committee members, Dr. Linda Hirst and Dr. Kara McCloskey for their questions to assist my understanding in what is expected for a graduate student to become an independent researcher.

Without my positive experiences from my past teachers and professors, I would never have entered and continued to pursue physics. For that, I would like to especially thank my high school teacher Mr. Dave Schalek; my College of Wooster professors Dr. Todd McAlpine, Dr. Donald Jacobs, Dr. John Lindner, and Dr. Susan Lehman; and my adviser at Miami University, Dr. Paul Urayama.

I thank my fiancé Bryan Maelfeyt for all his love and support throughout our time at the University of California, Merced together. My life has changed for the better ever since we have been together, and I am excited to see what our future holds.

Last but not least, I thank my parents for all their love, dedication, and efforts

to turn me into the person I became. My education would have never gotten this far without their constant guidance and support. Although we have had disagreements (especially through my teenage years), I have nothing but love and respect for them.

This dissertation was funded in part by the University of California, Merced Physics Graduate Student Summer Fellowship from 2013 to 2017, as well as the University of California Merced Dean's Distinguished Scholars Award in Spring of 2016.

Alison Huff
(310) 736-8358
ahuff@ucmerced.edu

EDUCATION

Ph.D., Physics
University of California, Merced, Expected August 2018
GPA: 3.72

M.S., Physics
Miami University, August 2012
GPA: 3.54

B.A., Physics
College of Wooster, May 2010
GPA: 3.22

EXPERIENCE

Graduate Student Researcher 2012-present
University of California, Merced
Dr. Sharping's Applied Photonics Laboratory
Projects:

- Developed a parametrically driven pendulum for an upper-division undergraduate laboratory
- Studied the trapping characteristics for a dual-beam optical trap with low refractive index contrast

Teaching Assistant 2012-present
University of California, Merced
Courses:

- Introductory Physics I for Physical Sciences, Discussion and Laboratory
- Introductory Physics I for Biological Sciences, Discussion and Laboratory
- Introductory Physics II for Physical Sciences, Discussion and Laboratory
- Introductory Physics II for Biological Sciences, Discussion and Laboratory
- Introductory Physics III for Physical Sciences, Laboratory

Duties:

- Present lectures as requested by faculty
- Lead discussion and laboratory classes - weekly for Physics I and II, bi-weekly for Physics III
- Develop mini-lectures based on weekly learning outcomes
- Assess student comprehension of material
- Hold office hours
- Provide external resources to assist student learning

Graduate Pedagogy Association, Vice President and Secretary 2015-present
University of California, Merced

- Founding member and officer of the first graduate club at the university
- Internal point of contact
- Provide simple and effective resources for graduate students to aid their teaching practices
- Create an environment for graduate students to encourage continuous improvement in teaching strategies

Center for Engaged Teaching and Learning Instructional Intern 2015-2017
University of California, Merced

- Attended, summarized, and co-presented all three workshops offered by CETL
- Assisted with Teaching Assistant Orientation during graduate student orientation
- Designed, implemented, and presented an educational research project, in conjunction with the Assessment as Pedagogy and Planning Project.

Assessment as Pedagogy and Planning Project Member Fall 2015
University of California, Merced Research:

- Identified undergraduate student learning needs for Physics I
- Analyzed student results utilizing an active learning strategy
- Developed related teaching documents
- Summarized and documented conclusions

Research Assistant 2011-2012
Miami University
Research: Developed a high pressure perfusion system for real-time physiological studies

Teaching Assistant 2010-2011
Miami University
Courses:

- General Physics I Laboratory
- General Phyiscs II Laboratory

Duties:

- Led weekly laboratory classes
- Assess student laboratory reports
- Held weekly office hours

Laboratory Assistant 2009-2010
College of Wooster
Courses:

- Modern Physics
- Junior Independent Study

Tutor 2009-2011
College of Wooster and Miami University
Courses:

- General Physics I
- General Physics II
- Modern Physics
- Mathematical Methods

Grading Assistant 2008-2010
College of Wooster
Courses:

- General Physics I
- Mathematical Methods

RESEARCH SKILLS

Thorough knowledge of LabVIEW programming environment; familiar with Igor Pro, Origin, and MATLAB data analysis software; extensive use of LaTeX typesetting language, Microsoft Office, and Open Office.

PUBLICATIONS

Alison Huff, Charles N. Melton, Linda S. Hirst, Jay E. Sharping. Stability and instability for low refractive-index-contrast particle trapping in a dual-beam optical trap. *Biomed. Opt. Express*, 2015, 6 (10), pp 3812-3819.

Jeff Maltas, Zac Long, Alison Huff, Ryan Maloney, Jordan Ryan, Paul Urayama. Note: A micro-perfusion system for use during real-time physiological studies under high pressure. *Rev. Sci. Instrum.*, 2014, 85 (10).

Alison Huff, Kelly Patton, Hosanna Odhner, Donald T. Jacobs, Bryna C. Clover, Sandra C. Greer. Micellization and Phase Separation for Triblock Copolymer 17R4 in H_2O and in D_2O. *Langmuir*, 2011, 27 (5), pp 1707-1712.

PRESENTATIONS

Alison Huff, Johnathon Thompson, Jacob Pate, Hannah Kim, Raymond Chiao, Jay Sharping (2017). "Resonance Threshold and Bistability in a Parametrically-Driven Pendulum". Presented at the October 2017 American Physical Society Far West Section Meeting.

Alison Huff, Johnathon Thompson, Jacob Pate, Hannah Kim, Raymond Chiao, Jay Sharping (2017). "A Parametric Oscillator Experiment for Undergraduates". Presented at the March 2017 American Physical Society Meeting.

Alison Huff (2015). "Work Together, Fight Alone: How Does Presenting Problems in Groups Improve the Robustness of an Individuals Problem-Solving Process?" Poster presented at the Third Annual UC Merced Research Week, Assessment as Research Symposium: Sharing Practices, Successes, and Lessons Learned section.

Alison Huff, Charles Melton, Linda Hirst, Jay Sharping (2015). "Stability Conditions for Trapping of Low Index Contrast Particles Dual Beam Optical Trap". Presented at the October 2015 American Physical Society Far West Section Meeting.

Hosanna Odhner, Alison Huff, Kelly Patton, Donald T. Jacobs, Bryna C. Clover, Sandra C. Greer (2011). "Miscellization and Phase Transitions in a Triblock Copolymer-D_20 System". Poster presented at the March 2011 American Physical Society Meeting.

Alison Huff, Kelly Patton, D.T. Jacobs, Bryna Clover, S.C. Greer (2010). "Micellization and Phase Transitions in a Triblock Copolymer-Water System". Poster presented at the March 2010 American Physical Society Meeting.

Todd McAlpine, Alison Huff (2009). "Simulation of the Dynamics of a Plane Pendulum with Positional Dependent Torque". Poster presented at the March 2009 American Physical Society Meeting.

AWARDS AND HONORS

Outstanding Teaching Award, 2018

Physics Graduate Group Annual Excellence Award, Outstanding Performance as a Teaching Assistant, 2015, 2017

Physics Graduate Student Summer Fellowship, 2013-2017

Dean's Distinguished Scholars Award, Spring 2016

Developing Teaching Strategies Certificate, 2015

Certificate of Recognition through the Instructional Internship Program, 2015

Mastering the Classroom with First Generation College Students Certificate, 2015

Improving Teaching by Assessing Learning Certificate, 2015

Abstract

Optical Trapping, Parametric Oscillations, and Active Learning
by
Alison Aiko Huff
Doctor of Philosophy in Physics
University of California, Merced
Professor Linda Hirst, Chair

This dissertation consists of three distinct projects: optical trapping, parametrically-driven oscillator, and physics education research. We trapped trap poly(methyl methacrylate) (PMMA) microspheres using radiation pressure forces when the refractive index ratio between the particles and the liquid medium suspending them was nearly one. This contrast resulted in a unique trapping landscape which was verified through our simulations. In the case of our parametrically oscillating pendulum, we modulated a parameter of the system, in this case the length of the pendulum, which gave rise to an instability which gradually increased the total energy of the oscillating pendulum. This system is an upper-level undergraduate laboratory experiment, where students would explore mechanical parametric oscillations and extract key linear pendulum features, such as the damping constant and the quality factor, and nonlinear dynamical features, such as frequency shifts and bistability. In the physics education research, I tested whether students would improve their ability to understand the material in the first semester of general physics (the majority of which are related to forces) if they were constantly required to develop robust solutions with low-stakes assignments. The results presented show that a positive correlation existed

between implementing class presentations where students are required to solve problems robustly in groups and with both low and high stakes assignments.

Contents

Acknowledgments **v**

Curriculum Vitae **vii**

Abstract **x**

1 Introduction **1**

2 Optical Trapping **6**

2.1 Theory of Trapping In a Dual-Beam Setup 7

2.2 The Dual-Beam Optical Trap 10

2.3 Characterizing the Stability of the Trap 12

2.3.1 Simulations 12

2.3.2 Beads in Index Matching Liquid 12

2.3.3 Determining Particle Size 14

2.3.4 Results 14

2.4 Soft Matter Trapping 19

2.4.1 How Soft Particles Stretch in the Trap 20

2.4.2 Oil Droplets in Water 21

2.4.3 Stem Cells in PBS 22

2.4.4 Results 22

2.5 Discussion 24

2.5.1 Issues and Resolutions 24

2.5.2 Improvement Opportunities 26

2.6 Conclusion 30
2.7 Recent Research 31

3 Parametrically Oscillating Pendulum **33**
3.1 Undergraduate Laboratory Objectives 34
3.2 How the Pendulum is Able to Parametrically Oscillate 35
3.3 Our Pendulum Setup 36
3.4 Data Collection 37
3.5 Modulation Depth Calibration 38
3.6 Derivation of Threshold Conditions 38
3.7 Frequency Shift for Peak Energy 41
3.8 Results 44
3.8.1 Raw Data 44
3.8.2 Pendulum Characteristics 46
3.8.3 Threshold Data 46
3.8.4 Bistability 51
3.9 Discussion 53
3.9.1 Issues and Resolutions 54
3.9.2 Improvement Opportunities 55
3.9.3 Research Impact 55
3.10 Conclusion 56

4 Group Presentations and Solution Robustness **57**
4.1 The Student Body 59
4.2 The Presentations 60
4.3 Results 61
4.4 Conclusions 64

5 Conclusions and Future Direction **66**
5.1 Future Exploration 67

A Optical Trapping Codes **73**
A.1 Pixel Sizes and Distances 73
A.2 Trapping Efficiency Plots 75
A.3 Trapping Contour Plots 81

B Parametric Oscillator Codes **86**
B.1 Driving the Pendulum 86
B.2 Oscillator Contour Plots 89

C Supplemental Assessment Documents **95**
C.1 Expectations 95
C.2 Entrance Survey 97
C.3 Sample Pre-Presentation Lesson Plan 100
C.4 Homework Notebook Rubric 102
C.5 Sample Presentation Lesson Plan 104
C.6 Presentation Rubric 106
C.7 Mid-semester Survey 108

Bibliography **110**

List of Figures

1.1 Road map of this dissertation. 2
1.2 Schematic of a particle in a well undergoing parametric oscillation. . . 3

2.1 Schematic of the trapping forces. 8
2.2 Schematics of the trapping experiment. 10
2.3 Flow chart of the simulations used to create trapping efficiency plots. 13
2.4 Calibration method for determining particle size. 14
2.5 Comparison of trapping efficiency simulations to experimental data. . 15
2.6 Contour plot describing the expected stability at the center of the trap. 16
2.7 Bifurcation plots showing the axial stability locations vs. particle radius for three different fiber separations. 17
2.8 Bifurcation plots of the axial stability locations as a function of fiber separation. 19
2.9 Soft matter stretching in a dual-beam optical trap. 20
2.10 Oil droplets trapped in water. 23
2.11 Stem cells trapped in PBS. 24
2.12 Stem cell sizes at each trapping power. 25
2.13 Oil droplet in a container of water with a surfactant. 27

3.1 Schematic of the parametrically-driven pendulum. 37
3.2 Relation between the change in length of the pendulum to the servo angle. 38
3.3 Graph representing period and frequency shift as peak energy increases. 43
3.4 Sample data output by the Arduino microcontroller and analyzed. . . 44

3.5 Ringdown and ringup of the pendulum. 45
3.6 Plot of oscillator energy ($2E/m$) as a function of time for five different modulation depths. 47
3.7 Steady-state energy plotted as a function of driving parameters. . . . 48
3.8 Simulated steady-state energy as a function of modulation depths at various driving frequencies. 49
3.9 Contour plot of the steady-state energy of the parametric oscillator as functions of frequency and modulation depth. 50
3.10 Bistability of the pendulum at various modulation depths. 51
3.11 Simulation depicting pendulum's sensitivity to initial conditions. . . . 52

4.1 Score averages over the course of a semester. 62

5.1 Sample Poincaré section for a pendulum undergoing chaos. 69
5.2 Sample bifurcation diagram for the motion of a pendulum undergoing chaos. 70

Chapter 1

Introduction

This dissertation combines both my physics and teaching interests, and overlaps with one of the large goals of Dr. Jay Sharping's Applied Photonics Research Group: to combine the fiber optical parametric oscillator with the dual-beam optical trap. My six years at the University of California has allowed me to tackle three projects; the dual-beam optical trap and the parametrically-driven pendulum with Dr. Jay Sharping, and a physics education project with the Assessment in Pedagogy and Planning Project and the Instructional Internship Program through the Center for Engaged Teaching and Learning. Because the three research topics presented here vary in both background and methods, I have organized my dissertation in a slightly unconventional way; all the contents for each project are in their own chapter. The visual road map for this dissertation is provided in Fig. 1.1

In Chapter 2, I talk about the dual-beam optical trap. An optical trap is a tool developed by Arthur Ashkin in 1970 [1] that is used to trap microscopic particles with radiation pressure forces. These traps fall under two main types, depending on the used number of beams. A single beam optical trap, more commonly known as an optical tweezer, utilizes a single, highly focused beam. A dual-beam optical trap, on the other hand, consists of two coaxially aligned, counter-propagating beams that diverge. This setup requires less power to trap microscopic particles, which reduces the photodamage applied by the beams compared to the single beam setup [2], which

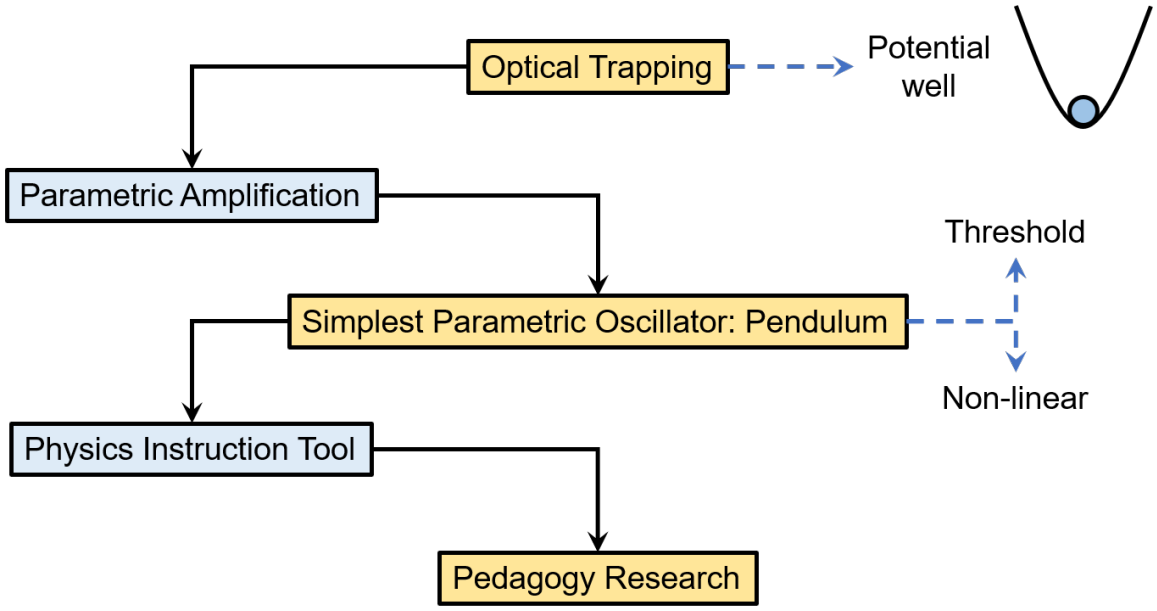

Figure 1.1: Road map of this dissertation. The center column with the yellow boxes are my research topics, and the blue boxes on the left are how the topics are related.

is advantageous when examining biological cells. The non-invasiveness of the dual-beam optical trap also allows micromanipulation and examination of these cells *in situ* [3]. Our main motivation of understanding the dual-beam optical trap stems from previous research from our lab done by Piñon *et al.* [4]; we wanted to understand how particles would trap in low refractive index contrast scenarios so that we could implement the methods on soft matter particles, then trap and stretch these particles to understand how their membranes are affected by radiation pressure forces. Our research shows that the location of stable trapping depends on the size of the particles and the distance between the optical fiber ends.

Particles that are stably trapped are considered to be in a stable optical potential well [1, 5], as pictured in Fig. 1.1; if we were to offset the position of the particle, it would return to the position corresponding to the bottom of the well. However, if we were to drive the particle by adjusting a trapping parameter at twice the natural frequency of the system (or resonance), we could cause the particle to oscillate about the stable equilibrium; this process is known as parametric oscillation. If the particle were already oscillating, and we modified a parameter in the same way to cause

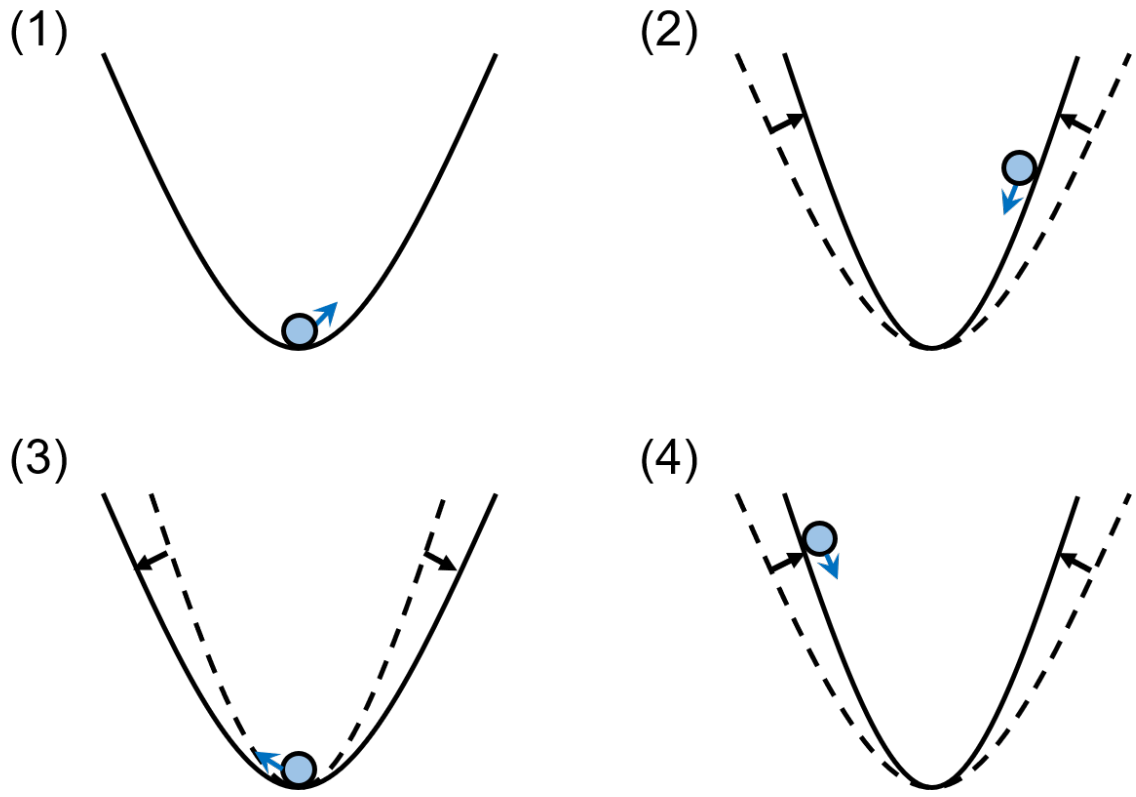

Figure 1.2: Schematic of a particle in a well undergoing parametric oscillation. By periodically changing the width of the well, the particle starts to oscillate (1). As it oscillates, we can continue to adjust the width (2-4), causing the amplitude of oscillation to increase.

larger oscillations, we are creating parametric amplification. This phenomenon was first noticed by Michael Faraday in 1831 [6], where by changing the parameter of the oscillating system periodically, the amplitude of the oscillations would increase. A schematic of parametric oscillation is shown in Fig. 1.2, where a particle is located at the bottom of a well. The well width is changed periodically (1), and after some time, the particle starts to roll up and down the sides of the well. The well is adjusted such that the width is narrowest when the particle is at its peak height (2) and widest at the minimum (3), which allows the particle to increase its energy and reach higher positions (4) until some maximum has been obtained.

Parametric oscillation is a key field in our Applied Photonics Research Group,

where we have projects in optical parametric oscillators. These oscillators are able to generate light with a variety of optical frequencies with laser-like quality [6]; our lab has built a fiber optic parametric oscillator with over 30 nm of tunability centered at 980 nm [7]. This is the wavelength we use with our dual-beam optical trap, so combining with the two would create a project that would allow us to explore the trapping profile of the system whilst adjusting a parameter of the trapping light.

In an effort to align my research with combining optical trapping with optical parametric oscillations, I decided to switch gears to the parametrically-oscillating pendulum project described in Chapter 3. This provides a hands-on approach to exploring both linear and nonlinear regimes of parametric oscillators. In lower division undergraduate classes, the simple pendulum is often used to explain oscillatory physics, as many students have been introduced to swings at a young age. Most people tend to increase the amplitude of oscillation by driving it; however, as William Case demonstrated, the swing can start to oscillate by periodically changing the location of the center of mass, effectively changing the length of the swing [8]. Our system is more closely related to a typical simple pendulum, where a wooden sphere is at the end of a string, and the length of this string is changing periodically. By doing so, we were able to examine the threshold conditions for this oscillator in the linear regime, as well as understand how the nonlinear regime affects the frequency to observe peak energy and demonstrates bistability.

The parametrically-oscillating pendulum project was also designed with the intention for it to be an experiment for an upper-level undergraduate laboratory setting, which aligned with my future plans in college teaching. Through this experiment, we want undergraduate students to have a chance to explore the physics of parametric oscillators. With their knowledge background, students should be able to use Newtonian physics to predict the behaviors in the linear regime, allowing them to theoretically determine threshold conditions. They should also be able to compare and contrast their experimental results, as well as observe the interesting physics that occurs due to nonlinearity.

My physics education project, on the other hand, focused on lower-division undergraduate students; specifically those in the first semester of general physics. In

academia, a common goal among educators is to develop students into critical thinkers; in General Physics I for Physics and Engineering Students (Physics 08) at the University of California, Merced, this is often monitored through the robustness of homework and exam solutions. Students have shown to retain and advance to high orders of knowledge through the process of active learning, which can be promoted through group work. However, one issue that many of these students have is effectively communicating solutions to the instructors and teaching assistants of the course, which is a result of the inability to present a robust solution. In addition, a small group of students would passively do worksheet problems during discussion sections, which would result in them not understanding how to apply key physics concepts.

Therefore, in Chapter 4, I talk about how I decided to implement group presentations, where the elements of robust solutions were broken up into three roles, and together would develop a solution to present to their peers. These were then scored based on the robustness of the problem-solving process by both the teaching assistant and their classmates. Through these presentations, the average homework score improved at a higher rate than with purely feedback alone. These results indicate that this method can help students start to develop a robust solution with individual work; however, due to the short-term application of these presentations, further testing must be conducted to fully assess the improvements in student work.

Chapter 2

Optical Trapping

Optical trapping uses the radiation pressure force from one or more lasers to trap microscopic particles. Since Arthur Ashkin's discovery of this phenomena in 1970 [1], optically trapped particles have been of interest in a wide variety of fields, from determining forces applied to *E. coli* with optical tweezers [9] to measuring frequency shifts from colliding cesium atoms cooled using a magneto-optical atom trap [10]. From these forces, we are able to trap dielectric particles using a dual-beam optical trap as demonstrated by Ashkin [1], where the beams are counter-propagating and are aligned coaxially. These systems require less power to trap particles, which results in less photodamage [2], making it more favorable for biological samples. Due to this advantage, the dual-beam optical trap has been used to study elasticity of soft matter particles, such as giant unilamellar vesicles (GUVs) [11,12] and red blood cells [13–15], by trapping and stretching the particles to reveal the stress/strain response of the particle membrane.

The use of an optical trap to controllably immobilize and deform GUVs provides a unique method to study biological and synthetic membrane mechanics. Minimal biophysical systems such as the GUV allow basic physical parameters such as elasticity moduli to be measured with the option of adding in additional complexity (different lipids, proteins) in a systematic fashion. This approach complements previous recent studies carried out on whole cells by Guck et al. [13–15]. Recently membrane mechanics have been studied via methods involving direct contact with the membrane,

such as micropipette aspiration [16]. While these methods can provide reliable data, they only provide measurements for one area of the membrane, and do not characterize it as a whole. With this in mind, a non-invasive method of testing such as an optical trap is necessary to characterize a bulk response of the membrane due to time-dependent forces. A dual beam optical trap has recently been shown, by our research group, to successfully stretch a GUV [4] well beyond previously reported stretching regimes in similar experimental setups [11]. However, it was shown to be fairly difficult to successfully trap the GUVs between the two fibers.

The work presented in this chapter first focuses on understanding trapping characteristics of the dual-beam optical trap by examining the locations of stable and unstable trapping when the refractive indices between the particle and surrounding medium are nearly identical ($n_{\text{particle}}/n_{\text{medium}} < 1.01$). By understanding trapping characteristics at low refractive index contrasts, we can increase the effectiveness of trapping soft matter particles and more accurately quantify the forces present within the trap. Using this information and experimental techniques, we then attempted trapping and stretching two types of soft matter particles.

2.1 Theory of Trapping In a Dual-Beam Setup

In an optical trap, a light beam interacts with a particle made from an optically denser material than its environment. For conditions where the particle size is comparable to or larger than the wavelength of light, a ray-optics approach is used and the beam is decomposed into a set of rays. Each ray interacts with the particle, as shown in Fig. 2.1; the forces due to each ray are decomposed into a scattering force F_s and a gradient force F_g. The scattering force lies parallel to the incident ray, while the gradient force is defined to be perpendicular to the incident ray. For a single beam of small angular divergence such as that emerging from the end of an optical fiber, integration over the entire beam results in a particle that is drawn towards the axis of the beam as a result of gradient forces. For two counter-propagating beams aligned coaxially, the particle will then trap in a stable location along the beam axis due to the combination of gradient and scattering forces.

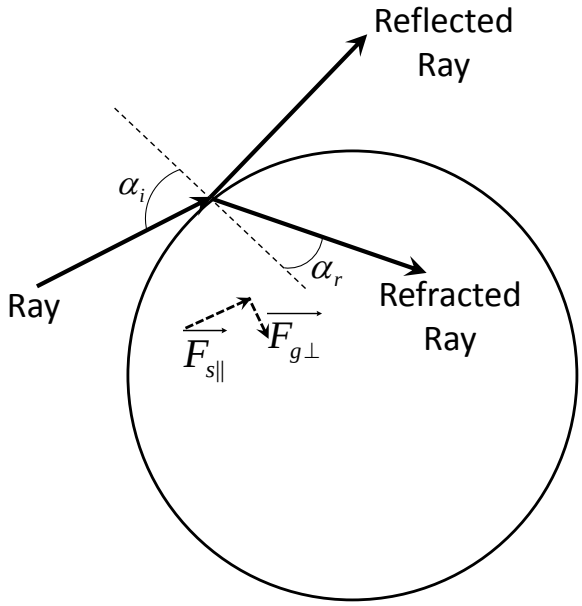

Figure 2.1: Schematic of the trapping forces [17]. An incoming ray strikes a particle, applying a force that can be split into a scattering and gradient force F_s and F_g. The particle traps if it has a larger refractive index than the surrounding medium. Reprinted from Ref. [18] with permission from the Optical Society of America, Inc.

In the case where the refractive index ratio between the particle and medium is relatively large ($n_{\text{particle}}/n_{\text{medium}} > 1.01$) and the particle size satisfies the criteria for a Mie scattering treatment, $2\pi R/\lambda \gg 1$ [19], the particle will trap halfway between the two fibers in the dual beam optical trap. In this case, the scattering forces are dominant along the beam axis. The trapping location is the point where the scattering forces arising from each beam are equal in magnitude but opposite in direction, and give rise to a restoring force when the particle is displaced away from that equilibrium point along the axis. However, we have observed that this trap exhibits unusual trapping behaviors when the refractive indices between the dielectric particle and the surrounding liquid are nearly equal ($n_{\text{particle}}/n_{\text{medium}} < 1.01$). This occurs because F_s decreases more rapidly than F_g as a function of the refractive index contrast and eventually F_g becomes dominant in the axial direction as well.

As shown in Sidick *et al.* [17], integrating the total force over all space and utilizing

the symmetry of the particle, we find that the total force on the particle by a single beam takes the form of

$$\mathbf{F} = \frac{n_1 P_0}{c}\mathbf{Q}, \tag{2.1}$$

where n_1 is the refractive index of the medium, P_0 is the total power transmitted by the beam, $\mathbf{Q}$ is the trapping efficiency factor of the particle, and c is the speed of light in a vacuum. For a beam centered on the particle, $\mathbf{Q}$ is reduced to a single dimension, where

$$Q_z = 2r_0^2 \int_0^{\theta_{\max}} \mathrm{d}\theta \, \sin 2\theta \, \frac{\exp(-2r^2/w^2)}{w^2} \, q_z. \tag{2.2}$$

Here, z indicates the axial direction, r_0 is the particle radius, θ is the angle between the normal of the surface and the beam axis, r is the distance from the surface to the beam axis, w is the beam radius, and q_z indicates what fraction of the momentum transferred from the beam to the particle that is parallel to the beam axis. This fraction is determined using

$$\begin{aligned} q_z = &\cos(\alpha_i - \theta) + R\cos(\alpha_i + \theta) \\ &- T^2 \frac{\cos(\alpha_i + \theta - 2\alpha_r) + R\cos(\alpha_i + \theta)}{1 + R^2 + 2R\cos 2\alpha_r}, \end{aligned} \tag{2.3}$$

where R and T are the reflectance and transmittance at the particle surface, respectively.

For the case of two counterpropagating beams, the force vectors from each beam are added together, such that along the beam axis, we see the net force $F_{z,\mathrm{tot}}$ is

$$F_{z,\mathrm{tot}} = \frac{n_1(P_1 + P_2)}{c}\left(\frac{P_1 Q_{z1}}{P_1 + P_2} - \frac{P_2 Q_{z2}}{P_1 + P_2}\right), \tag{2.4}$$

where beam 1 propagates towards the right and beam 2 propagates towards the left. Since w is dependent on the position from the fiber end along z, we are able to use Eq. 2.4 with Eq. 2.2 and 2.3 to create simulations showing how $Q_{z,\mathrm{tot}}$ depends on z. By defining the separation of the fibers and the particle radius, we are able to see the stable and unstable trapping locations along our beam axis.

2.2 The Dual-Beam Optical Trap

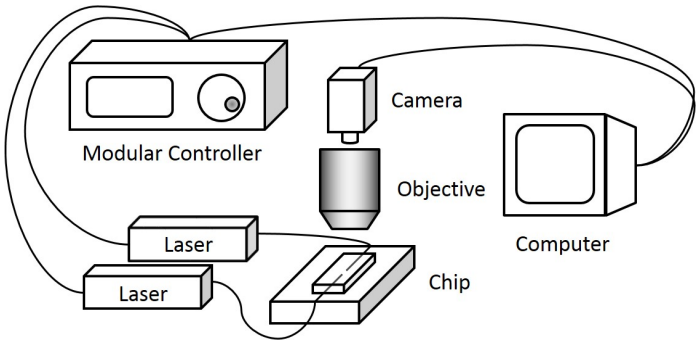

(a)

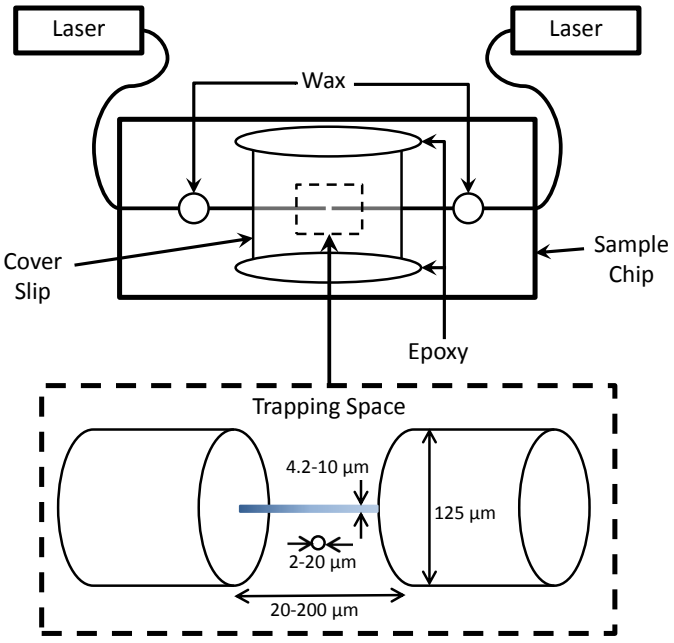

(b)

Figure 2.2: Schematics of the trapping experiment. (a) Schematic of the experimental setup. (b) Schematic of the sample chip. The single-mode fibers are secured in place with drops of wax. A cover slip fastened with epoxy aligns the fibers in the trapping space and provides a flat field of view. The trapping space is expanded to show the relative sizes of the particles, beam and fibers. The fiber separation is fixed during chip assembly. A microscope is used to observe trapped particles and a computer controls the laser power from two separate 980 nm laser diodes. Reprinted from Ref. [18] with permission from the Optical Society of America, Inc.

Our dual-beam optical trap, shown in Fig. 2.2a, utilizes two 980-nm pump lasers (Bookham LC95), which are monitored using a modular controller (Newport Model 8008) and LabVIEW software. Optical powers in the range of 50-250 mW from each fiber are typically used within the trap. The beams are guided by single mode fibers (Fiber Instrument Sales, HI9806) to a Plexiglass sample chip (OPTIX Acrylic 1AG3622A), where the fibers are aligned along a groove. This groove is created using a 36 gauge nichrome wire (Jacobs Online NW36250) parallel to the surface and pressed down with a second Plexiglass chip and additional weight, where a 0.61 A current runs through the wire for 60 s. Once the fibers are aligned to the desired separation, they are secured in the groove with household wax with a glass cover slip cut from a microscope slide to approximate dimensions of 12.5 mm $\times$ 7.0 mm and a thickness of 1.0 mm is set with five minute epoxy to ensure alignment. The microscope uses a Mitutoyo M Plan Apo 5$\times$ objective and images are recorded using a video camera attached to the eyepiece. PMMA sample droplets are placed along the glass coverslip edge with a syringe, such that the sample flows through the regime due to capillary action. Everytime we added droplets from our syringe, we would vigorously shake it for ten seconds to ensure that our sample was as uniformly distributed as possible, and that aggregated particles were separated.

During data collection, we needed to examined the system as it moved with a low flow rate, such that any particle that would interact with the beam would more easily trap because Brownian motion would be minimized. When we begin with an empty sample chip, we would wait a couple of minutes after filling up our sample chamber until we were able to observe particles to visibly interact with the beam; this meant the particle would either change its trajectory but keep moving through the trap, or it would stop moving and become trapped. For each particle, we would test what type of trap we observed by turning the laser off for a few seconds to allow the particle to move away from its trapping location, then turn the lasers back on; if the particle snapped back into place, it was stably trapped, otherwise, we had an unstable trap.

Occasionally, the system's flow would be slow enough that either particles would not move out of the trap, or we would be unable to observe particles flow between the fiber ends. When this occurred, we would first mechanically agitate the system by

lightly tapping on the cover slip to encourage flow. If this did not help our situation, we would add a couple new drops of our sample with the syringe from one side while placing a Kimwipe on the other side, such that we would see a more drastic flow, and minimize the chance of air bubbles to appear in our sample chamber.

2.3 Characterizing the Stability of the Trap

To understand the physics of how radiation pressure forces from the dual-beam optical trap affects soft matter, such as GUVs, we first needed to examine where these particles would trap between the fibers. Initially, we hypothesized that the particles would stably trap at the center (half-way between the fiber ends); however, the following proved otherwise.

2.3.1 Simulations

Our simulations to determine the theoretical trapping landscape is shown as a flow chart in Fig. 2.3. Once inputting the parameters of the system, the MatLAB code determined the possible range where the particle's center could be located along the beam axis. For a specific position in this range, the code examined the possible locations on the particle's surface that could interact with a single laser beam. At each of these points, the momentum transfered to the particle q_z was calculated using Eq. 2.3. By summing these momenta, we effectively used Eq. 2.2, allowing us to examine the trapping efficiency from a single laser beam. The code repeated this for the second laser beam and output a graph of the net Q_z as a function of position. Since F_z is proportional to Q_z, a $Q_z = 0$ implies an equilibrium position.

2.3.2 Beads in Index Matching Liquid

Our samples for our low refractive index constrast experiments consisted of PMMA beads (MICROBEADS® SPHEROMERS® CA6, CA10, and CA15; Bangs Laboratories, Inc. Dry PMMA beads BB01N) in a refractive index liquid medium (Cargille

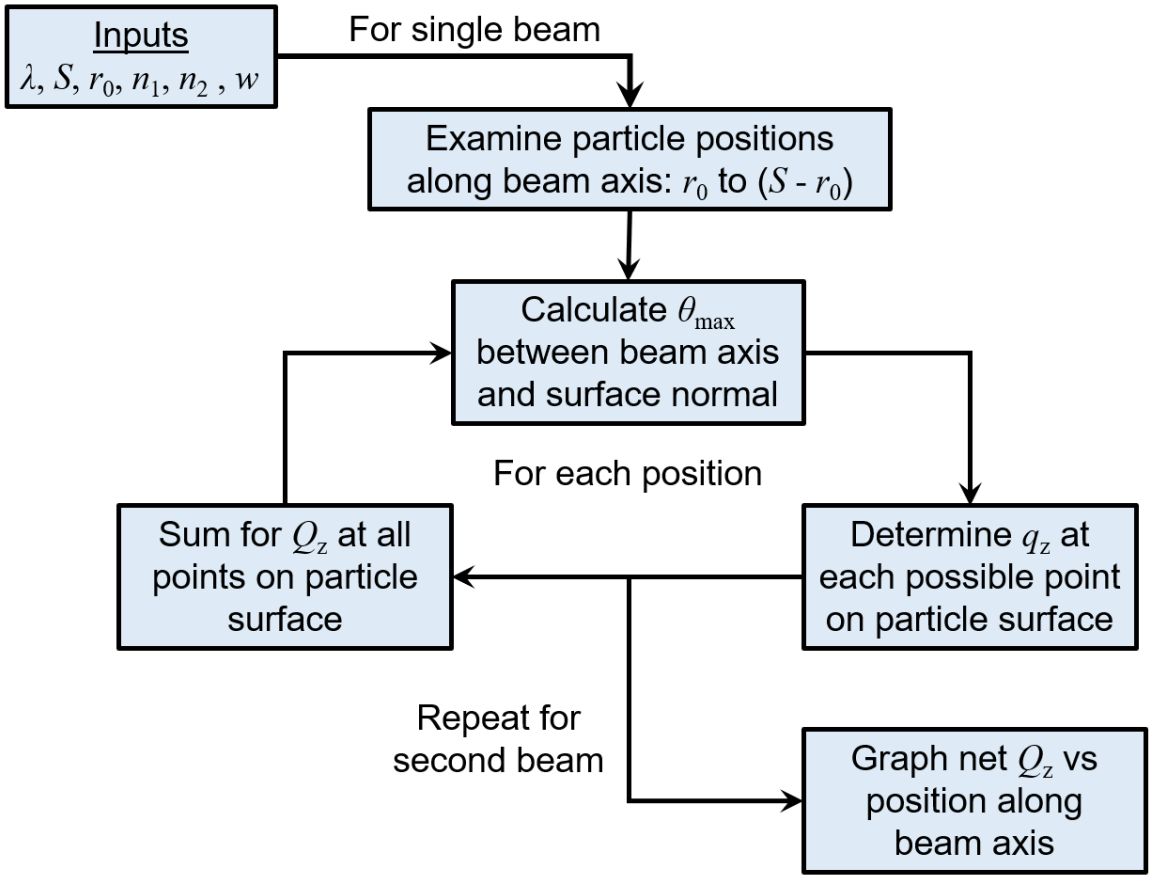

Figure 2.3: Flow chart of the simulations used to create trapping efficiency plots. By generating these at multiple fiber separations and particle radii, we were able to examine the theoretical trapping landscape at low refractive index contrasts. The MatLAB code is provided in A.2.

Laboratories, Series A). The PMMA bead sizes ranged from 2 to 20 μm (Mie scattering according to $2\pi R/\lambda \gg 1$ applies [19]) and had a refractive index of 1.482 ± 0.002, while the medium had a refractive index of 1.4700 ± 0.0002. The sample was inserted into a 3 cc syringe and shaken well for 10 s in order to separate aggregated particles. The samples were held and experiments were performed at room temperature, and we expected laser-induced heating to be minimal ($< 2^\circ$ C) [19]. Our simulations used room-temperature refractive indices and assume no thermal effects. Using the approach of Peterman *et al.*, we expected $< 2^\circ$ C of heating in the center of the trap [20].

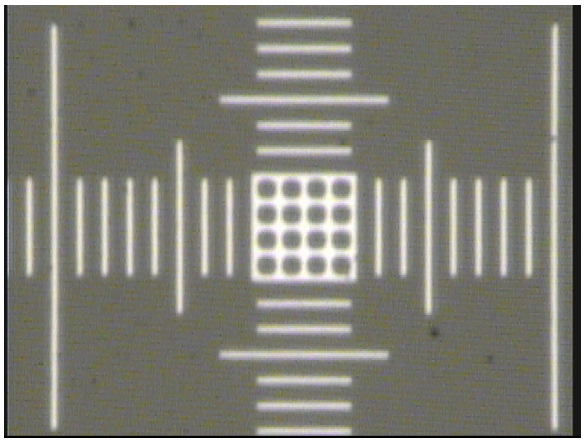

Figure 2.4: Calibration method for determining particle size. The lines are spaced 0.01 mm apart. The longest vertical lines near the edges of the figure were used for our calibration.

2.3.3 Determining Particle Size

To determine the size of each of our trapped particle, we used a microscope stage micrometer calibration slide (Microyntechm TS-M2), shown in Fig. 2.4, where the line spacing is 0.01 mm. With `mycursors.m`, available for download through the File Exchange on MatLAB Central through MathWorks, we determined the conversion between pixel count at our magnification setting and the length by measuring the distances between the inner and outer edges of longest lines in Fig. 2.4. We found with our system that 1386.9 pixels corresponded to a length of 200 μm.

2.3.4 Results

Our research began with comparing simulations using equations presented in Sidick *et al.* [17] and our experimental results of stability positions along the fiber axis. Using Eq. 2.2, we generated simulations of Q_z with respect to the location along beam axis at various separations and particle sizes, as shown in Fig. 2.5a. Since F_z is proportional to Q_z and is a restoring force, we see the positions where Q_z is zero and have a negative slope are stable equilibria, while having a positive slope indicates an unstable equilibrium. Due to the similarity in refractive index of the particle and

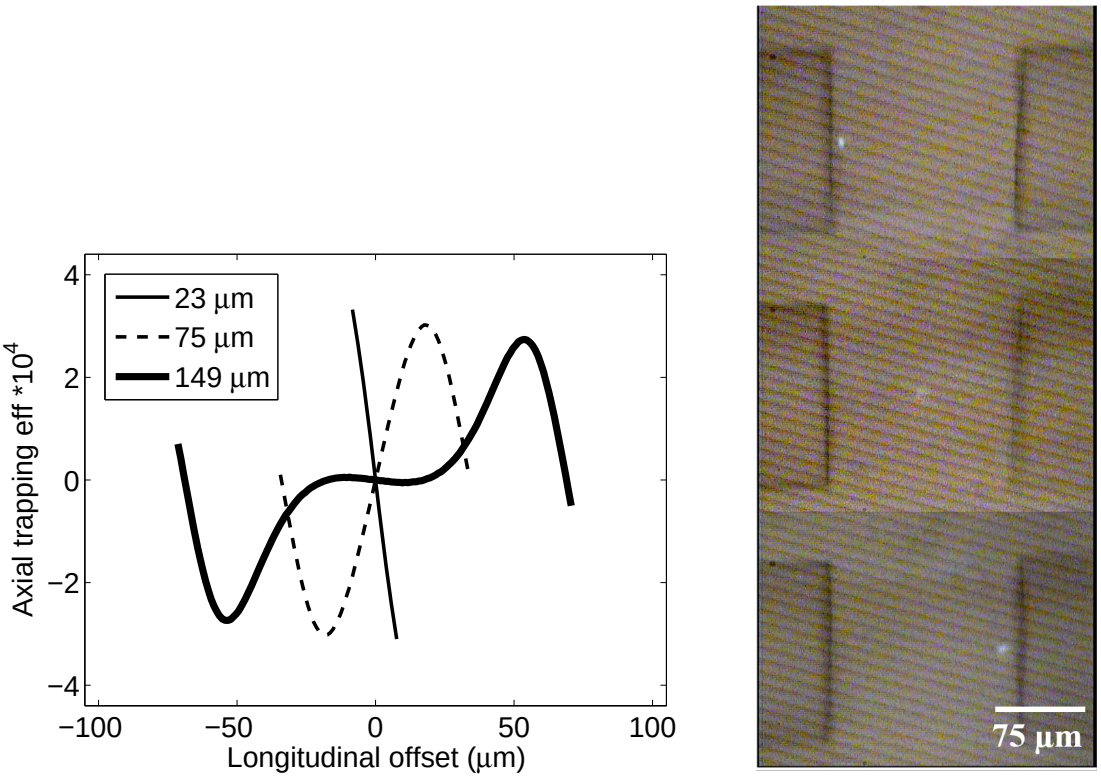

(a) (b)

Figure 2.5: Comparison of trapping efficiency simulations to experimental data. (a) Simulations of the dimensionless trapping efficiency Q_z along the beam axis z when the particle radius is 3.15 μm and the fiber separation are 23 μm, 75 μm, and 149 μm. The trap center is located at $z = 0$. (b) Pictures of experimentally trapped particles at a fiber separation of 129.1 μm. The bright spots indicate the location of the microspheres. The contrast and brightness were adjusted to better view the particle and fibers. Reprinted from Ref. [18] with permission from the Optical Society of America, Inc.

surrounding medium, we see in Fig. 2.5a that the stable trapping positions are based on separation and particle size; for a 3.15 μm particle radius, we see that a single stable equilibrium occurs when the fiber separation is small (23 μm). However, an increase to an intermediate separation (75 μm) moves the equilibria location near the fiber tips. At large separations (149 μm), we see both the center and near the fiber ends become equilibria, yet the center is not as strong of an equilibrium as the fiber ends. The three equilibrium positions are experimentally verified, as shown in Fig.

2.5b.

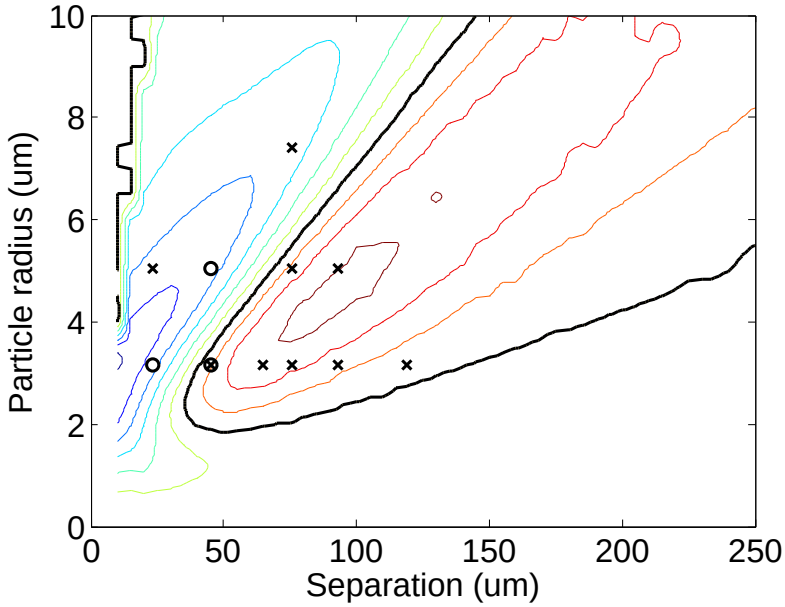

Figure 2.6: Contour plot describing the expected stability at the center of the trap. The warmer colors indicate an unstable trapping regime, while the cooler colors indicate a stable trapping regime. The thick black zero line indicates location where the center is neither stable nor unstable. The contours are obtained from the simulations. Experimental data is given by markers. Open circles represent the particles observed to be trapped at $z = 0$ (indicating a stable equilibrium point at $z = 0$), while the crosses represent particles which drift away from $z = 0$ (indicating an unstable equilibrium point at $z = 0$). Reprinted from Ref. [18] with permission from the Optical Society of America, Inc.

To further understand trapping characteristics for a low refractive index contrast sample, we compiled these simulations with various fiber separations and particle radii into a contour plot describing the stability of the center of the trap, as shown in Fig. 2.6. The steepness of the slope at the center from Fig. 2.5a is indicated with the color, where a steep positive slope is represented as dark red, and a steep negative slope is dark blue. The black line represents a slope of zero, where the trap is neither stable nor unstable. Comparing our experimental data to the simulations, we see that the particles do drift away from the center when the contour plot displays

an unstable trap at the center, and that they stabilize at the center when it indicates a stable trap.

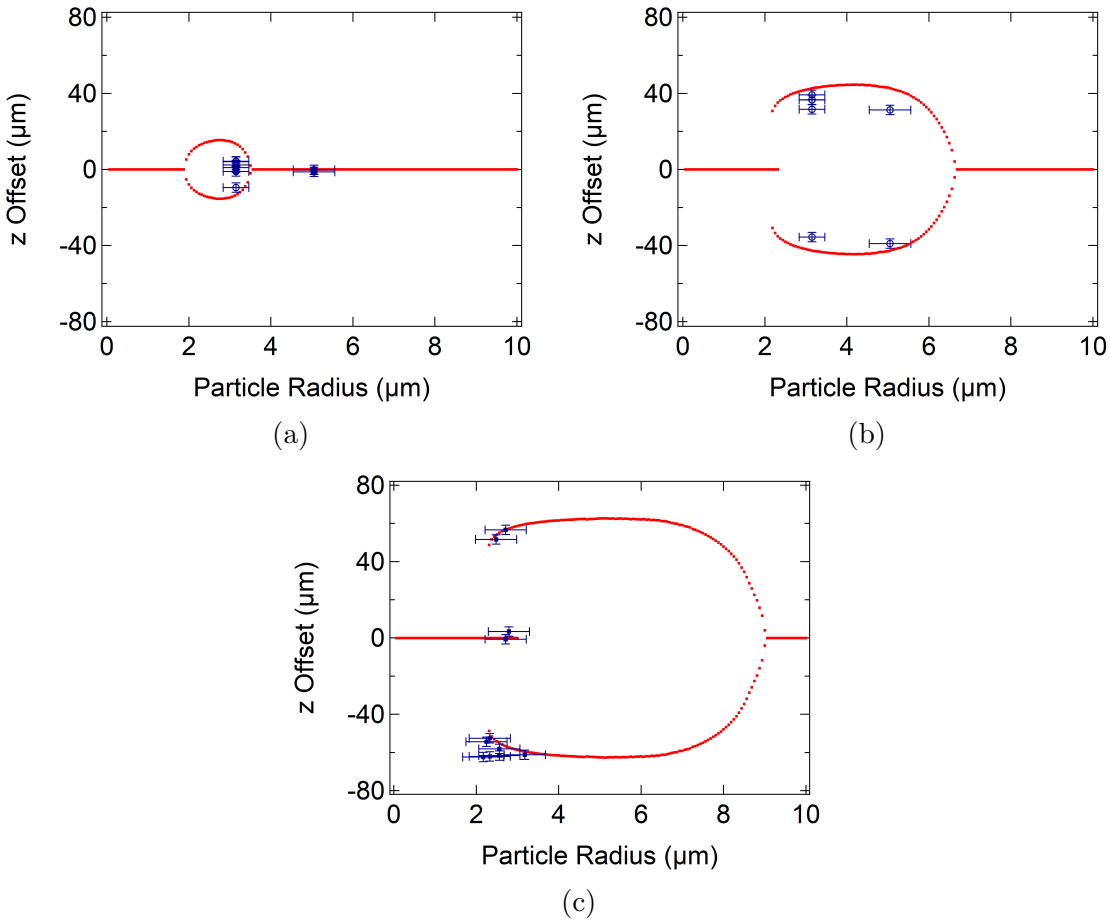

Figure 2.7: Bifurcation plots showing the axial stability locations vs. particle radius for three different traps with fiber separations of (a) 45 μm, (b) 92.9 μm, and (c) 129.1 μm. The red dots represent the simulated stable trapping location, and the symbols represent experimentally observed stably trapped particles. The trap center is located at z=0. Trapping locations are shown schematically within (c). The error bars were determined empirically through measurements of the inner and outer edges of both the fiber and beads. Reprinted from Ref. [18] with permission from the Optical Society of America, Inc.

In order to see how the stability locations are dependent on particle size, we analyzed multiple Q_z simulations for a given fiber separation and developed bifurcation plots, as shown in Fig. 2.7. The refractive index of the medium and particle are

1.4700 and 1.482, respectively for all fiber separations. We see that the bifurcation points match the zero-line position in Fig. 2.6. In Fig. 2.7a, we see that particles with radii between 2.0 μm and 3.5 μm would not be stably trapped at the center; this applies to radii between 2.4 μm and 6.9 μm in Fig. 2.7b, and between 3.0 μm and 9.0 μm in Fig. 2.7c. In these "unstable ranges", the particle may be stably trapped close to the fiber ends as verified experimentally, due to F_g dominating over F_s. We also see that the unstable range increases and begins at larger particle sizes as the fiber separation increases; this can be understood by considering the particle size relative to the beam diameter. When the particle radius is either much larger or smaller than the beam radius, α_i and α_r at $\theta_{\max}$ approach 0 or $\pi/2$, respectively; these result in F_s dominating over F_g. However, when the radius is within the unstable range, F_g is larger than F_s. Since the beam diameter increases as z increases and the particle interacts with both beams, at larger separations the double stable point occurs over a larger particle size range and begins at a larger size.

Interestingly, at larger separations we see sections with three stable trapping locations, as shown in Fig. 2.7c for particle radii between 2.3 μm and 3.0 μm. The three-location range is a mixture of the two scenarios; a particle entering the beam closer to the fiber ends will be pulled close to the fiber tip and trap due to the dominance of F_g in that region. On the other hand, if the particle enters the beam near the trap center, then it will trap there due to the local dominance of F_s. This is due to the z-dependence of both F_g and F_s; F_g dissipates more rapidly than F_s as a function of z, so after a certain distance the center becomes a stable point. It is important to note that the center is a weaker stable point than the ends; this is apparent in Fig. 2.5a for the 149 μm separation when comparing the stable location slopes. Therefore, the particle will more easily trap near the fiber ends, rather than the center.

To better observe the bifurcation trend, we also analyzed multiple Q_z simulations for a given particle radius and created another set of bifurcation plots, as shown in Fig. 2.8. Utilizing the same refractive indices, we notice the bifurcation points are located at the same position as the zero line in Fig. 2.6. At smaller separations, particles are stably trapped in the center due to F_s being stronger than F_g. As the separation increases, F_g begins to dominate, resulting in two stable trapping locations;

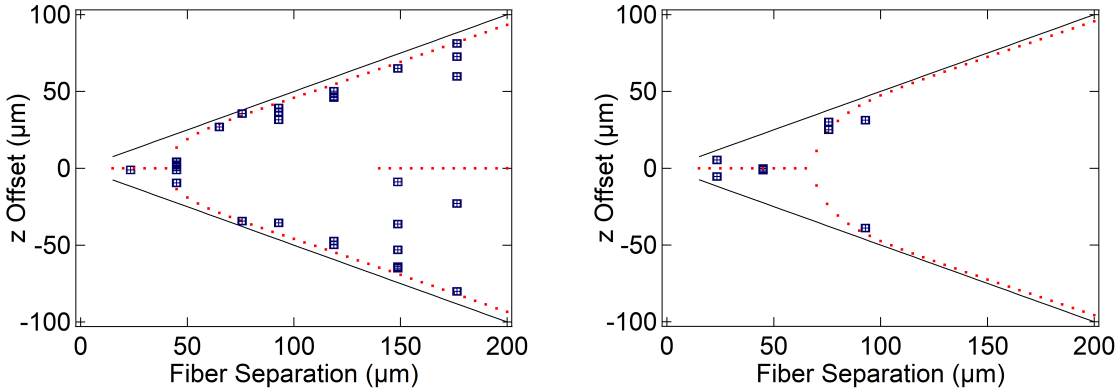

(a) (b)

Figure 2.8: Bifurcation plots of the axial stability locations as a function of fiber separation for particles of radius: (a) 3.15 μm and (b) 5.05 μm. The red dots indicate the simulated stable trapping location, the black lines show the location of the fiber ends, and the blue data points represent the observed stably trapped particles. The trap center is located at $z = 0$. The error bars were determined empirically through measurements of the inner and outer edges of both the fiber and beads. Reprinted from Ref. [18] with permission from the Optical Society of America, Inc.

this occurs at a 45 μm separation in Fig. 2.8a and a 70 μm separation in Fig. 2.8b. Similar to Fig. 2.7, we notice the range of dual-stability locations increases, and the transition point occurs at larger separations for larger particle sizes.

In addition, analogous to Fig. 2.7c, we experimentally and computationally observe a section with three stable trapping locations appearing after a 140 μm-fiber separation for particles with radii of 3.15 μm, as shown in Fig. 2.8a. As stated previously, this is due to the relative strengths of F_s and F_g along the z-axis; we also see the center is a weaker stable trapping location than the fiber ends, so particles will trap more easily near the fiber ends than the center.

2.4 Soft Matter Trapping

Armed with the understanding of where particles stably trapped in our dual-beam optical trap, we decided to venture into researching membrane mechanics. Unlike most of these studies which focus on area effects, as shown by Evans [16], we wanted

to observe bulk response of membranes using our setup. In order to do this, we needed to trap and stretch soft matter particles with different membrane types, so we chose oil droplets in water, and stem cells, donated from the McCloskey Lab.

2.4.1 How Soft Particles Stretch in the Trap

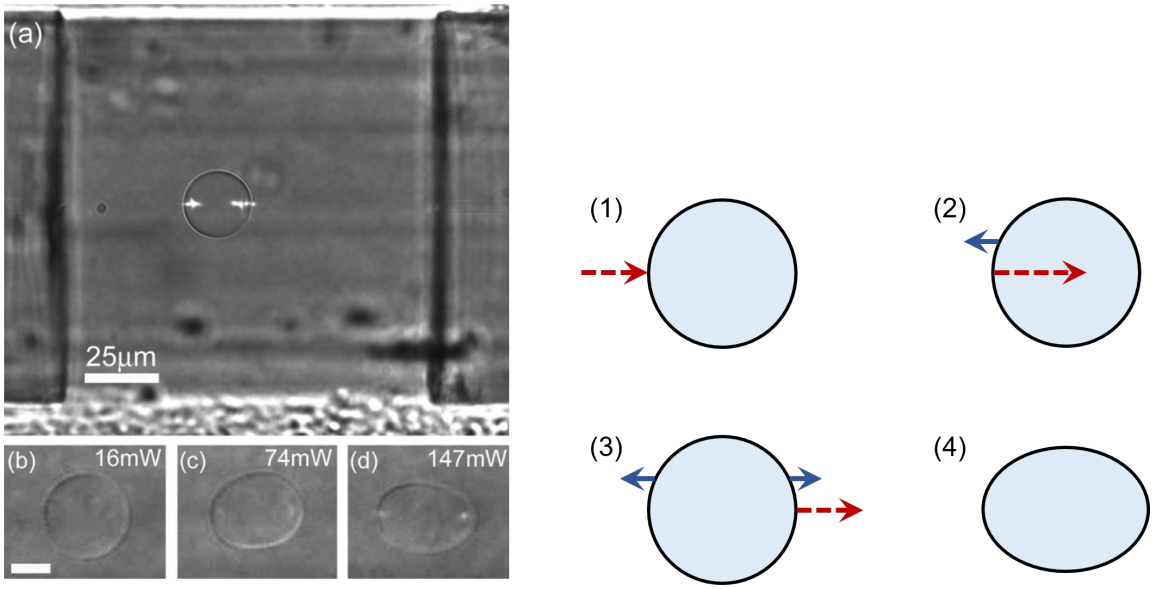

Figure 2.9: Soft matter stretching in a dual-beam optical trap. (a) GUVs trapped and stretched in a dual-beam optical trap [4]. The power at which the vesicles are trapped and stretched are written on each image. (b) Momenta and forces from light-particle interactions causing stretching, derived from Guck *et al.* [13]. The red dashed arrows represent the momenta of light, while the blue solid arrows are forces. The light with some momentum approaching the particle (1) enters the particle and applies a net force on the surface (2). The light then leaves the particle and applies a force on the other side (3), causing particle stretching (4).

Our dual-beam optical trap was originally built to trap and stretch GUVs, as demonstrated in Fig 2.9a. As shown in Guck *et al.* [13], we can start by examining the effects of a single light ray interacting with a dielectric soft matter particle without a membrane. Due to the relativistic nature of photons, we start with the Minkowski

form of momentum density, or the canonical momentum [21]

$$p = \frac{nE}{c}, \tag{2.5}$$

where p is the momentum of the photon, n is the refractive index through which the photon is traveling, E is the energy of the photon, and c is the speed of light in a vacuum. We can see the schematic of a light ray interacting with a dielectric soft matter particle in Fig. 2.9b. Since the refractive index of the particle is larger than the refractive index of the surrounding medium, momentum increases as the light enters the particle; this results in the surface gaining momentum in the opposite direction, due to momentum conservation. Similarly, when the light exits the particle, the momentum decreases, resulting in the surface gaining momentum in the same direction as light propagation. In addition, a portion of the light reflects off the surface during entry and exit, which results in the surface gaining momentum in the direction of light propagation at both points. Since $F = \dot{p}$, this results in forces applied on the surface of the particle, as shown in Fig. 2.9b(3). Due to volume conservation, the result is the particle stretching along the beam axis [14], as observed in Fig. 2.9a, while the resulting force pushes it in the direction of light propagation, as described in Fig. 2.9b(4). With a second, coaxially aligned beam propagating in the opposite direction, the particle can be trapped, while the momentum applied on the surface of the particle is increased.

2.4.2 Oil Droplets in Water

Our oil droplets in water samples consisted of 3 μL standard vegetable oil and 300 μL distilled water. The sample was placed in a sonicator (Microson Misonix Ultrasonic Cell Disruptor) for ten seconds to create droplets of oil throughout the water that were stable for sixty minutes. The particle sizes ranged from 2.0 to 5.0 μm and had a refractive index of $n_{\text{oil}} = 1.47$ [22], while the distilled water had an refractive index of $n_{\text{water}} = 1.33$. The sample was held at and the trapping was conducted at room temperature. The sample was inserted into a 3 cc syringe to allow for better control when flowing it into the sample chamber.

2.4.3 Stem Cells in PBS

Our stem cell samples were provided by the McCloskey Lab, and the methods (provided by Edwin Shen) were as follows: Matrigel coated plates were prepared by incubating 1.125% Matrigel (Corning) in DMEM F12 (Gibco) on tissue culture plastic for 1 hour. Human induced pluripotent stem cells (hiPS, DF19-9-7T from WiCell) were cultured on Matrigel coated tissue culture plastic at an initial density of 3500 cells/cm^2. Culture media was refreshed daily with mTeSR1 (Stem Cell Technologies) and passaged every 3 - 4 days with Accutase (Innovative Cell Technologies). Immediately before trapping, cells were lifted with Accutase and resuspended in a phosphate buffer solution (PBS) with a refractive index of $n_{\mathrm{PBS}} = 1.335$ [23] at a density of 250000 cells/mL; this density allowed for frequent single cell trapping, as enough were present in the sample to flow through the trapping region, but was not high enough for the majority of the cells to cluster together. The cells were estimated to have a refractive index range equivalent to that of cytoplasm ($n_{\mathrm{cytoplasm}} = 1.37 - 1.38$ [24, 25]). The sample was inserted into a 3 cc syringe to allow for better control when flowing it into the sample chamber.

2.4.4 Results

Our experiment with soft matter particles started with trying to see if the oil droplets would be trapped in our dual-beam optical trap. Using the same methods as for PMMA beads, we ran simulations using equations presented in Sidick *et al.* [17] and created bifurcation plots for our new mixture, as shown with red dots in Fig. 2.10a. After the theory confirmed that the particles could be trapped, we experimentally verified this, as demonstrated with blue symbols in Fig. 2.10a. An average-sized oil droplet trapped is shown in Fig. 2.10b, which, albeit exciting, presents the main issue with the oil-in-water sample; these particles were far too small to observe any form of stretching with our system.

We then examined how stem cells in PBS would interact with our dual-beam optical trap. Like the case with oil in water, we used the same methods as for the PMMA beads and ran simulations using the equations presented in Sidick *et al.* [17]

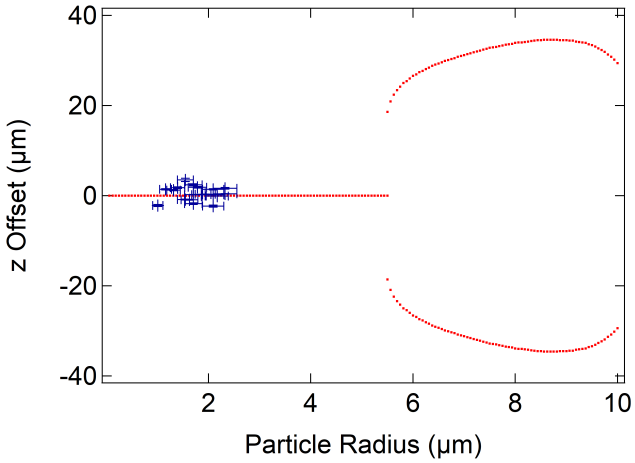

(a)

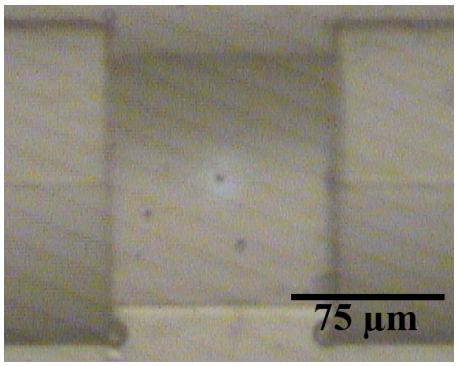

(b)

Figure 2.10: Oil droplets trapped in water. (a) Bifurcation plot showing the axial stability locations vs. oil droplet radius within a trap with a fiber separation of 87.6 μm. The red dots represent the simulated stable trapping location, and the blue symbols represent experimentally observed stably trapped oil droplets. The trap center is located at z=0. The error bars were determined empirically through measurements of the inner and outer edges of both the fiber and droplets. (b) A picture of a stably trapped oil droplet with the same fiber separation. The contrast and brightness were adjusted to better view the particle and fibers.

to created bifurcation plots for our new mixture, as shown with red dots in Fig. 2.11a. Fortunately, the stem cells were, on average, much larger; the radii of the stem cells ranged between 2.0 μm and 13.5 μm, with the majority of those trapped were above 7.0 μm, such as Fig. 2.11b. These cells also successfully trapped at large separations and relatively close to the center of the trap, as shown in Fig. 2.11a.

However, an issue arose when we tried to stretch these cells. Fig. 2.12 depicts four stably trapped cells, where each was trapped at a total power of 200mW (100 mW from each fiber). The power was increased in increments of 100 mW and left to stabilize for five minutes at each setting, then decreased in a similar manner. Unfortunately, we were unable to observe any noticable stretching of cells in our trap.

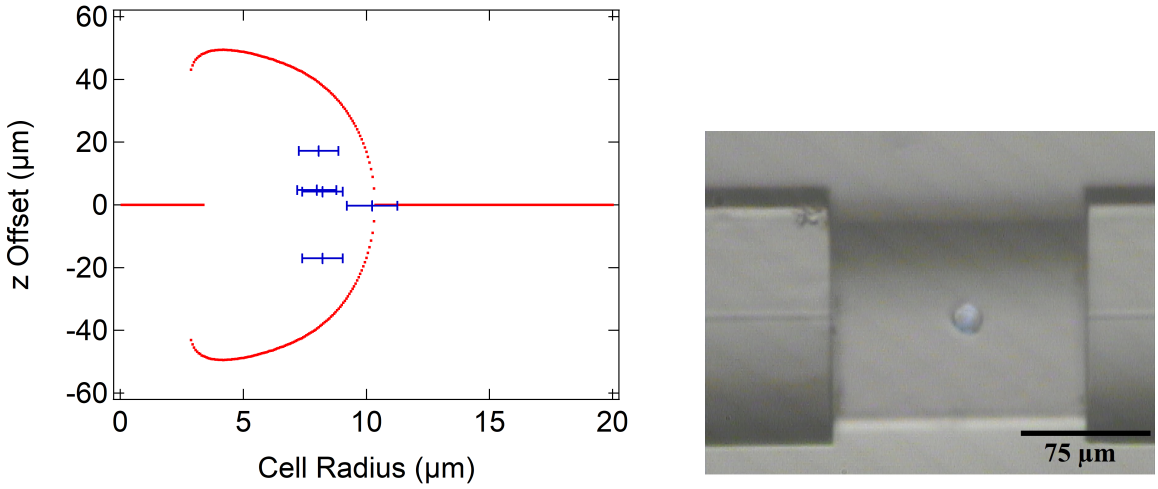

(a) (b)

Figure 2.11: Stem cells trapped in PBS. (a) Bifurcation plot showing the axial stability locations vs. stem cell radius radius within a trap with a fiber separation of 127 μm. The red dots represent the simulated stable trapping location, and the blue symbols represent experimentally observed stably trapped stem cells. The trap center is located at z=0. The error bars were determined empirically through measurements of the inner and outer edges of both the fiber and cells. (b) An average sized cell trapped in the dual-beam optical trap at a total power of 400 mW.

2.5 Discussion

In this section, I will discuss both the issues I have encountered during my optical trapping experiments and what can be done to improve the experiments I have conducted.

2.5.1 Issues and Resolutions

Sample Chip

When we started making our sample chips as described in Section 2.2, we initially decided to secure both our fibers and the cover glass slip with wax. However, by doing so, we noticed that the cover glass would occasionally come off, resulting in our fibers to be slightly misaligned. We then moved on to securing all components

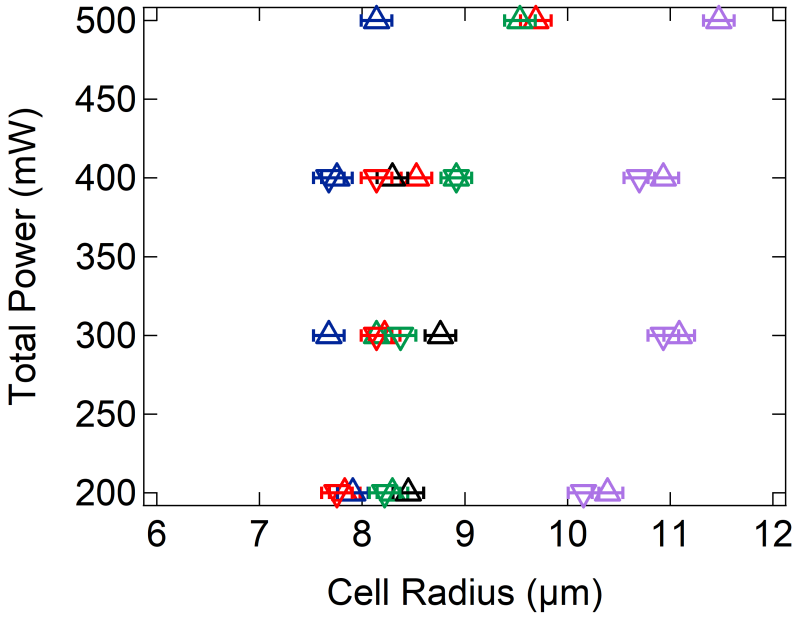

Figure 2.12: Stem cell sizes at each trapping power. The triangles pointing up were data collected as the power increased, while the triangles pointing down were collected as the power decreased. Each color represents a single stem cell. The error bars were determined empirically through measurements of the inner and outer edges of both the fiber and cells.

with 5-minute epoxy. This prevented our cover slip from moving; unfortunately, the fibers were too secure, and we were not able to change the separation between the fiber ends as well. Occasionally, we would also put too much epoxy down to secure the cover glass; therefore, we made sure to use as little as possible, and increased our drying time from the recommended 90 minutes to 120 minutes.

Particle Density

Particle density was an issue when it came to both our PMMA and stem cell samples. For PMMA in the refractive index matching liquid, I noticed that the optimal concentration occurred when, once the system was mixed, the fluid had a slight, but noticeable opacity, with a hint of a milky color. If the opacity did not change, the particles would be present, but would be hesitant to flow between the fiber ends; however, a more opaque sample resulted in the PMMA beads clumping together, and

we would rarely see single beads flow through the trap.

For stem cells, I was provided with samples containing 125, 250, and 500 kilo-cells per milliliter. I noticed that 250 kilo-cells per milliliter was the optimal particle density; similar to the situation for PMMA beads, the 125 kilo-cells per milliliter resulted in minimal (almost non-existent) interaction with the trap, while the 500 kilo-cells per milliliter was filled with cells clumping together, and almost no single cells that could be trapped.

Contour to Bifurcation Plot

When starting on the trapping project, all the experimental data points were placed on the contour plot, as we were predicting all particles to trap at the center; however, the contour plot solely displayed whether or not the center of the trap was stable based off of the simulations. This prevented us from fully exploring the trap, and caused confusion with our experimental results, where we observed particles trapping at other longitudinal positions, but had no way of presenting that on the contour plot.

This part of the project was where I really learned the importance of going back to our roots (or our simulation source, in this situation). By re-examining our axial trapping efficiency plots, we noticed that the center was always a trapping location, as we predicted. Contrary to our initial prediction, the system also contained other stable trapping locations, which was dependent on the particle size and fiber separation. This allowed us to change our method of comparing our simulations to our experimental results; by examining the stable trapping locations based off of our simulations as a function of either particle size or fiber separation, we better understood what was occurring in our trap when we had low refractive index contrast.

2.5.2 Improvement Opportunities

Increasing Oil Droplet Sizes for Stretching

Oil droplets are particles made up of lipids and are both viscous and elastic [26]. However, due to its hydrophobic nature, oil and hydrophilic liquids form an immiscible

mixture; in our system of oil droplets in water, after a long period of time, a clear layer of oil and water would form. We assessed that our oil droplets maintained their sizes over a period of an hour. However, combining the fact that oil droplets have a lower density than that of water and that they are hydrophobic implies that if we increase our observation time, we would be able to have larger oil droplets as they would merge to decrease the amount of surface area in contact with water. If we wait long enough for our oil droplets to have radii between 6.0 and 8.0 μm and flow our mixture into our sample chamber, we can better assess whether oil droplets can stretch in our trap.

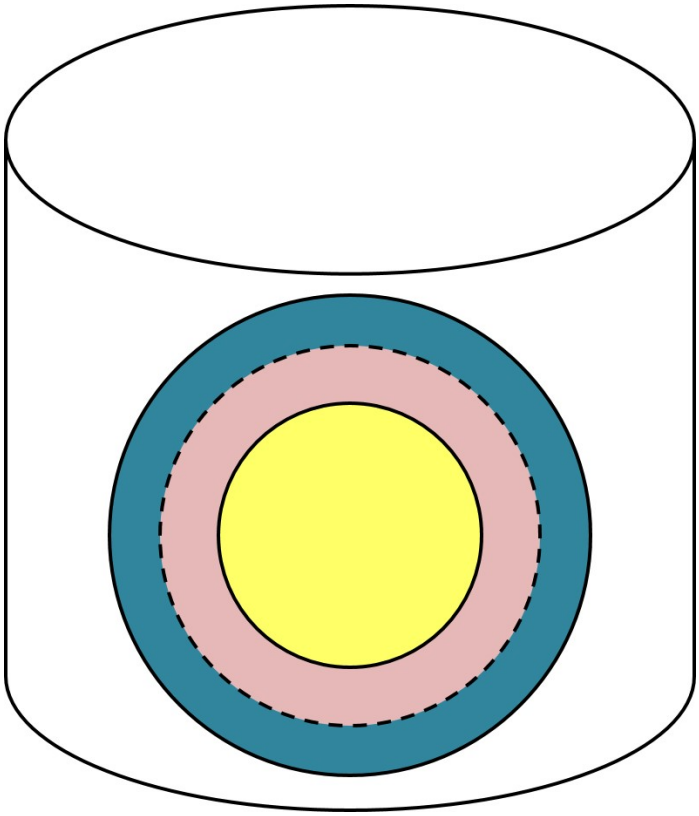

Figure 2.13: Oil droplet in a container of water with a surfactant. The yellow circle represents the oil droplet, while the pink and cyan represent the hydrophobic and hydrophilic portions of the surfactant, respectively.

Another interesting experiment would be to add a surfactant and observe how this addition affects stretching of oil droplets. By adding a surfactant at the right time,

we can maintain our particle size in the desired range, such that the oil and water would never separate into two layers. This emulsifier must have a hydrophobic and hydrophilic portion, and must attach to the oil droplets as shown in Fig. 2.13. For oil droplets to be successfully immersed in water, we must refer to the hydrophile-lipophile balance (HLB) of the emulsifier [27]. Due to our system, we need to look for an HLB value that is larger than ten [27]. However, with the addition of a surfactant, we end up with a membrane with entropic characteristics due to the resemblance of the lipid bilayer of biological cells.

Shear Modulus: Comparison to Other Cells

Our inability to observe stretching of stem cells in our trap is most likely due to the relationship between the forces applied by the laser and the various elastic moduli of the cell- Young's modulus E, the shear modulus G, and the bulk modulus K. Young's modulus represents an object's resistance to length change and is equal to the tensile stress divided by the strain [28, 29]; this modulus typically represents the spring constant of the molecular bonds, or the molecules in the lipid bilayer in our case [29]. The shear modulus indicates an object's resistance to area change whilst the volume is held constant, and the bulk modulus describes an object's resistance to volume change [28, 29]. Since we are examining a the soft matter particle stretch along the beam axis with a constant volume maintained, we are focusing on the shear modulus.

The shear modulus for a thin film is $G = Eh/(1 - \nu^2)$, where h is the bilayer thickness and ν is the Poisson ratio [30, 31]. The lipid bilayer is, on average, 4-6 nm thick [31, 32]; using $h = 5$ nm and $\nu = 0.5$ [30], we can estimate the shear modulus with a given Young's modulus. For a stem cell, the elastic modulus of the membrane is on the order of 10^3 N/m^2 [33–36], which results in an approximate shear modulus on the order of 10^{-6} N/m. The maximum amount of force our lasers would apply on our average-sized trapped particle (radius of 7.5 μm at a total power of 500 mW) was on the order of 10^{-13} N. This implies that the maximum stretching we would see is on the order of 10^{-7} m, which would not be detectable with our equipment, as it would be less than a pixel in difference. Therefore, the force applied by the

dual-beam optical trap was large enough to overcome the shear modulus of the stem cells, but we would not be able to observe them stretching in our trap, unlike what was observed with GUVs in Fig. 2.9a.

This shear modulus is on the same order as other cell membranes, including that for a human erythrocyte [37] and the red blood cell [38]. However, the quantity Eh for GUVs are on the order of 10^{-7} N/m, which results in an approximate shear modulus order of 10^{-7} N/m [32]. This corresponds to a maximum stretching on the order of 10^{-6} m, which is easily detectable with our setup. Therefore, the best way to observe stretching with our current setup is to trap GUVs.

How to Observe Optimal Stem Cell Stretching

The key issue we had with our stem cell experiment was that the maximum force our modular controller would allow us to output was on the order of 10^{-13} N, which would not allow us to overcome the area elastic modulus. By modifying our system in various ways, we may be able to generate enough force to overcome this. One option is to change the wavelength of the laser. The energy of light (or a photon) can be defined as

$$E = \frac{hc}{\lambda},$$

where E is the energy of the photon, h is Planck's constant, c is the speed of light in a vacuum, and λ is the wavelength of light. If we can increase the energy of the photons, we are increasing the momentum of light, which results in a larger force applied on the particle, since $\mathbf{F} = \dot{\mathbf{p}}$, where $\mathbf{F}$ is the force vector applied on the particle, and $\dot{\mathbf{p}}$ is the time-derivative of the momentum vector. To increase our energy, we must decrease our wavelength; for example, we can start by utilizing a laser in the visible range. The advantage of using a wavelength low enough is that we still attempt to keep photodamage to a minimum.

Another possibility is to utilize the same system, but prevent the modular controller from limiting the maximum power for each laser. Currently, our modular controller prevents us from reliably going over a total power of 500 mW; on an averaged-sized stem cell of 7.5 μm, this applies forces on the order of 10^{-13} N per laser. If

we can safely increase each of our laser powers to be on the order of 10^4 mW, then we are able to obtain forces on the order of 10^{-7} N. This is not only impossible with our pump lasers, which have a maximum output of 400 mW, but is also incredibly dangerous, and defeats the purpose of using a dual-beam optical trap, as any particle that has any light sensitivity will encounter photodamage.

In addition, to guarantee that we are trapping the stem cells at the center, we can increase the fiber separation until our simulations indicate that we would have a single stable trap. Unfortunately, this would mean that our optimal magnification would not be able to show both fiber ends. In order to circumvent the issue, we can add particles of known sizes that have a noticeably different appearance than the cells, decrease the magnification, determine our fiber separation, and reset the magnification back to our optimal setting with one fiber end visible. This way, we would be able to determine our separation and measure the particle position with respect to a fiber end, which would allow us to determine the longitudinal position with respect to the trap center.

2.6 Conclusion

We have characterized low refractive-index-contrast optical trapping in a dual-beam fiber-optical trap behavior using PMMA beads. Our simulations and experimental data show a shift between stable and unstable trapping behavior for some fiber separations and particle sizes which is due to the interplay between net gradient and net scattering forces in the axial direction. For certain fiber separations and particle sizes we find that stable trapping in the center of such a trap is not possible. When trapping near the center is possible, it is frequently accompanied by weak restoring forces in the trap. Additionally, we find that stable trapping is possible near a single fiber tip, and this single-fiber gradient force trap will exhibit a much larger restoring force (about five times larger than at the center).

Through our understanding trapping characteristics at low refractive index contrasts, we attempted to trap and stretch soft matter particles. For both the case of oil droplets in water and stem cells in PBS, we were able to successfully and stably trap

our particles. However, due to size (oil) and shear modulus (stem cells) constraints, we were unable to successfully observe stretching in our dual-beam optical trap.

2.7 Recent Research

The dual-beam optical trap is still studied and used in unique ways in various research groups.

Brzobohatý *et al.* trapped spheroids using a dual-beam optical trap whose counter-propagating laser light is circularly polarized and observed rotational motion of the trapped particles [39]. They found that the number of spheroids trapped caused different results. For a single particle, the spheroid would rotate depending on the trapping orientation; when the minor axis was parallel to the beam axis, the spheroid rotation was not visible, while trapping with the minor axis perpendicular to the beam axis resulted in easily detectable rotation. When two spheroids were trapped, they oriented themselves such that the minor axis was perpendicular to the beam axis and each other, and they would rotate with this condition unperturbed. Three spheroids would form a quasi-linear trimer, where they would align with their major axes "connected". This resulted in two oscillations; a periodic motion such that they would circulate their center of mass in a plane that was parallel to light propagation, and small oscillations about the axis of the ensemble. Lastly, they examined four spheroids, which resulted in two dimer pairs; here, they noticed that the pairs would distance themselves until they were positioned at a stable equilibrium.

Xiao *et al.* also examined rotation in the dual-beam optical trap; however observed how misaligning the counter-propagating light would cause orbital rotation of the trapped particle. [40]. They found that the frequency of the orbital rotation was proportional to the power output from the laser, while the trajectory of the particle was dependent on how the trap was misaligned, rather than its initial position. Their simulations utilizing the ray-optics model also matched their experimental results.

The two dual-beam optical traps used by Brzobohatý *et al.* and Xiao *et al.* were like our experiments in that the particles were being trapped in a liquid medium. However, trapping with this system can also be done with other fluids; for example,

Jauffred *et al.* have been successful in trapping gold nanoparticles in air, where the sizes of gold ranged from 80 nm to 200 nm [41]. They determined that gold was easier to trap that silica or polystyrene beads with the same size range, but trapping gold in air was ten times more difficult than in water, most likely due to the larger drift present. In addition, they noticed that metallic nanoparticles were heated to a higher temperature than when trapped in water, and they plan to explore how this phenomenon affects optical trapping.

Chapter 3

Parametrically Oscillating Pendulum

Parametric amplification and oscillation are integral to modern experimental physics [42–46]; parametric devices provide experimental access to quantum vacuum or zero-point fluctuations, and the effects of these fluctuations are pervasive in physics. The Lamb shift [47], emergence of large scale structure [48], and the cosmological constant [49] are good examples of phenomena where vacuum fluctuations contribute. Due to the ongoing collaborations between our group and the Ray Chiao Gravitational Radiation Group, we are particularly interested in the dynamical Casimir effect [50,51] wherein real photons (or perhaps even gravitons [52]) are born from the vacuum due to a time-varying cavity boundary condition. It is then interesting that the threshold for parametric oscillation can be derived using only classical mechanics, and that stimulating experimental conclusions can be drawn from a parametrically-excited simple pendulum.

In what follows, we describe a pendulum whose parametric excitation is controlled by an open-source Arduino microcontroller. In comparison with past classroom demonstrations of parametric oscillators, the microcontroller combines unprecedented flexibility in determining the driving frequency (or frequencies) and parameter modulation depth, while also enabling automated data acquisition of the position and/or

velocity of the pendulum bob as a function of time. It combines intuitive and quantitative understanding in an inexpensive and simple system.

The pendulum is a powerful tool for teaching physics [53]. The linearized pendulum is a simple harmonic oscillator exhibiting the parabolic potential which is a cornerstone concept in quantum mechanics. Driving an underdamped pendulum is presented in undergraduate mechanics textbooks [54]. It is possible, however, to excite the motion of an oscillator by varying a *parameter*, such as the length or effective acceleration due to gravity. [55] These *parametric processes* actually amplify the existing motion (including vacuum fluctuations) of the pendulum such that, assuming that the effective *parametric gain* is greater than the loss due to dissipation, the pendulum's motion will grow exponentially to a large amplitude [55], which incorporates a pendulum hanging from a vertically-oscillating platform, and to that of Ref. [56], which utilized a pendulum with a periodically driven length. Our analysis is consistent with the theory presented in Ref. [56] and Ref. [57] for a linear oscillator. Our system and analytical treatment includes damping in the analysis and uses a programmable Arduino microcontroller for greater flexibility in the driving frequencies. Moreover, we believe that the interesting physics is more transparent in combining the best aspects of Ref. [55] and [57]. Finally, we employ an Arduino microcontroller which is an incredible tool in a student laboratory setting; not only is it a low-cost device, the open-source nature of it has encouraged a plethora of educational projects to develop, ranging from creating a LED-display stopwatch [58] to electronically verifying the time-varying behavior of RC circuits [59].

3.1 Undergraduate Laboratory Objectives

This pendulum was developed for an upper-division undergraduate laboratory class, such that physics students can better observe and understand parametric oscillations. The learning objectives and learning outcomes for such a setting are listed below.

Learning Objectives

1. Experimentally observe and quantify damped harmonic motion of a pendulum.
2. Derive the threshold condition for the lowest and next-lowest order parametric

oscillations.

3. Predict the modulation depth required to induce parametric oscillations.
4. Experimentally observe and quantify the parametrically-driven pendulum motion.

Learning Outcomes

1. Students will demonstrate the ability to
   (a) assemble and debug a simple, weakly damped pendulum having a single mode of oscillation and identify the likely key sources of dissipation.
   (b) record and extract relevant data from sensors, and integrate the computer-controlled servo motor.
   (c) use Newtonian mechanics to derive equations of motion and to manipulate those equations into forms that predict or explain observed experimental behavior.
   (d) generate and interpret plots of experimental data in both the time domain and frequency domain, allowing them to extract key features of the oscillator such as dissipation or gain, resonance frequency, and quality factor Q.
2. Students will be able to explain
   (a) the difference between a standard driven pendulum and a parametrically driven pendulum
   (b) the concept of a threshold of oscillation and enumerate the conditions for parametric oscillation above threshold.

3.2 How the Pendulum is Able to Parametrically Oscillate

In general physics, we learn that motion in perpendicular directions are independent of each other. How, then, would a pendulum driven in a single dimension, be able to start swinging in two dimensions? For this, we need to examine the system at the atomic level, rather than the macroscopic level.

At first glance, a pendulum "at rest" seems to have a clear, measurable position and momentum, and an energy of zero. However, this is if we examine the system macroscopically; when we zoom in to our system until we can no longer ignore quantum effects, we see that atomic particles neither have a exact position nor momentum, and our energy is, in fact, non-zero. Instead, we see that our atoms have a probability "cloud", where we know the approximate position and momentum; the uncertainty in these two elements must follow the Heisenburg's Uncertainty Principle, which states $\Delta x \Delta p \geq \hbar/2$ [60, 61]. Here, Δx and Δp are the range of uncertainty for the position and momentum of the atom, respectively, and $\hbar$ is the reduced Plank's constant. In our system, this uncertainty occurs in all three dimensions.

Driving out pendulum at the right frequency (resonance) initially looks like we are only driving the system vertically at the macroscopic level; however, at the microscopic level, the atoms are still moving in three dimensions whilst becoming excited. Since the atoms have more energy they move faster, which eventually causes our pendulum to start oscillating, which we have controlled to be one-dimensional, as explained in Section 3.3.

3.3 Our Pendulum Setup

Our parametric oscillator setup is shown in Fig. 3.1. A 27.4 $\pm$ 0.5 cm long simple pendulum was created using a wooden ball with a diameter of 2.56 $\pm$ 0.01 cm and nylon cord. The "V" shape constricted the pendulum's motion to a single plane. The cord was passed through eyelets and secured on a spool such that the cord was parallet with the horizontal supporting rod. The spool was rotated by a servo motor (SpringRC SM-S2309S), which was operated through an Arduino microcontroller (Uno). This configuration allowed the pendulum length to vary sinusoidally and smoothly, to minimize energy dissipation. The driving frequency and servo motor angular amplitudes (servo angle) were user-defined variables. The modulation depth h was calibrated experimentally.

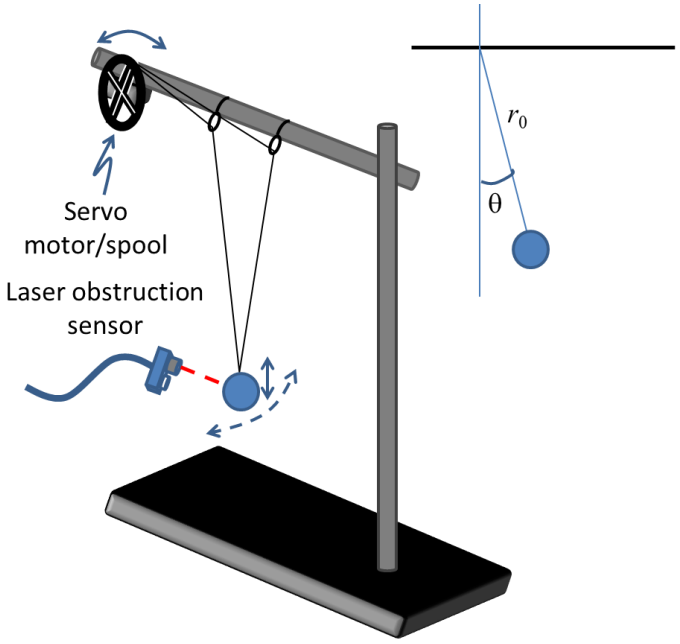

Figure 3.1: Schematic of the parametrically-driven pendulum. The motion of the servo motor results in a variation in the length of the pendulum as a function of time. The quantities r_0 and θ are given as shown in the inset.

3.4 Data Collection

The experimental data was collected using the laser obstruction sensor (Waveshare Laser Receiver Module Laser Sensor Module) shown in Fig. 3.1, which, like the servo motor, was operated with the same Arduino microcontroller. The sensor detected when the laser beam is obstructed by the pendulum bob, which the microcontroller used to determine the duration of the blockage as a function of time; we call this duration a passage time, as it represents the amount of time it takes for the ball to pass across the beam. This data were then compiled and saved using a SD shield (HiLetgo Mini Logging Recorder Data Logger Module Shield V1.0) and an SD memory card.

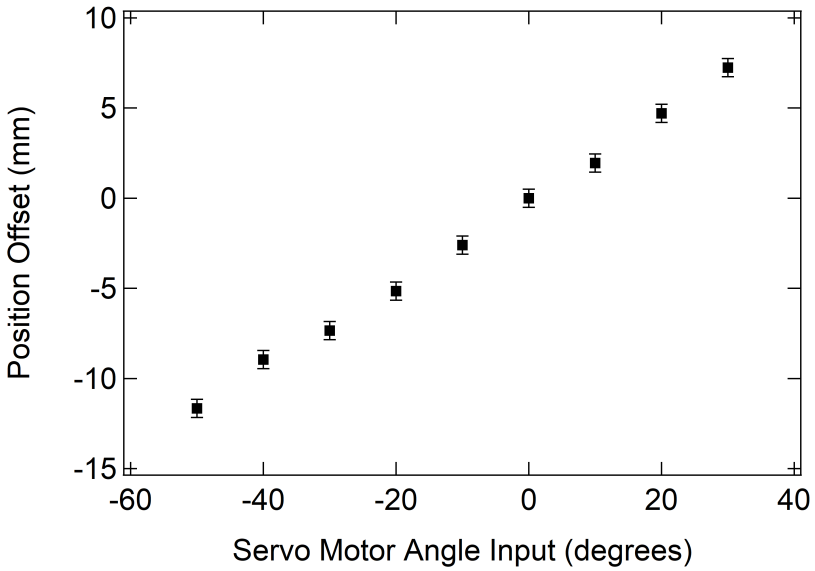

Figure 3.2: Relation between the change in length of the pendulum to the servo angle. The more positive the servo angle, the shorter the pendulum length. The zero case for both occurs when the pendulum is at its natural length r_0.

3.5 Modulation Depth Calibration

The servo angle was converted into a modulation depth by determining the relationship between the pendulum length change δr and the servo angle. We measured the position of the bottom of the ball with respect to the surface onto which the surface was mounted at a range of servo angles. By determining the position offset from the natural pendulum length r_0 at an input angle of zero degrees, we could create the plot shown in Fig. 3.2, which, when linearly fit, yielded $\delta r = (0.235 \pm 0.004 \text{ mm/deg})\,\theta_{\text{servo}}$, where θ_{servo} is the inputted servo angle. Using this, we were able to convert our servo angle to a modulation depth using the expression $h = \delta r / r_0$.

3.6 Derivation of Threshold Conditions

This derivation was adapted from Johnathon Thompson.

For any type of parametric oscillator, the modulation depth must be greater than that of the threshold in order to sustain oscillatory motion. We can derive this

threshold condition from first principles, where we start with the equation of motion and the general solution for a weakly-damped pendulum,

$$\ddot{\theta} + 2\gamma\dot{\theta} + \omega_0^2\theta = 0 \tag{3.1}$$

and

$$\theta(t) = Ae^{-\gamma t}\sin(\omega_0 t) + Be^{-\gamma t}\cos(\omega_0 t), \tag{3.2}$$

respectively, where θ is a small displacement angle, γ is the damping parameter, $\omega_0 = \sqrt{g/r_0}$ is the natural resonance frequency of a pendulum with length r_0, and g is gravitational acceleration. However, our pendulum length varies in a sinusoidal manner, so we must modify Eq. 3.1 and 3.2 to include a time dependent pendulum length $r(t)$, which is given by

$$r\left(t\right) = r_0\left(1 + h\sin\left(2\omega_0 t\right)\right), \tag{3.3}$$

where $h = \frac{\delta r}{r_0}$ is a modulation depth. Damping is added as an angular-velocity-dependent term to give a new equation of motion

$$\ddot{\theta} + 2\frac{\dot{r}\left(t\right)}{r\left(t\right)}\dot{\theta} + 2\gamma\dot{\theta} + \frac{g}{r\left(t\right)}\theta = 0, \tag{3.4}$$

where we see that a damping coefficient γ is included in the standard form of a damped simple harmonic oscillator as seen in Eq. 3.1. We will look for solutions of the form

$$\theta\left(t\right) = a\left(t\right)\sin\left(\omega_0 t\right) + b\left(t\right)\cos\left(\omega_0 t\right), \tag{3.5}$$

where

$$\begin{aligned} a\left(t\right) &\propto e^{\mu t} \\ b\left(t\right) &\propto e^{\mu t}, \end{aligned} \tag{3.6}$$

represent slowly varying envelope functions, and μ is the exponential amplitude gain coefficient. Parametric driving requires amplification, which occurs when $\mu > 0$ and

is real.

When we plug Eq. 3.3, 3.5, and 3.6 into Eq. 3.4, we can obtain a system of two equations for a(t) and b(t). Ignoring the second derivatives, as they are relatively small and will not affect the threshold calculation, we obtain

$$\left(a(t)\Big(\frac{3}{2}h\omega_0^2+2\mu\omega_0+2\gamma\omega_0+\gamma\mu h\Big)+b(t)\Big(2\gamma\mu+2h\mu\omega_0-h\mu\omega_0-h\gamma\omega_0\Big)\right)=0 \quad (3.7)$$

for the cosine term and

$$\left(a(t)\Big(2\gamma\mu-2h\mu\omega_0+h\mu\omega_0+h\gamma\omega_0\Big)+b(t)\Big(\frac{3}{2}h\omega_0^2-2\mu\omega_0-2\gamma\omega_0+\gamma\mu h\Big)\right)=0 \quad (3.8)$$

for the sine term. For the purposes of establishing a threshold of oscillation, we seek out the terms of Eq. 3.7 and 3.8 only up to first order in h. With only these terms written in matrix form we have

$$\begin{bmatrix} \frac{3}{2}h\omega_0^2+2\mu\omega_0+2\gamma\omega_0 & 2\gamma\mu \\ 2\gamma\mu & \frac{3}{2}h\omega_0^2-2\mu\omega_0-2\gamma\omega_0 \end{bmatrix}\begin{bmatrix} a(t) \\ b(t) \end{bmatrix}=0$$

. Upon evaluating the determinant of the left-most matrix and setting it equal to zero, we identify the conditions when this system gives a positive value for μ, which is the condition for exponential growth in the amplitude of the oscillations. The threshold is given by

$$h \geq \frac{4\gamma}{3\omega_0}=\frac{2}{3Q}, \quad (3.9)$$

where Q is the quality factor of the pendulum. Note that $h=\delta r/r_0$ is an amplitude modulation depth.

The quality factor that results in Eq. 3.9 is of interest as it describes physical concepts associated with oscillators [54], but is most often described three ways. As shown in Eq. 3.9, $Q=\omega_0/2\gamma$ is the reciprocal of the sharpness of the resonance peak when plotting the system's energy against the driving frequency. Therefore, a large Q would indicate a narrow resonance, and a small Q would imply a wide resonance. We can also use $Q=\pi$(decay time/period), which relates the number of oscillations

the system undergoes during the decay time; a large Q implies that the oscillator rings for a longer time and, therefore, has low damping, while a small Q rings for a smaller time and has high damping. We can also express our quality factor in terms of energy storage during a single cycle as $Q = 2\pi$(energy stored/energy dissipated). A large Q indicates the system is able to store a large amount of energy compared to the amount dissipated. For our pendulum, $Q = 173 \pm 3$.

3.7 Frequency Shift for Peak Energy

As shown in Baker and Blackburn [53], when our pendulum has an angular amplitude that can no longer be considered small, we cannot approximate $\sin\theta \cong \theta$; this shifts our pendulum from the linear to non-linear regime. This causes our period T, and therefore, our frequency f, to no longer be solely dependent on system parameters, but also the amplitude of the pendulum swing. We can show this by first starting with the equation of motion of a simple pendulum

$$\ddot{\theta} = \frac{g}{r_0}\sin\theta, \tag{3.10}$$

where θ now represents any angular displacement of the pendulum. Using $\mathrm{d}\theta = \dot{\theta}\,\mathrm{d}t$, we can rewrite Eq. 3.10 as

$$\dot{\theta}\ddot{\theta}\,\mathrm{d}t = -\frac{g}{r_0}\sin\theta\,\mathrm{d}\theta. \tag{3.11}$$

When we integrate Eq. 3.11, we end up with the first integral of motion

$$\dot{\theta}^2 = \frac{2g}{r_0}\cos\theta + \text{constant}. \tag{3.12}$$

Since the total energy E is equal to sum of the kinetic energy ($mr_0\dot{\theta}^2/2$) and potential energy ($mgl(1-\cos\theta)$), solving for the angular speed in the form of Eq. 3.12 results in

$$\dot{\theta}^2 = \frac{2g}{r_0}\cos\theta + \frac{2E}{mr_0^2} - \frac{2g}{r_0}. \tag{3.13}$$

When the pendulum reaches it's maximum angular amplitude α, E is equal to the

potential energy at that amplitude. Plugging in $E = mgl(1 - \cos\alpha)$ into Eq. 3.13, we see

$$\dot{\theta}^2 = \frac{2g}{r_0}\left(\cos\theta - \cos\alpha\right), \tag{3.14}$$

which, when using the trigonometric identity $\cos\theta = 1 - 2\sin^2(\theta/2)$, becomes

$$\dot{\theta} = 2\sqrt{\frac{g}{r_0}\left[\sin^2\left(\frac{\alpha}{2}\right) - \sin^2\left(\frac{\theta}{2}\right)\right]}. \tag{3.15}$$

Rearranging this to allow for integration results in

$$\mathrm{d}t = \frac{\mathrm{d}\theta}{2\sqrt{\frac{g}{r_0}\left[\sin^2\left(\frac{\alpha}{2}\right) - \sin^2\left(\frac{\theta}{2}\right)\right]}}. \tag{3.16}$$

To simplify this integration, we can let $\sin(\theta/2) = \sin(\alpha/2)\sin\phi$ and $k^2 = \sin^2(\alpha/2)$, such that

$$\mathrm{d}t = \sqrt{\frac{r_0}{g}}\,\frac{\mathrm{d}\phi}{\sqrt{1 - k^2\sin^2\phi}}. \tag{3.17}$$

When we examine the time the pendulum takes to swing from its lowest point (where kinetic energy is highest and $t = 0$) to α, we are looking at a quarter of the oscillation. In addition, when $\theta = \alpha$, $\phi = \pi/2$, so solving for a period with Eq. 3.17 results in

$$T = 4\sqrt{\frac{r_0}{g}}\int_0^{\pi/2}\frac{\mathrm{d}\phi}{\sqrt{1 - k^2\sin^2\phi}}. \tag{3.18}$$

To solve Eq. 3.18, we can use the binomial expansion, where

$$(1 - k^2\sin^2\phi)^{-1/2} = 1 + \left(\frac{1}{2}\right)k^2\sin^2\phi + \left(\frac{1\cdot 3}{2\cdot 4}\right)k^4\sin^4\phi \tag{3.19}$$

$$+ \cdots + \left(\frac{1\cdot 3\cdot 5\cdots(2n-1)}{2\cdot 4\cdot 6\cdots 2n}\right)k^{2n}\sin^{2n}\phi. \tag{3.20}$$

Using the integration technique

$$\int_0^{pi/2}\sin^{2n}\phi\,\mathrm{d}\phi = \left(\frac{1\cdot 3\cdot 5\cdots(2n-1)}{2\cdot 4\cdot 6\cdots 2n}\right)\frac{\pi}{2}, \tag{3.21}$$

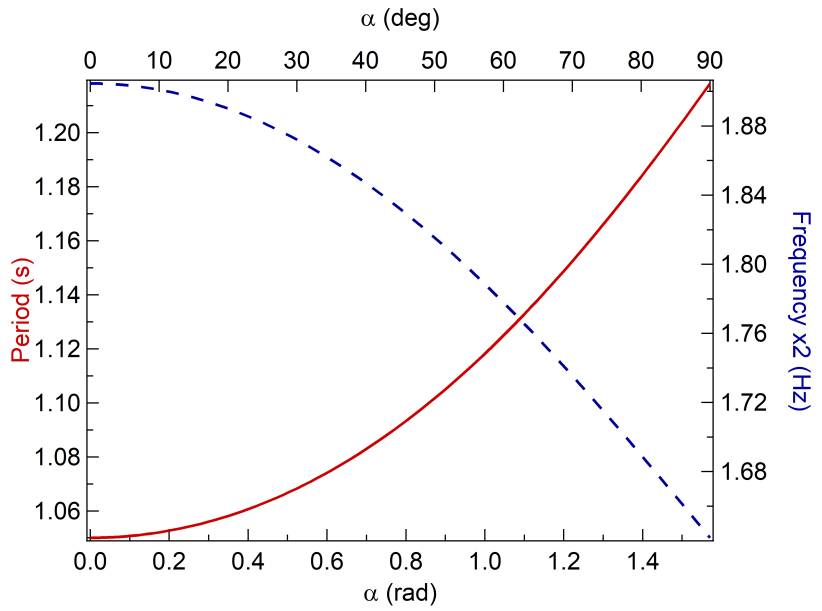

Figure 3.3: Graph representing period and frequency shift as peak energy increases. The solid red line corresponds to the period of the pendulum, while the dashed blue line represents the frequency about the second harmonic.

we can integrate each term in Eq. 3.20 separately. We calculate the period using the first three terms, as the other terms have a negligible impact on the result. We can determine how the amplitude affects the peak energy location about the second harmonic frequency using the relation $f = 1/T$, both of which are plotted as a function of the maximum angular amplitude in Fig. 3.3.

The total energy of the pendulum is related to the maximum angular displacement as $E = mgr_0(1 - \cos\alpha)$. Therefore, as α increases, E also increases, and in order for our pendulum to have large E, we need to drive our system at larger modulations depths. As indicated by the dashed blue curve in Fig. 3.3, as our energy increases, our frequency of the pendulum decreases. This implies that driving our 27.4-cm long pendulum at the second harmonic frequency (1.90 Hz) would cause the pendulum to swing if the modulation depth were small, or near threshold. However, as we increase the modulation depth, we would need to drive the system at a frequency lower than 1.90 Hz to maximize the total energy.

3.8 Results

3.8.1 Raw Data

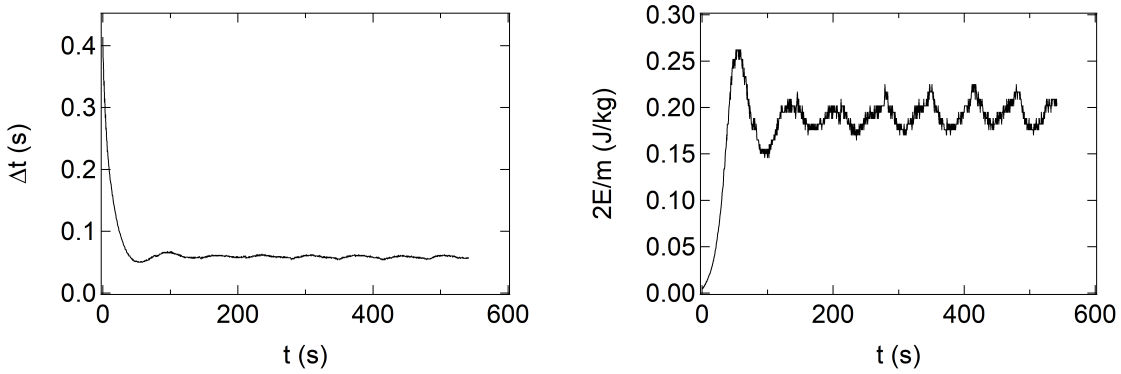

(a) (b)

Figure 3.4: Sample data output by the Arduino microcontroller and analyzed. (a) Raw data output by the Arduino microcontroller. The duration of beam blockage as a function of time when the modulation depth and driving frequency are set to 0.0256 and 1.91 Hz, respectively. (b) Energy equivalent from the same set of data as a function of time. Note that as time increases, the energy approaches a steady-state.

As previously indicated in Section 3.4, the Arduino microcontroller recorded the time and duration that the pendulum mass blocked the laser beam. When we plot the raw data with the appropriate modulation depth and driving frequency, we can obtain graphs similar to Fig. 3.4a. As the pendulum starts to parametrically oscillate, we notice that the passage time exponentially decrease as a function of time and reach some steady-state. We convert this passage time into an energy equivalent E/m using simple kinematics ($v_{\text{avg}} = d/t_{\text{pass}}$) and the expression for kinetic energy ($E = mv_{\text{avg}}^2/2$), where v_{avg} is the average speed of the pendulum with mass m as the diameter of the ball d blocks the beam for some duration t_{pass}. Plotting this energy equivalent as a function of time results in Fig. 3.4b, where we can see that the system reaches some steady-state when driven for some time.

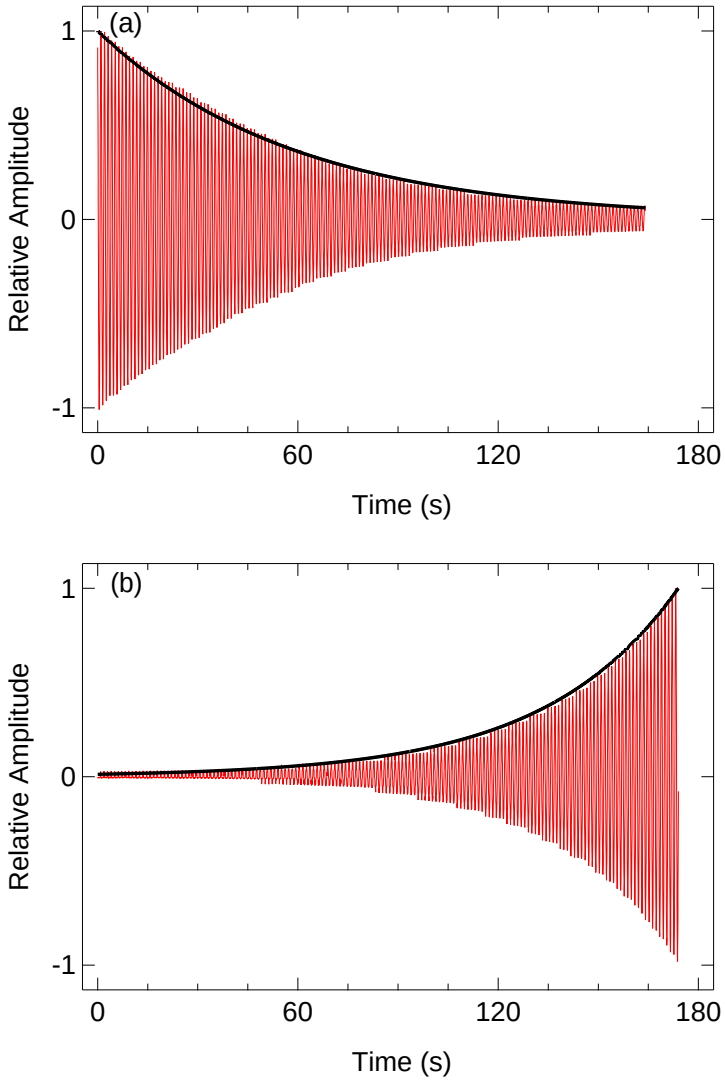

Figure 3.5: Ringdown and ringup of the pendulum. (a) Relative amplitude of an *undriven* pendulum as a function of time (red thin lines). The plot shows the ringdown in the damped harmonic motion. The damping parameter $\gamma = 0.017$ s^{-1} is obtained by fitting a curve to the slowly varying envelope (heavy black line) of the oscillations. (b) Relative amplitude as a function of time for the same oscillator subject to a time-dependent length r_0, *i.e.,* parametric excitation (red thin lines). The exponential slowly-varying envelope, showing net gain in the energy of the pendulum, is plotted as a heavy black line.

3.8.2 Pendulum Characteristics

A couple examples of collected data for a pendulum length of 28.5 ± 0.5 cm are shown in Fig. 3.5. The case for an undriven pendulum is shown in Fig. 3.5a, where we can see the system ringdown over time. By fitting the peak relative amplitude as a function of time to an exponential decay curve as demonstrated with the heavy black line, we determined that the damping parameter of the pendulum was $\gamma = 0.017\ \mathrm{s}^{-1}$. The majority of the data we collect, however, is of a parametrically-driven pendulum, as shown in Fig. 3.5b. Here, we are able to observe the system undergoing a ringup over time. We can fit our increasing relative amplitude to an exponential gain curve, resulting in an exponential amplitude gain coefficient $\mu = 0.025\ \mathrm{s}^{-1}$. In order for us to observe parametric oscillations, we must (a) set our driving frequency to twice the characteristic resonance frequency, and (b) have a modulation depth that is large enough to exceed the threshold conditions. In the case of Fig. 3.5b, the system was driven at a frequency of 1.88 Hz and at a modulation depth $h = 0.014$, which is 87% larger than our experimentally-observed threshold value ($\mathrm{h_{exp}} = 0.0075 \pm 0.0005$).

3.8.3 Threshold Data

The temporal behavior of the parametric oscillator is depicted in Fig. 3.6 where we plot the steady-state energy in a 27.4 ± 0.5-cm long pendulum as a function of time for five different modulation depths. As expected, the ring-up time is shorter and the steady-state energy is larger as the modulation depth increases. For the case of larger modulation depths, we also observe transient oscillations which die out as the system reaches steady-state.

We study the oscillation threshold and frequency response by observing the steady-state energy of as a function of modulation depth and modulation frequency, respectively. The response of the system as a function of frequency is plotted in Fig. 3.7a for the case of a modulation depth of $h = \frac{\delta r}{r_0} = 0.031$, which is well above the threshold for the lowest order resonance. The peak in energy is not located at the second-harmonic driving frequency of $f = 2f_0 = 1.90 \pm 0.02$ Hz. Rather it is shifted to a lower value of 1.86 Hz. This is a consequence of the large angular amplitude of oscillation obtained

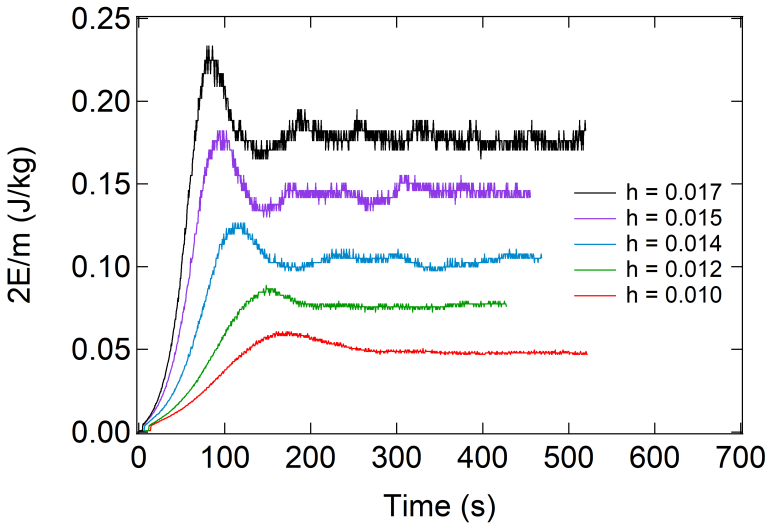

Figure 3.6: Plot of oscillator energy ($2E/m$) as a function of time for five different modulation depths. Larger modulation depths produce a rapid ring-up time and result in higher steady-state energies after transient variations dissipate.

and the need to relax the small-angle approximation which linearizes the simple pendulum, as demonstrated in Section 3.7. Due to the nonlinearity of the system, we expect that the resonance frequency of a pendulum will decrease by as much as 9.57% for the largest amplitudes observed here [53], but we will not observe that much shift. In the measurements presented in Fig. 3.7a, the pendulum starts at rest so the shift in modulation frequency corresponding to peak energy is not as pronounced as that predicted by the large angle theory.

The threshold behavior is plotted in Fig. 3.7b. Experimentally, for modulation depths less than $h = 0.0085$ the pendulum is not excited, and the energy remains zero; when we take a linear fit to the first few data above threshold, we see that the extrapolation yields a threshold of $h_{\text{exp}} = 0.0075 \pm 0.0005$. The energy increases suddenly when the modulation depth increases beyond the threshold. The energy continues to increase as a function of modulation depth, which reflects the fact that the parametric amplification per cycle increases, but it is important to note that the case of energy greater than ~ 0.1 J/kg already already exceeds the point at which the pendulum can be considered "linear". The experimentally-obtained value for the

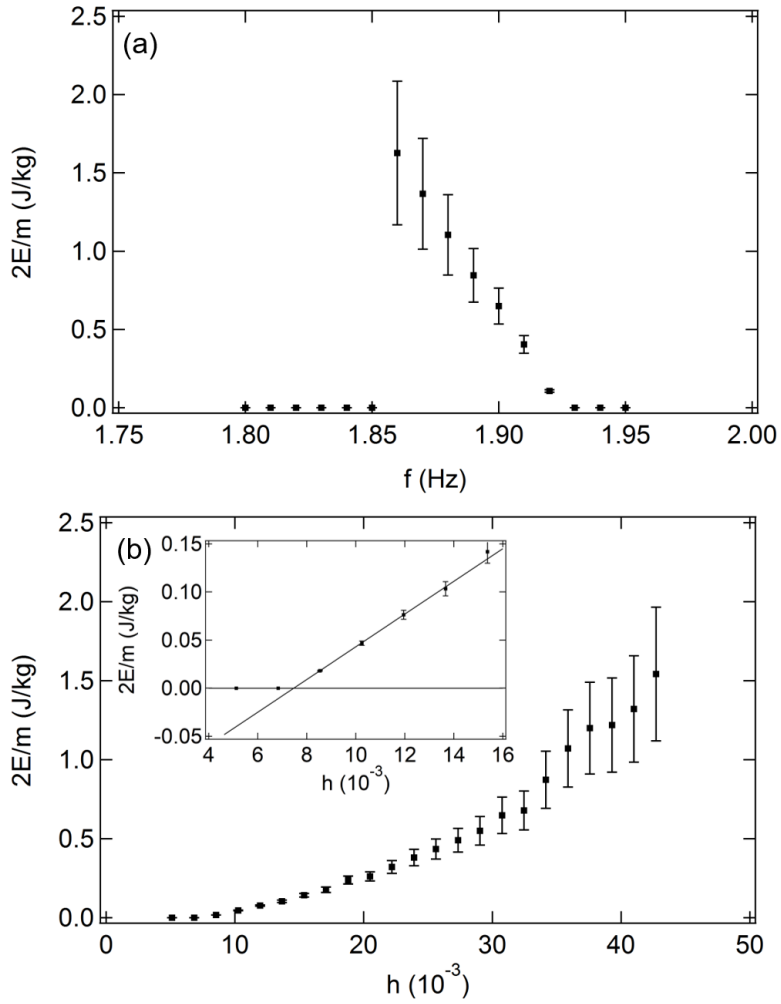

Figure 3.7: Steady-state energy plotted as a function of driving parameters. (a) Steady-state energy of the parametric amplifier at various modulation frequencies for a modulation depth of 0.031. (b) Steady-state energy of the parametric amplifier at various modulation depths, when the modulation frequency is twice the fundamental frequency, at 1.90 Hz. The inset graph shows the linear fit of the first few data points above the experimental threshold.

threshold modulation depth ($h_{\rm exp} = 0.0075 \pm 0.0005$) is nearly double the theoretically expected value given in Eq. 3.9 to be $h_{\rm theory} = \frac{\delta r}{r_0} = 0.00379 \pm 0.00003$, which assumes our experimentally measured value for dissipation ($\gamma = 0.017$ s^{-1}) from the data in Fig. 3.5a. For our pendulum, $Q = 173 \pm 3$.

We also see in both plots in Fig. 3.7 that the error bars increase as a function of

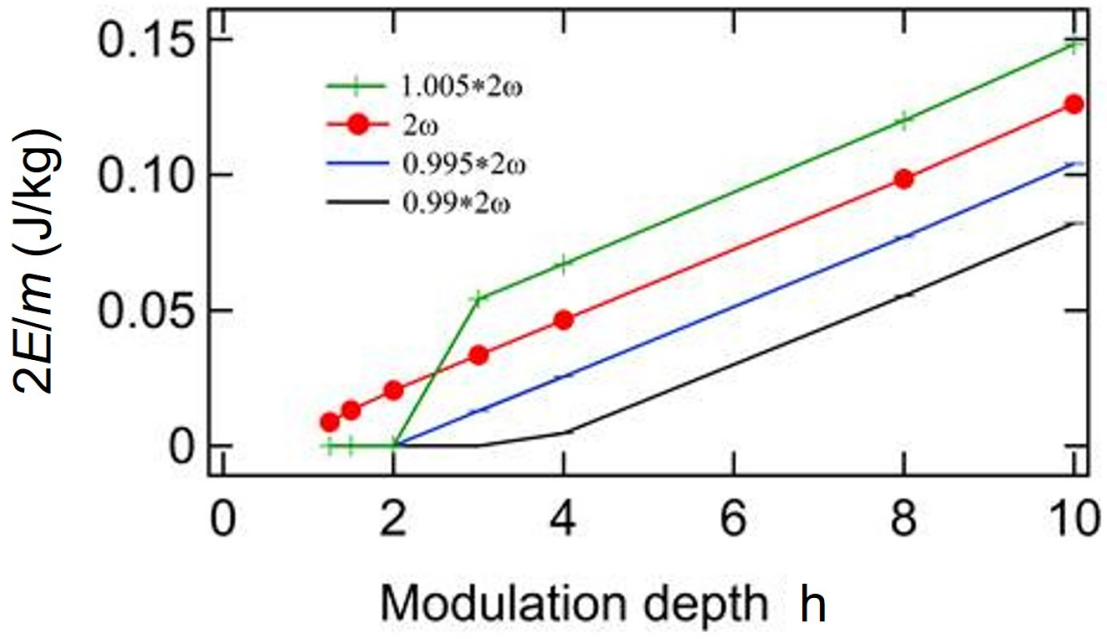

Figure 3.8: Simulated steady-state energy as a function of modulation depths at various driving frequencies. The red curve is the second harmonic frequency. The blue and green curves are for a driving frequency 0.5% less than and greater than resonance, respectively. The black curve is for a driving frequency 1% less than resonance.

energy; this is due to the laser sensor recording the passage time with an uncertainty of about 4 ms resulting in an increase in the uncertainty in the calculation of velocity and thus the energy as well. This uncertainty can be seen in the width of the temporal plots (Fig.3.6) near steady state. The contradiction in our threshold occurs due to the sensitivity to the parameters. By using Eq. 3.4 with driving frequencies near and at the second harmonic, we can simulate the threshold condition. As shown in Fig. 3.8, we see that by increasing or decreasing the driving frequency by less than 1%, the threshold condition for the modulation depth increases by about a factor of two. This lies within our experimental uncertainties of our frequencies, indicating that our experimentally set driving frequencies are not as accurate as we can obtain through simulations.

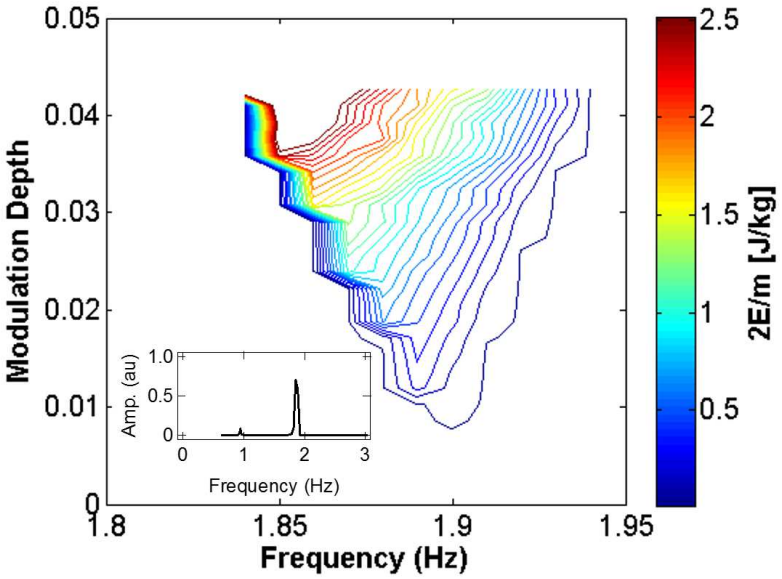

Figure 3.9: Contour plot of the steady-state energy of the parametric oscillator as functions of frequency and modulation depth. Zero energy is indicated by the solid black line. The inset graph shows the relative oscillation amplitude over a larger frequency span revealing a small amplitude at the fundamental frequency and a much larger amplitude for parametric driving.

We combine all the steady-state energy data for various modulation frequencies and depths into one contour plot, as shown in Fig. 3.9. Here, the pendulum was driven in the neighborhood of the second-harmonic frequency. We observe the increase in the frequency range over which parametric oscillations build up as a function of modulation depth. The threshold modulation depth $h = 0.0085$ and an accurate value of the second-harmonic frequency $2f_0 = 1.90 \pm 0.02$ Hz for small amplitude is evident. The maximum energy observed corresponds to the pendulum oscillating with a maximum angular displacement of 80-90 degrees. As observed in Fig. 3.7a, we see that the non-linearity of the system results in this peak energy to occur at a driving frequency of 1.84 Hz, 3.16% from the calculated second-harmonic frequency. The inset graph in Fig. 3.9 depicts the relative amplitude of the oscillator over a larger range of frequencies. Two resonances are observed, one weak resonance at the fundamental frequency of 0.95 Hz and a stronger resonance at the second

harmonic frequency of 1.90 Hz. As obtained in the previous section, the lowest-order (and highest gain) parametric instability is observed when driving near the second harmonic. The weak resonance at the fundamental frequency corresponds to the next-lowest-order instability.

3.8.4 Bistability

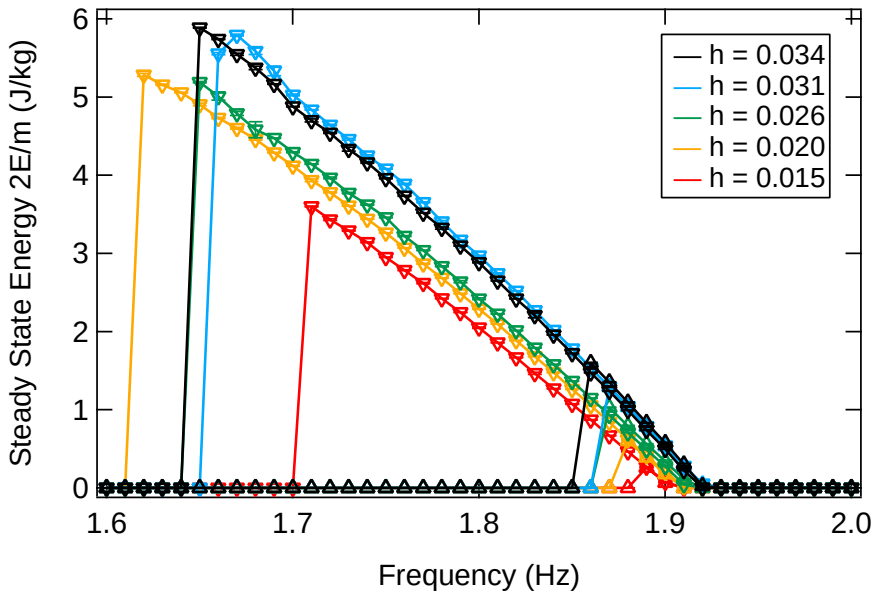

Figure 3.10: Bistability of the pendulum at various modulation depths. Each color represents one modulation depth. The upward-pointing triangles represent increasing frequencies, while the downward-pointing triangles indicate decreasing frequencies.

Another phenomenon of this parametric oscillator is the presence of bistabililty in its steady-state energy. A system is bistable if it has two stable equilibrium states, which are dependent on the initial conditions of the system. By collecting time and passage time data while increasing or decreasing the frequency in steps without pausing in-between increments or decrements, we notice a range of frequencies where the direction of change causes a variation in the steady-state energy. In Fig. 3.10, we see for all modulation depths, when the driving frequency increases, the data correlate with the present data in Fig. 3.9 and, as indicated previously, the highest

energy occurs at a frequency less than the second harmonic. In addition, all of these points overlap with the data when the driving frequency decreases for each modulation depth.

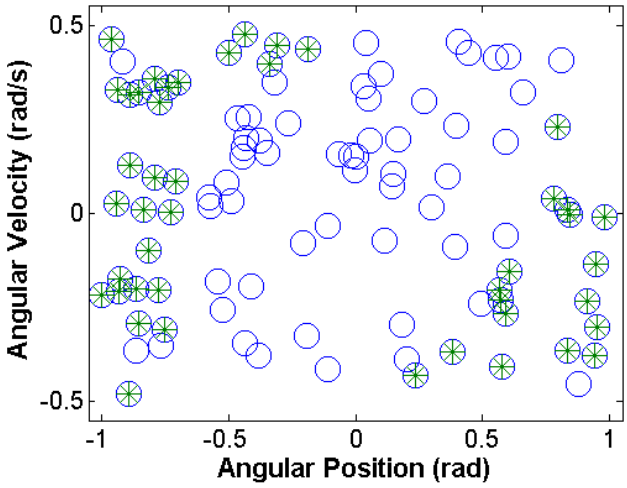

(a)

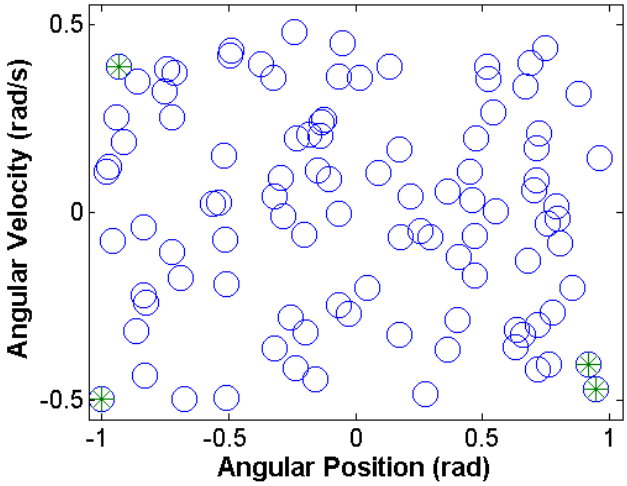

(b)

Figure 3.11: Simulation depicting pendulum's sensitivity to initial conditions. Various initial conditions of angular position and velocity for a modulation depth of 0.011 and a driving frequency of (a) 1.80 Hz and (b) 1.65 Hz. The blue open circles are the initial conditions, and the green asterisks represent the conditions where non-zero energy was present.

However, the interesting data occurs outside of the range shown in Fig 3.9. When the driving frequency decreases past this range, we notice the bistability occurs; the energy continues to increase until a sudden drop-off at $f = 1.65 \pm 0.05$ Hz. As demonstrated in Belyakov *et al.* [56], this pendulum has chaotic properties, and this sudden drop-off frequency is sensitive to initial conditions; this is clearly depicted in Fig. 3.11.

We ran a simulation at a specific driving frequency, where we had a program randomly generate one hundred different pairs of initial angular positions and angular speeds between -1 to 1 rad, and -0.5 to 0.5 rad/s, respectively. Using the equations of motion of the system, we were able to determine which pairs would result in a non-zero energy after 30 minutes. In both graphs, we see that the results are initial-condition-dependent; namely, if the pendulum does not have a certain position and momentum when the frequency parameter changes, the pendulum will not be able to parametrically oscillate. We also see that the further away the driving frequency is from the left edge of the contour plot in Fig. 3.9, the less likely the system will be driven to oscillate. When we look at Fig. 3.11a, which is for a modulation depth of 0.011 and a driving frequency of 1.80 Hz, we see that the system will most likely end up with a non-zero energy if it starts with a larger position or speed. However, if we compare this to Fig. 3.11b, which is for a modulation depth of 0.011 and a driving frequency of 1.65 Hz, we see that the system will not as likely end up with a non-zero energy, but needs to have a larger angular position and velocity for the pendulum to have a chance at being parametrically oscillated.

3.9 Discussion

In this section, I will discuss both the issues I have encountered during my parametrically driven pendulum experiments, what can be done to improve the experiments I have conducted, as well as the impact of my research.

3.9.1 Issues and Resolutions

Servo Motor Skips

The main issue encountered during the parametric oscillator experiment was the occasional skipping that occurred with the stepper motor while collecting data. I noticed that this seemed to occur more frequently when the system had been running for an extended period of time, such as during the bistability experiments. Unfortunately, the best resolution is to minimize this by letting the equipment rest. For example, although the easiest way to collect the steady-state data was to let the system run through all the parameters, it would be best to run through the driving frequencies for a specific modulation depth, let the system rest for 20-30 minutes, then move on to the next modulation depth. This also minimized the amount of times that power outages would interfere with our data collection.

Pendulum Slippage

The other issue I frequently encountered was the string of the pendulum slipping as the experiment was running, causing the pendulum length to change or, in the worst case scenario, the string to no longer be taut enough for the system to be driven. We found the optimal solution for this was to take a box cutter and create a nick in the wheel that the string was wrapped around, secure both ends of the string into the nick, and tape the string both to the nick and along the surface of the wheel that the string was wrapped around. Since this has been implemented, the string has not slipped, and the length of the pendulum has been maintained.

String and Eyelet Issues

A one-time-occurrence of the string fraying allowed us to upgrade our system (slightly). Initially, our eyelets were O-ring-like, and, although they did not interfere with our results, caused enough friction over time to cause the string to start to fray. Therefore, we switched out rubber eyelets to fishing eyelets, and the string to a braided fishing line to make the system more robust.

3.9.2 Improvement Opportunities

Currently, our pendulum stand is made out of wide pieces of wood; even though this results in a cheaper setup, the width of the wood, especially the top part holding the servo motor, spool, and eyelets as shown in Fig. 3.1, can occasionally interact with the motion of the pendulum at large angular amplitudes. To prevent this, which is especially crucial when observing chaos due to system sensitivities, a more robust system can be created with metal bars or pipes with a narrower width. The two pieces should also be bolted together, instead of securely clamped, as this can add unnecessary weight to the system.

In terms of furthering our understanding of the mechanical parametric oscillator, a robust exploration is described in Chapter 5.

3.9.3 Research Impact

A mechanical parametric oscillator is not just a fantastic tool to encourage students to explore complex systems; these systems are also intriguing for researchers, as they can undergo linear, non-linear, and chaotic behavior.

Butikov simulated two free-to-move identical masses connected by a rigid rod, which was attached to an elastic spiral spring [57]. By symmetrically and periodically moving the two masses, Butikov created a time-dependent moment of inertia which resulted in periodic motion. With this, he explored the boundaries of parametric motion, as well as examined resonances at various orders.

Belyakov *et al.* simulated a pendulum composed of a rigid rod with a mass periodically moving along the rod, essentially periodically varying the pendulum length [56], similar to our system. They used this system to explore the linear and chaotic motions of the system at various parameters. They noticed that, depending on the system parameters, the system can transition into chaos two different ways. The first is when the system undergoes a period-doubling cascade, or where the periodicity doubles at certain points [62] as the modulation depth increases. The second is when the system suddenly enters chaos.

As mentioned above in the two examples mechanical parametric oscillator research, most groups explore these systems computationally. We have presented, and will continue to pursue, the experimental equivalent, which could help strengthen the understanding of non-linearity in these systems.

3.10 Conclusion

We have described an experiment which exhibits parametric driving of a simple pendulum in a manner where theory and experiment are clearly interpreted. The fact that "the pendulum swings with large amplitude in one direction as a result of driving it in another dimension" is fascinating to first graders and physics graduate students alike. Moreover, a thorough understanding of this experiment provides a foundation for current research in quantum information and opto-mechanics where damped harmonic motion, Q, and parametric amplification are central. In addition, this experiment also demonstrates chaotic properties, allowing students to experimentally observe nonlinear dynamics.

Chapter 4

Group Presentations and Solution Robustness

The advancement of academia requires the constant questioning and answering of one phrase: "why?" Since humans are strongly curiosity-driven, we have a desire to pursue this type of questioning, starting with a young mindset. In academia, an individual's young mindset begins developing during their undergraduate studies, where a variety of subject matters are offered, starting with a set of detailed fundamentals classes. Unfortunately, in order for students to develop into distinguished scholars in a specific field, they must first create a solid base of fundamental knowledge within these classes, associated with remembering, understanding, and applying knowledge in Bloom's taxonomy [63]; otherwise, these students cannot successfully obtain mastery of the subject matter, which requires analyzing, evaluating, and creating knowledge [63].

As educators, one of our goals is developing our students into critical thinkers, which also lies with the higher orders in Bloom's taxonomy [63]. However, this is a time-consuming process, and we are unable to dedicate all of our time to every student; this is why active learning is beneficial for both involved parties. The requirement for students to successfully create a solid base of fundamental knowledge and advance to higher orders of knowledge is for them to actively learn; that is, to actively engage in their learning process. To demonstrate its importance, Franklin *et al.*

compared the knowledge retained by students through quizzes and exams in a traditional lecture-based class and an activity-based reformed class [64]. From the results, Franklin *et al.* concluded that the short-term knowledge gain was about the same in both class settings; however, the students in the lecture-based classes showed a rapid decay of this gain over the course of weeks, while the students in the reform-based classes retained this gain and saw an enhancement by subsequent instruction [64]. In addition, Kober *et al.* indicates that metacognition, which is "the mind's ability to monitor and control its own activities" [65], is an important component to student learning [65]. If a student consistently questions their understanding of concepts or methods while solving problems, or assess their knowledge, they will be able to more quickly see any errors and fix them accordingly [65].

One method of actively engaging students in their learning is having them work in small groups. In a large group environment, such as in a lecture hall, a few students tend to dominate the discussion, causing the majority of the remainder to either not pay attention or be confused. By assigning small groups, within which the abilities are either similar or slightly varied; this way, one member cannot do all the problems for the others, and the entire group benefits by communicating and working together. Through collaboration, students are able to retain knowledge better than a traditional lecture-format, as the method encourages active-learning [65]. This has also been viewed with elementary and junior high school students, where working in small groups have had "favorable effects on achievement and productivity, psychological health and self-esteem, intergroup attitudes, and attitudes towards learning" [66]. In addition, by students practicing communication skills with their peers, they will be able to communicate their ideas more effectively in their responses on exams.

The first semester of general physics (Physics 08) addresses classical mechanics, where the topics range from kinematics (motion) to energy conservation. Due to the large range, the course goals, teaching objectives, and learning outcomes are generalized, as presented in Appendix C.1. From the list of expectations, I chose to focus on two of the learning outcomes: "You should be able to demonstrate your expertise in this subject by utilizing the definitions, language, and mathematical tools (geometry, algebra, and calculus) to discuss classical mechanics problems verbally, in writing,

and mathematically," and "You should be able to analyze a written problem or observed phenomena, simplify it, identify the key known and unknown features, make predictions, and evaluate those predictions based on the principles of physics." Using these, I wanted to research if, and how, the problem-solving process for individuals would improve with presenting a robust solution to a problem in small groups.

4.1 The Student Body

The first semester of general physics (Physics 08) is intended for an undergraduate audience associated with physical sciences and engineering. To better understand my students, I administered an entrance survey on the first day of discussion, with three types of questions; student background, student intuition, and student expectations (pulled from the Maryland Physics Expectations Survey [67]), as presented in Appendix C.2. From the responses, I found the majority of my students were first- and second-years in the School of Natural Science or School of Engineering. Although the majority of the students had not taken physics previously, their math backgrounds were strong based on the classes they had taken, as well as their ability to recall and apply basic mathematical rules to a specific problem. The students hinted, through current post-graduation plans and study habits, that they were a motivated, or goal-oriented student body. They also indicated that they preferred studying in groups, and the majority were visual learners, though many were also kinesthetic learners.

The physics problems answered in the entrance survey showed that their physics intuition is weak, which aligns with their inexperience with physics classes. The responses were heavily associated with their "gut-feeling," which was backed up with neither conceptual nor mathematical logic. In addition, students have not been required to apply the knowledge from one subject to another in high school. This may have subconsciously caused them to categorize concepts obtained in mathematics separately from physics, which could partially result in underdeveloped intuition in physics. Their dissociation of mathematics and physics also appeared in their idea that the mathematics in physics were only associated with numbers, rather than thinking about the physical meaning behind them, as well as not fully realizing that

all the equations in physics are derivable.

4.2 The Presentations

The standard style used during discussion sections for Physics 08 utilizes group work centered around a worksheet created by the instructor of record. As shown in Appendix C.3, the teaching assistant spends a relatively short period of time reviewing the concepts covered in class, then has the students work at the white boards, followed up by a brief recap at the end to summarize the take-home messages. Although this type of group work helps students discuss and develop methods of solving physics problems, it does not demonstrate the importance of developing a robust problem solving process. This has been observed with past responses to long problems on physics exams, where students will often leave out key elements or not analyze whether their final answer is a realistic result.

In order to have students accustomed to assessing their solutions, I decided to expand on the rubric used for their homework notebooks and have students present a problem from their discussion worksheet. As shown in Appendix C.4, these homework notebooks are graded on a scale of 0 to 3 based on the robustness of the solution provided by the student, rather than the accuracy of the answer. The purpose of these homework notebooks is to get students in the habit of providing robust solutions while doing their homework, such that their responses to problems on the mid-term and final examinations earn them better scores; a robust solution will show how and why a problem was solved with a specific method. However, the students will not always work directly in these notebooks; instead, they choose to work the problems, see if they are correct, then will write the solution in their notebook. This creates a better-looking notebook, but eliminates the entire thought process that the student goes through, including their reasoning for how they obtained an incorrect numerical answer.

In order to encourage discussion among my students, I started to enforce presentations during the seventh week and arranged them groups of three. As shown in Appendix C.5, these groups were assigned one problem, and were given 40 minutes

to develop a robust solution and decide their roles during the presentation. One person was responsible for board work, which required them to model the problem and identify the question, then set up and work through the solution, whilst keeping everything organized and legible. The second student was required to describe and identify the concepts in the problem, explain the method used in the the solution, and assess the final answer. The third member moderated the presentation and answered all questions from the class after the solution was presented; each group in the audience was required to ask one question, which had to be answered with clear reasoning. Once the entire group had completed their presentation, all audience members graded their peers using the rubric shown in Appendix C.6. By following this process, I hypothesized that students would be learning the requirements for a solution to be classified as robust, which they would then apply to their homework notebooks and exams, resulting in an increase in their scores. In addition, these presentations addressed each type of learning style, as the presenters provided both a visual and oral solution to the problem, and the audience had the opportunity to take notes.

4.3 Results

After the group presentations were implemented for a couple of weeks, I had the students fill out a mid-semester survey as presented in Appendix C.7. This allowed me to see how their opinions in regards to the presentations, as well as their views about physics were changing through the Maryland Physics Expectations Survey. In addition, I monitored how their homework notebook scores were improving since the implementation, as well as comparing their average midterm scores to that of the class. The majority of the students had two main comments: they wanted to see more worked out examples, particularly of more advanced problems, and they were concerned that they were not getting the most out of these presentations. However, while monitoring their homework notebook scores, I noticed a significant improvement, which is visible with the larger increase in the average between October 13th and October 22nd in Fig. 4.1a, as well as the continuing increasing trend. The

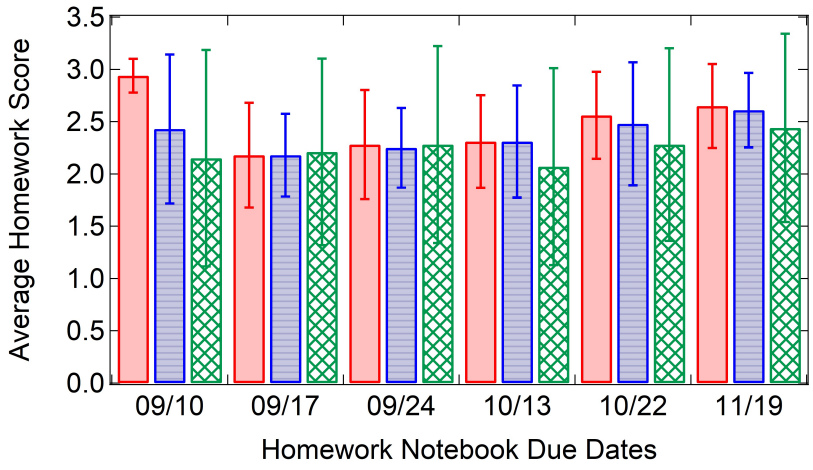

(a)

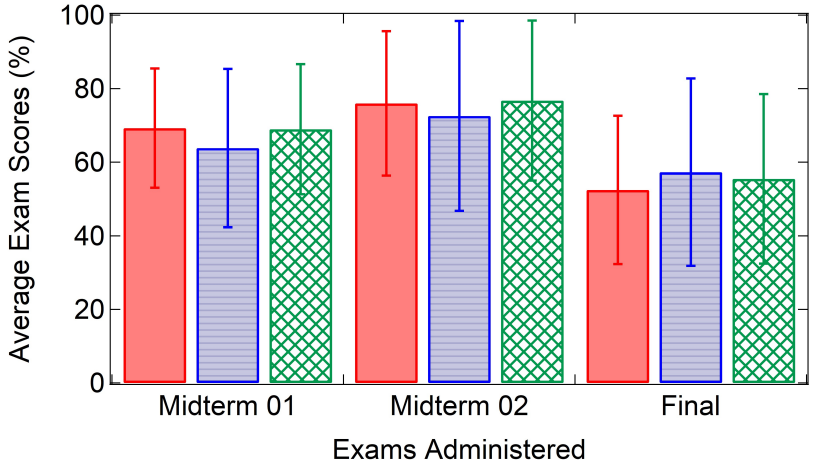

(b)

Figure 4.1: Score averages over the course of a semester. (a) Homework notebook averages from the class and two discussion sections, 23 and 24. These averages do not include the scores from the students who did not turn anything in, nor the first homework notebook score, as it was a homework set based on becoming familiar with Mastering Physics, the website through which the instructor assigned homework. (b) Exam averages from the entire class and discussion sections 23 and 24. These averages include scores from students who have informally dropped the class. In both graphs, the solid red bars are the average score for discussion section 23, the horizontally-lined blue bars are for discussion section 24, and the meshed green bars represent the averages of the entire class.

earlier dates do show an increase, which is likely a result of the students becoming familiar with the homework notebook methods and the feedback I had written, but after the presentations began, the students seemed to have understood more of what was required in a robust solution and had applied the method in their notebooks. Their scores were also higher than that of the class average, which also indicates that the presentations helped align their understanding of a robust solution to our expectations.

Although the homework notebook scores seemed to indicate that the robustness of the solutions were improving, through interacting with the various groups, I had also become wary of the initial method; when groups had completed their assigned problems, they were reluctant to continue with the worksheet, regardless of whether I instructed them to "get back on track". This is evident in Fig. 4.1, especially in Fig. 4.1b, where the class average was larger than the average from my discussion sections, and the amount the averages increased were similar. Therefore, when I conducted the presentations the second time, I modified the problem assignments; instead of assigning each group one problem, I had all groups get through as many of the problems from the beginning of the worksheet, and would let the groups know which problem they would present five minutes prior. This forced them to stay on task, and would optimize the amount of practice they had with the problems. Another difference was the time I dedicated at the beginning of class; initially, I would spend minimal time to quickly explain the concepts covered within the worksheet, but by showing them how to solve one problem from the worksheet in detail (or a separate problem, if the worksheet was on the shorter side), the solutions during the presentations also became more complete.

The change in problem assignment, as well as presenting a detailed example problem at the beginning of class, resulted in a noticeable change between the second midterm and the final exam. Both the average scores of the class and my two discussion sections decreased for the final as shown in Fig. 4.1b, which may be a result of a combination of the final based purely on the material covered from the second midterm, the quantity of material covered during this duration, the length of time the students had to process all the information, and the tragic incident that affected our

school. However, when comparing the change of scores, the amount the class average decreased is two percentage points lower than the average for discussion section 23, but six percentage points higher than the average for discussion section 24. In fact, the final average for section 24 was two percentage points higher than the class average. In addition, the presentation scores also increased, where the average score from the first set was 7.15 (out of 8 points possible) and the second set was 7.45, which indicated that requiring the students to do more problems did not take away from their ability to provide a robust solution. Both the exam and the homework notebook trends imply that the presentation method can enhance individual student learning and solution robustness when combined with the opportunity to practice problem solving in small groups. However, to fully confirm this, this should be implemented from the first day of classes and compared with those that have not embedded this into the discussion sections, to eliminate additional resistance that may have occurred from requiring this of students half-way into the semester.

4.4 Conclusions

In an introductory physics class, the most effective way for students to communicate their knowledge to others is by providing a robust solution to a problem. Although this requirement is built into the curriculum with their homework notebooks, many students usually do not do their homework problems directly in the notebooks, which takes away from the robustness, as students will not include any errors they make with or assessments of their methods. In order to provide students with more practice in developing robust solutions, discussion sections were broken up into groups of three, where students were given time to develop a response to and present physics problems. By having students present and assess one another through the use of rubrics, their homework notebook scores increased, demonstrating the possible effectiveness of this method. However, the exam scores did not portray this trend in the same way; although the average final exam score of my discussion sections did have less of a decrease than the class average, a decrease was still present. Therefore, in order to more accurately demonstrate the effectiveness of group presentations for robust

solutions from an individual, a comparison between the standard approach and this method must be conducted from the first discussion date.

Chapter 5

Conclusions and Future Direction

The main conclusions from my dissertation are summarized below:

- The stable trapping location of an optically trapped particle depends on the particle's size and the separation between fiber ends for a low refractive index contrast system.
- Oil droplets can stably trap, but were too small to observe stretching in our optical trap.
- Stem cells can stably trap and are large enough to observe stretching, but the shear modulus is too large to observe noticeable stretching within our system.
- The parametrically-driven pendulum acts linearly near threshold, and we observe peak energy to occur at the second harmonic frequency.
- A parametrically-driven pendulum driven in the non-linear regime has a peak energy as a lower frequency than the second harmonic frequency.
- The parametrically-driven pendulum undergoes bistability, which depends on the direction of the driving frequency scan. In addition, we observe sudden drop-offs which could indicate possible chaos, as whether the pendulum continues to oscillate or not as it enters a new driving frequency is dependent on initial conditions.

5.1 Future Exploration

One of the key areas of study in the Applied Photonics lab is the experimental applications of parametric amplification and oscillation. For example, we aim to parametrically excite processes within particles which are trapped in the dual-beam optical trap. We have been unable to do so thus far because of the large damping which is always present in our microfluidic dual-beam traps. Exploring the trapping and subsequent excitation of particles in air, or even in vacuum, is one exciting future direction.

In this chapter, I decided to explore another interesting direction, which is the experimental study of nonlinear dynamics in our parametrically driven pendulum. Through the effort, we will obtain a thorough experimental understanding of the range of nonlinear dynamical behavior we may observe in any parametrically-driven system.

One of the large goals within the Applied Optics lab is to combine the optical trapping experiment with the optical parametric oscillator. In order to do so, we need to further understand the nonlinearity of the parametrically oscillating pendulum and observe whether the system truly undergoes chaos.

A crucial difference between linear and nonlinear motion is whether that linear equations of motion obey the superposition principle, but not nonlinear equations [62]. We can understand this better by looking at a homogeneous, second order linear equation

$$a(t)\ddot{x}(t) + b(t)\dot{x}(t) + c(t)x(t) = 0 \tag{5.1}$$

where $x(t)$ is the unknown variable and $a(t)$, $b(t)$, and $c(t)$ are known and fixed variables. For equations where the superposition principle is applicable, if $x(t)$ is a solution of Eq. 5.1 and ζ is a constant, then $\zeta x(t)$ is also solution. In addition, if $x_1(t)$ and $x_2(t)$ are both solutions, then so are linear combinations of the two, such as $x_1(t) + x_2(t)$. We can easily see these rules do not apply to nonlinear equations by rewriting Eq. 5.1 as

$$a(t)\ddot{x}(t) + b(t)\dot{x}(t) + c(t)\sqrt{x(t)} = 0. \tag{5.2}$$

In addition, if we look at an inhomogeneous equation like

$$a(t)\ddot{x}(t) + b(t)\dot{x}(t) + c(t)x(t) = \frac{F(t)}{m} \tag{5.3}$$

for a linear equation, if $x_a(t)$ is a solution to the nth order inhomogeneous equation (here, $n = 2$), then all solutions are a linear combination of $x_a(t)$ and n independent solutions of the homogeneous equation. This does not apply for nonlinear expressions.

Our system models that of a simple pendulum, where we have a mass attached to a string. Although a true simple pendulum does not undergo chaos, our pendulum is damped and driven, which, depending on the parameters, can be a chaotic system [62]. For a system to be chaotic, it must fulfill two requirements: the system must be sensitive to initial conditions, as demonstrated by Henri Poincaré [68], and the behavior of the oscillations must be erratic, even after any transient behavior [62].

To test whether a system is chaotic, we can start our pendulum to oscillate at various angular amplitudes for a specific modulation depth and frequency in the range shown in Fig. 3.9, including areas near the boundary of the plot, such as $h = 0.025$ and $f = 1.85$ Hz, and record each angular position as a function of time; this will allow us to explore the bistability shown in Fig. 3.10 in more detail. Using this data in pairs of different initial conditions, we can graph the difference in angular position $\Delta\theta(t) = \theta_1(t) - \theta_2(t)$ over time, and observe the envelope of the graph, which should follow $|\Delta\theta(t)| \sim Ae^{\lambda t}$; here, A is a positive constant, and λ is the Liapunov constant. If λ is negative, then our system is not chaotic, as the system is attracted to a periodic oscillation. However, if λ is positive, then we have a chaotic system [62].

We can also examine whether a system is undergoing chaos through Poincaré sections. By plotting $\dot{\theta}(t)$ against $\theta(t)$ at a constant rate, we can observe the motion of the system in more detail for a specific frequency and modulation depth, which can allow us to assess whether or not the oscillation has some structure. If we are looking at a simple, linear pendulum, we would expect dots on the graph that formed a circle or ellipse due to its periodicity. However, a chaotic system would result in dots that do not have a clear structure, as shown in Fig. 5.1 [69].

When we accumulate multiple Poincaré sections for a range of a driving parameter,

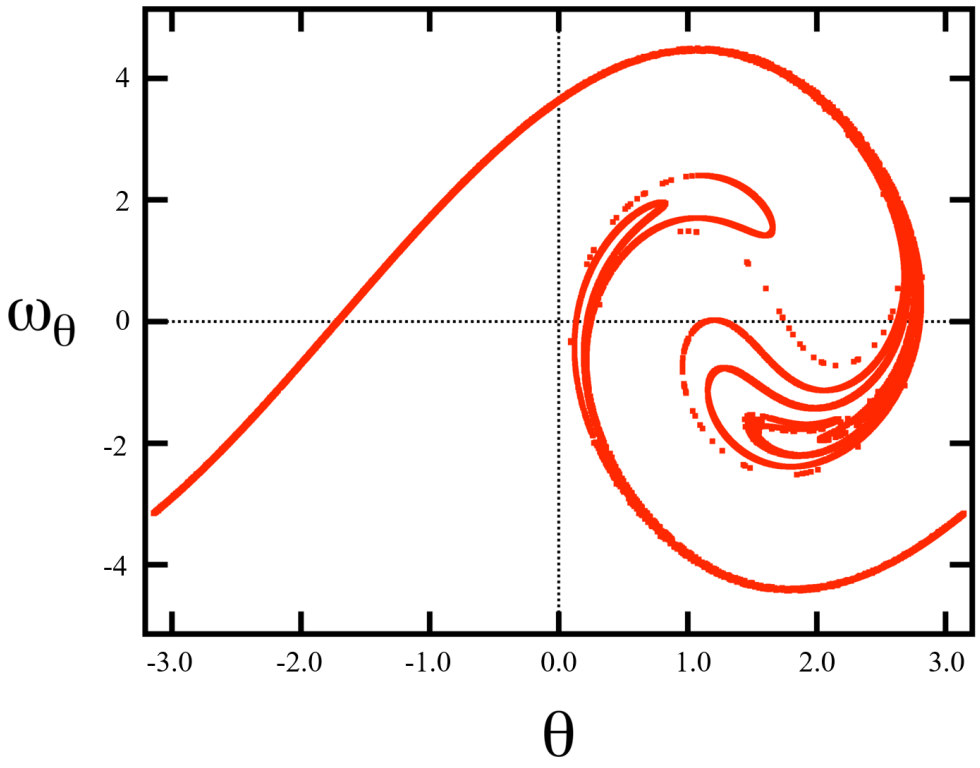

Figure 5.1: Sample Poincaré section for a pendulum undergoing chaos. A pendulum with a charge and mass in a changing electric field for a given driving amplitude results in a "strange attractor", which indicates chaotic motion [69].

we can project the data onto bifurcation diagrams, an example of which is shown in Fig. 5.2. When a system undergoes bifurcation, a stable equilibrium disappears and is replaced by two new equilibria; examples of these in Fig. 5.2 occur at diving amplitudes $A = 5.8$, 6.4, and 6.6. By simulating the steady state during a time frame where the transient behavior is not included over the range of the driving parameter with the same initial conditions for each simulation, we can better understand the nonlinear behavior of the pendulum. If the system is not chaotic, we are able to see distinct points at a given parameter, representing periodic motion; chaotic motion would result in multiple, indistinguishable dots, an example of which can seen in Fig. 5.2 when $7.7 < A < 8.2$.

The following list provides a more specific set of experimental instructions to

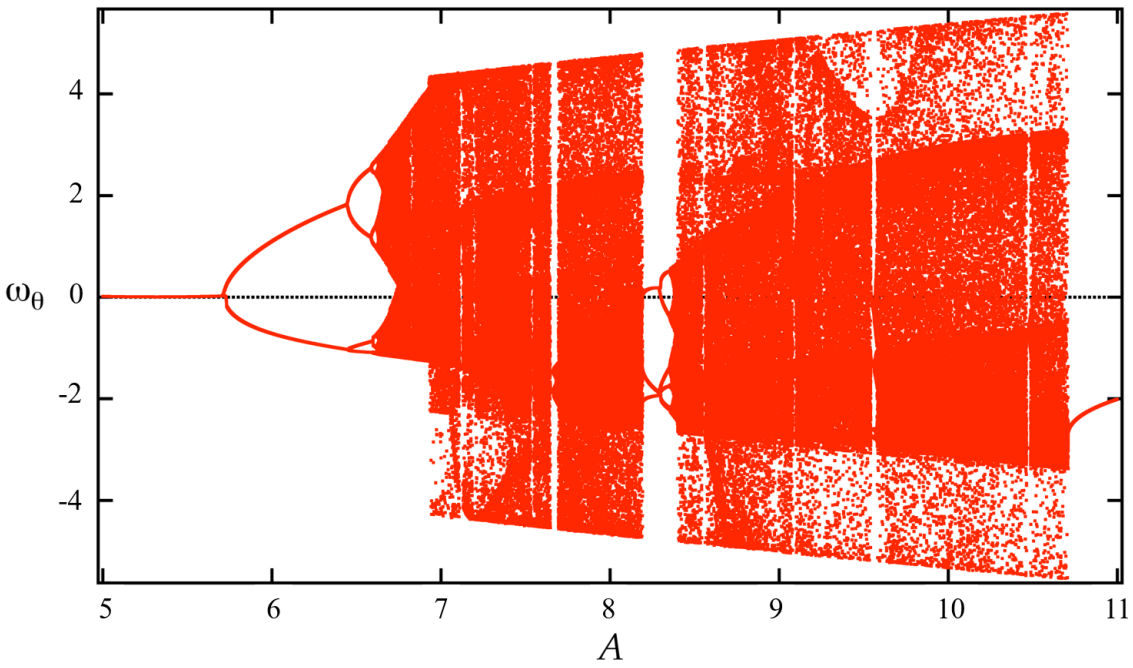

Figure 5.2: Sample bifurcation diagram for the motion of a pendulum undergoing chaos. Accumulating Poincaré sections for a pendulum with a charge and mass in a changing electric field can undergo both chaotic and non-chaotic motion [69].

better explore chaos with our parametric pendulum:

- **To explore the bistability in more detail**
  1. Use a camera, preferably with high-speed capability for better precision, to plot the pendulum's angular position as a function of time for various initial angular positions, angular speeds, modulation depths, and driving frequencies, especially on the left of the left edge of the contour plot shown in Fig. 3.9.
  2. Examine the plots in pairs, where the two have similar initial conditions, such as with the same initial position, modulation depth, and frequencies, but a slight difference in speeds.
  3. Plot the angular position *difference* as a function of time, and examine the envelope of the graph. Compare the envelope function to $e^{\lambda t}$, where λ is the Lyaponov exponent. If the exponent is positive, the system is

chaotic; otherwise it is either linear (if it decays to zero) or non-linear and non-chaotic.

- **For Poincaré sections**
  1. Use a camera, preferably with high-speed capability for better precision, to plot a phase-space diagram (the pendulum's angular speed as a function of angular position) at various modulation depths and driving frequencies for an extended period of time, so that transient behavior (oddities in the motion at the beginning) has died out and the pendulum undergoes several periods.
  2. On a separate phase-space diagram, plot the position and speed of the pendulum in period intervals after transient behavior has died out (T, $2T$, $3T$, etc.). Examine whether the graph (Poincaré section) has a clear structure, indicating non-chaotic motion, or is non-trivial and is seemingly unpredictable, implying chaos.
  3. To compare experimental results to simulations, start with parameters provided in Belyakov *et al.* [56].
- **For bifurcation diagrams**
  1. Compile multiple Poincaré sections for a range of modulation depths and driving frequencies.
  2. Plot either (a) the angular position against the modulation depths for a specific driving frequency or (b) the angular position as a function of driving frequency for a given modulation depth. Examine what portions of the bifurcation diagram has clear, distinct points (non-chaotic motion) and which parts contain multiple, indistinguishable dots (chaotic motion).
  3. To compare experimental results to simulations, start with parameters provided in Belyakov *et al.* [56].

By thoroughly understanding the properties of the mechanical parametric oscillator, we will have a stronger foundation to use to start implementing the optical parametric oscillator into the dual-beam optical trap experiment. In addition, we must explore how to trap with minimal damping, which is necessary in air, such that when the optical parametric oscillator is incorporated, the damping is still weak

enough to observe parametric oscillations with trapped particles.

Appendix A

Optical Trapping Codes

This portion of the appendix provides the MatLAB codes used with the dual-beam optical trapping experiment.

A.1 Pixel Sizes and Distances

The following code was used to determine the pixel separation between the fiber ends, as well as the size and position of the trapped particle. This was used in junction with mycursors.m, available for download through the File Exchange on MatLAB Central through MathWorks.

```
clear all
close all

imindex=0;
flist=dir('*.png');
[A B]=size(flist);
pct1=imread(flist(1).name);
figure(1);
imagesc(pct1);
bak=rgb2gray(pct1);
sep=3
```

```
lfibval=150;
rfibval=500;
lpart=300;
rpart=400;

for p=1:A


pct=imread(flist(p).name);
imagesc(pct);
FH=mycursors();
FH.off(1);
FH.add(lfibval);
FH.add(lpart);
FH.add(rpart);
FH.add(rfibval);
goodpic=(input('Picture OK? '));

lfibval=FH.val(1);
lpart=FH.val(2);
rpart=FH.val(3);
rfibval=FH.val(2);

if goodpic==1
    imindex=imindex+1;
    diams(imindex)= rpart-lpart;
    seps(imindex)=rfibval-lfibval;
    zoffp(imindex)=lpart-lfibval;
else
end
end

radii=diams/2;
```

```
zoff=zoffp+radii;
figure
plot(seps,radii,'o')

save('temp','seps','radii','zoff')
%save('temp','seps')
```

A.2 Trapping Efficiency Plots

The following MatLAB code was used to create trapping efficiency Q_z plots along the beam axis.

```
clear all
close all
r0=0.0625;
S=126.53125;

while r0<20.0625
   close all
   lam=.98;
   n1=1.335;
   n2=1.375;
   m=n2/n1;
   w0=2.1;
   rho=pi*n1*w0^2/lam;
   offst=0;

   zmid=S/2;
   s0=S/w0;
   normrad=r0/w0;

   zstart=r0-zmid;
   zfin=zmid-r0;
```

```
   dz=1;
   rstart=-1;
   rfin=1;
   dr=1;

   [zcoord,rcoord] = meshgrid(zstart:dz:zfin,rstart:dr:rfin);

   [rs,seps]=size(zcoord);

   for zctr=1:seps
       for rctr=1:rs
           zset=zcoord(rctr,zctr);
           z0=zmid+zset;
           dset=rcoord(rctr,zctr);
           if  rctr==1
               zset;
               dset;
           end
           Qzeff=quad2d(@(theta,phi) Qz(r0,theta,phi,z0,dset,n1,
w0,lam,n2,rho),0,thetamax(r0,dset,z0,n1,w0,lam),0,pi);
           if dset==0
               Qxeff=0;
           else
               Qxeff=-quad2d(@(theta,phi) Qx(r0,theta,phi,z0,dset,n1,
w0,lam,n2,rho),0,thetamax(r0,dset,z0,n1,w0,lam),0,pi);
           end
           qxmat(rctr,zctr)=Qxeff;
           qzmat(rctr,zctr)=Qzeff;
           z0=zmid-zset;
           dset=dset-offst;
           Qzeff=quad2d(@(theta,phi) Qz(r0,theta,phi,z0,dset,n1,
w0,lam,n2,rho),0,thetamax(r0,dset,z0,n1,w0,lam),0,pi);
           if dset==0
```

```
            Qxeff=0;
        else
            Qxeff=-quad2d(@(theta,phi) Qx(r0,theta,phi,z0,dset,n1,
w0,lam,n2,rho),0,thetamax(r0,dset,z0,n1,w0,lam),0,pi);
        end
        qxmat(rctr,zctr)=qxmat(rctr,zctr)+Qxeff;
        qzmat(rctr,zctr)=qzmat(rctr,zctr)-Qzeff;
    end
    %toc;
end

set(gca,'FontSize',16);
qzmatdisp=qzmat;
qxmatdisp=qxmat;


figure(1)
plot((zcoord(1,:)),qzmat(ceil(rs/2),:),'o')
xlabel('Longitudinal offset (um)');
ylabel('Axial trapping eff');

rval=-rfin;
zval=zstart;

for rr=1:rs
    zval=zstart;
    for cc=1:seps
        zcoord(rr,cc)=zval;
        rcoord(rr,cc)=rval;
        zval=zval+dz;
    end
    rval=rval+dr;
end
```

```
   saveas(gcf,['MPart' num2str(n2) '_Liquid' num2str(n1) '_Sep' num2str(S)
'_Rad' num2str(r0) '.fig'],'fig');
   eval(['print -djpeg Part' num2str(n2) '_Liquid' num2str(n1) '_Sep'
num2str(S) '_Rad' num2str(r0) '.jpeg']);

   r0=r0+0.0625;
   %S=S+5;
   keep r0 S


end
```

This code called three functions; Qz, thetamax, and Qx, shown below in black, blue, and red font, respectively.

```
function Q=Qz(r0,theta,phi,z0,d,n1,w0,lam,n2,rho)
%eparm;
zp=z0-r0*cos(theta);

Rc=zp.*(1+((pi*n1*w0^2)./(lam*zp)).^2);
rsq=d^2+(r0*sin(theta)).^2-2*d*r0*sin(theta).*cos(phi);

Rz=(Rc.^2-rsq).^0.5;

a=(d^2+(Rz+r0*cos(theta)).^2).^0.5;

gamma=acos((Rc.^2+a.^2-r0.^2)./(2.*a.*Rc));
gamma=real(gamma);

alphai=acos((d^2+(Rz+r0*cos(theta)).^2-r0^2-Rc.^2)./(2*r0.*Rc));
alphai=real(alphai);

alphat=asin((n1/n2)*sin(alphai));
```

```
alphat=real(alphat);

rp=-(sin(alphai-alphat)./sin(alphai+alphat));
rl=(tan(alphai-alphat)./tan(alphai+alphat));
RR=(rp.^2+rl.^2)/2;
if alphai==0
   RR=((n1-n2)/(n1+n2))^2;
end
TT=1-RR;

qs=1+RR.*cos(2*alphai)-TT.^2.*(cos(2*alphai-2*alphat)+RR.*cos(2*alphai))./
(1+RR.^2+2*RR.*cos(2*alphat));

qg=-RR.*sin(2*alphai)+TT.^2.*(sin(2*alphai-2*alphat)+RR.*sin(2*alphai))./
(1+RR.^2+2*RR.*cos(2*alphat));

wsq=w0^2*(1+(zp/rho).^2);

if d==0
    Q=(2/pi)*r0^2*sin(2*theta).*(exp(-2*rsq./wsq)./(wsq.*Rc)).*
(qs.*Rz-qg*r0.*sin(theta));
else
    Q=(2/pi)*r0^2*sin(2*theta).*(exp(-2*rsq./wsq)./(wsq.*Rc)).*
(qs.*Rz+qg./(tan(gamma)).*(Rz-(Rc.*(Rz+r0*cos(theta)))./
(a.*cos(gamma))));
end


function Q=thetamax(r0,d,z0,n1,w0,lam)
%eparm;
theta=0:0.001:pi/2;

zp=z0-r0*cos(theta);
Rc=zp.*(1+((pi*n1*w0^2)./(lam*zp)).^2);
```

```
rsq=(r0*sin(theta)).^2;
Rz=(Rc.^2-rsq).^0.5;

[garb minloc]=min(abs(d^2+(Rz+r0*cos(theta)).^2-r0^2-Rc.^2));

Q=1;



function Q=Qx(r0,theta,phi,z0,d,n1,w0,lam,n2,rho)
%eparm;
zp=z0-r0*cos(theta);

Rc=zp.*(1+((pi*n1*w0^2)./(lam*zp)).^2);
rsq=d^2+(r0*sin(theta)).^2-2*d*r0*sin(theta).*cos(phi);

Rz=(Rc.^2-rsq).^0.5;

a=(d^2+(Rz+r0*cos(theta)).^2).^0.5;

gamma=acos((Rc.^2+a.^2-r0.^2)./(2.*a.*Rc));
gamma=real(gamma);

alphai=acos((d^2+(Rz+r0*cos(theta)).^2-r0^2-Rc.^2)./(2*r0.*Rc));
alphai=real(alphai);

alphat=asin((n1/n2)*sin(alphai));
alphat=real(alphat);

rp=-(sin(alphai-alphat)./sin(alphai+alphat));
rl=(tan(alphai-alphat)./tan(alphai+alphat));
RR=(rp.^2+rl.^2)/2;
if alphai==0
   RR=((n1-n2)/(n1+n2))^2;
```

```
end
TT=1-RR;

qs=1+RR.*cos(2*alphai)-TT.^2.*(cos(2*alphai-2*alphat)+RR.*cos(2*alphai))./
(1+RR.^2+2*RR.*cos(2*alphat));

qg=-RR.*sin(2*alphai)+TT.^2.*(sin(2*alphai-2*alphat)+RR.*sin(2*alphai))./
(1+RR.^2+2*RR.*cos(2*alphat));

wsq=w0^2*(1+(zp/rho).^2);

if d==0
    Q=0;
else
    Q=(2/pi)*r0^2*sin(2*theta).*(exp(-2*rsq./wsq)./(wsq.*Rc)).*
(qs.*(r0.*sin(theta).*cos(phi)-d)+qg./(tan(gamma)).*((r0.*sin(theta).*
cos(phi))-d.*(1-Rc./(a.*cos(gamma)))));
end
```

A.3 Trapping Contour Plots

The following MatLAB code was used to create our contour plots depicting the stability of the dual-beam optical trap at its center along the beam axis.

```
clear all;
close all;
rads=0;
sepas=0;
radstart=0.5;
radstop=10.5;
drad=.5;
nrads=1+(radstop-radstart)/drad;
```

```
tic

sepastart=10;
sepastop=250;
dsepa=5;
nsepas=1+(sepastop-sepastart)/dsepa;

nrads

sparm=zeros(nrads,nsepas,2);
slpe=zeros(nrads,nsepas,1);

for r0=radstart:drad:radstop
    rads=rads+1;
    srads(rads)=r0;
    sepas=0;
    toc
    for S=sepastart:dsepa:sepastop
        if 2*r0<S-2
            sepas=sepas+1;
            savefile = 'Sandr0.mat';
            save(savefile, 'r0', 'S');
            StabilityStudy01;
            ssepss(sepas)=S;
            slpe(rads,sepas,1)=(qzmatdisp(2,3)-qzmatdisp(2,1))/dz;
        else
            sepas=sepas+1;
            ssepss(sepas)=S;
            slpe(rads,sepas,1)=0;
        end
    end
end
```

```
ZZ=size(slpe);
for j=1:ZZ(2)
    slpeinterp(:,j)=interp(slpe(:,j),10);
end

sradsinterp=interp(srads,10);

set(gca,'FontSize',16);

[C,h]=contour(ssepss,sradsinterp,slpeinterp);
set(h,'ShowText','on','TextStep',get(h,'LevelStep')*10)
xlabel('Separation (\mum)');
ylabel('Particle radius (\mum)');
xlim([0 sepastop])
ylim([0 radstop])
shading interp;
view([0 90]);

slpeinterpcalc=circshift(slpeinterp,1).*slpeinterp;

[slprows slpcols]=size(slpeinterpcalc);

sgnslpe=sign(slpeinterp);

clocctr=1;
for sr=1:slprows
    for sc=1:slpcols
        if slpeinterpcalc(sr,sc)<0
            cloc(1,clocctr)=sradsinterp(sr);
            cloc(2,clocctr)=ssepss(sc);
```

```
            clocctr=clocctr+1;
        end
    end
end
figure
set(gca,'FontSize',16);
plot(cloc(2,:),cloc(1,:),'o')
xlim([0 sepastop])
ylim([0 radstop])

xlabel('Separation (S)');
ylabel('Particle radius (r0)');

figure
set(gca,'FontSize',16);

surfc(ssepss,sradsinterp,sgnslpe);
xlim([0 sepastop])
ylim([0 radstop])
xlabel('Separation');
ylabel('Particle radius');
shading interp
view([0 90]);
```

This code, like that for the trapping efficiency plots, utilize Qz, thetamax, and Qx; however, the parameter file (eparm) is not commented out for this situation. This file is shown below.

```
lam=.98;
n1=1.335;
n2=1.375;
m=n2/n1;
load('Sandr0.mat');
w0=2.1;
```

```
rho=pi*n1*w0^2/lam;
offst=0;

zmid=S/2;
s0=S/w0;
normrad=r0/w0;

zstart=-1;
zfin=1;
dz=1;
rstart=-.1;
rfin=.1;
dr=.1;
```

Appendix B

Parametric Oscillator Codes

This portion of the appendix provides the Arduino and MatLAB codes used with the parametrically-driven pendulum experiment.

B.1 Driving the Pendulum

The following code was used with the Arduino microcontroller and open-source Arduino software to allow user inputs for both the servo motor angles (which is linearly proportional to the modulation depth) and driving frequencies for the pendulum, as well as record both the time and passage time for each setting.

```
#include <Servo.h>
#include <SD.h>
#include <SPI.h>

const int chipSelect = 10;

Servo myServo;
int servoPin=9;
int angle;
int angset=44;
```

```
const float pi=3.14;

const int sensePin = 8;
boolean isthere=false;

unsigned long sstime=6000000;
unsigned long looptime=0;

float freq0=1.90;
float freq=freq0;
float freqSpan=.10;
int freqPoints=10;
int freqInt=10000*freq;

boolean trigOn=false;
unsigned long startTime=0;
unsigned long stopTime=0;
unsigned long deltaTime=0;

void setup(){
  myServo.attach(servoPin);
  Serial.begin(9600);
  pinMode(sensePin, INPUT);
  Serial.print("Initializing SD card...");
  if (!SD.begin(chipSelect)) {
    Serial.println("Card failed, or not present");
      return;
  }
  Serial.println("card initialized.");
}
void loop(){
for (angset=10;angset<=10;angset=angset+2){
  for (freq=1.90;freq>=1.90;freq=freq-(freqSpan/freqPoints)) {
```

```
freqInt=10000*freq;
deltaTime=0;
String angpart=String(angset);
String freqpart=String(freqInt);
String fnameString=angpart+freqpart+".txt";
int str_len = fnameString.length() + 1;
char fname_array[str_len];
fnameString.toCharArray(fname_array, str_len);
Serial.print(freqpart);
Serial.print(",");
Serial.println(angpart);
looptime=millis();
while ((millis()-looptime)<sstime){

  angle=90-(angset/2)*(cos(2*pi*(freq)*millis()/1000));
  myServo.write(angle);

  isthere= !digitalRead(sensePin);
  if ((trigOn==false) && (isthere==true)){
  startTime=millis();
  trigOn=true;
  }

  if ((trigOn==true) && (isthere==false)){
  stopTime=millis();
  deltaTime=stopTime-startTime;
  trigOn=false;
  File dataFile = SD.open(fname_array, FILE_WRITE);

  if (dataFile) {
    dataFile.print(stopTime);
    dataFile.print(", ");
    dataFile.print(deltaTime);
```

```
    dataFile.println();
    dataFile.close();
  }
    else {
    Serial.println("error opening datalog.txt");
  }
  }
  }
if(deltaTime>0){
  delay(300000);
}
  }
}

myServo.write(90);
while(1); }
```

B.2 Oscillator Contour Plots

The following code was modified from a version developed by Jake Pate, and was used to create the steady-state energy contour plots as a function of modulation depth and driving frequency.

```
function [M] = plotter3D(ext_in,save_fig,savename,makeflist)
% This function (script) receives filenames as an input and plots the
% corresponding heatmap. The script (function) will take a series of files
% and plot them all to create a 3D plot or heatmap.
%% Initialize Parameters (uncomment for script mode)
%clearvars
%ext_in='TXT';
%savename='parametric_graph';
%save_fig=0;
%
```

```
switch nargin
    case 1
        save_fig='nosave';
        savename='parametric_graph';
        makeflist=0;
    case 2
        savename='parametric_graph';
        makeflist=0;
    case 3
        makeflist=0;
end

if ischar(ext_in)
else
    ext_in=char(ext_in);
end
d_units=25.4/1000; %Gives diameter of 1 inch in meters.
[~,listing]=f_search(ext_in);
[r,~]=size(listing);
listing=natsortfiles(listing);
figure
hold on
%r=1; %Uncomment for fast debugging
a_ind=1;
f_ind=1;
for i=1:r
    strname=strfind(listing{i},'.');
    A=dlmread(listing{i},',');
    y=A(:,1); % Time duration
    passtime=A(:,2); %Time ball blocked laser signal
    angamp(i)=[str2double(listing{i}(1:2))]; %Angular Amplitude
    freq(i)=[str2double(listing{i}(3:strname-1))]/1E4; %Frequency
    %Need to get correct velocity by changing units
```

```
    %
    z(1,i)={d_units./(mean(passtime(end-10:end))/1000)}; %Velocity
end
%
% SORT FILES FIRST, THEN READ THEM IN AND POPULATE APPROPRIATELY
funi=unique(freq); %Non-repeating frequencies
anguni=unique(angamp); %Non-repeating angular amplitudes
freqsize=length(funi);
angampsize=length(anguni);
M=zeros(angampsize,freqsize); %Matrix is row times column, so
% angampsize is row (ycolumn) and freqsize is column (x column).
%Create new loop that matches the filename string with the
%appropriate index in funi and anguni, then use that placeholder
%as the new index in M
% F=figure;
for k=1:r
    [~,cang]=find(angamp(k)==anguni); %Gives y coordinate for matrix
    [~,cfreq]=find(freq(k)==funi); %Gives x coordinate for matrix
    %Populate matrix that has been filled with zeros, essentially a poor
    %man's scatter plot.
    M(cang,cfreq)=z{k}.^2; %Since we are indexing through z again with k
    % the same size as i, the mapping should work the same.
end
% shading interp
%
%% Get Files needed to fill plot
%
if makeflist
    [rf,cf]=find(M==0);
    for p=1:length(rf)
        fneed(p)={[num2str(anguni(rf(p))),num2str(funi(cf(p))*1E4),'.txt']};
    end
    fneed=sort(fneed.');
```

```
    fid=fopen(['/Users/Jake/Documents/MATLAB/Jay_research/Files Needed/',
...'Filesneeded.txt'],'w');
    fprintf(fid,'%s\n',fneed{:});
    fclose(fid);
else
end
%
%% Plotting
%NOTE: surfc does not seem to want any repeating elements, so I'm using
%the unique() function, thankfully the file sorting above takes care of
%properly sorting the amplitudes and frequencies so that the unique
%function does not mess up the order (as it groups in numerical order).
%
% If I wanted to make sure it plots points appropriately (should be
% scattered), I could put it in a loop and update the surfc graph for
% each interation.
%s=surfc(funi,anguni',M); %For shaded
mrat=anguni*0.234/274;
%s=contour(funi,anguni',M,40); %For lines
YPT=[0.01:0.1:2.51];
mrat=[2*mrat(1)-mrat(2),mrat];
zline=zeros(1,freqsize);
M=[zline;M];
s=contour(funi,mrat',M,YPT); %For lines
%figure
set(gca,'FontSize',15,'box','on'); %For fontsize
view(2)
%shading interp %For shaded
colormap(jet);
h=colorbar('FontSize',15);
hold off
grid off
xlabel('Frequency (Hz)','FontWeight','bold','FontSize',15)
```

```
ylabel('Modulation Depth','FontWeight','bold','FontSize',15,
'Interpreter','tex')
axis([1.80,1.95,0,0.05])
ylabel(h, '2E/m [J/kg]','FontWeight','bold','FontSize',15,
'Interpreter','tex')

if strcmpi(save_fig,'save')
    print(savename,'-djpeg');
end
end
```

Within this code, f_search.m and natsortfiles.m were called in, the latter of which also calls in natsort.m. The first of these three scripts is shown below; natsortfile.m and natsort.m are both available for download through the File Exchange on MatLAB Central through MathWorks.

```
function [ ext_out, output_args] = f_search(ext_in)
%% File Search Tool Searches for files based upon specific extensions
%   Function returns filenames of various extensions as arrays.


i=0;
j=0;
l=0;
%% Grab the Images
    ls
    mylist=dir;

    [r,c]=size(mylist);
    %Create for loop to grab all the special files

    for i=3:r
        files(i,1)={mylist(i).name};
    end
```

```
    if nargin==0;
        ext_in=input('\n\n What type of file do you want to grab?
Ex: type .tiff: ','s');
    end
    % exp_tiff=('.tiff\W*');
    % exp_txt=('.txt\W*');
    % exp_csv=('.csv\W*');
    exp_other=([ext_in,'\W*']);
    ext_out=ext_in;
    file_ext=regexpi(files,exp_other,'match');

    %Note this works isequal(tiffs{1},{})
    %Determines which elements of the cell are empty and gets rid of them
    s_result=ones(r,1); %Pre-allocate memory

    for q=1:r
        s_result(q,1)=isequal(file_ext{q},{}); %1 if empty, 0 if false (good)
    end

    list_ind=find(s_result==0); %Get indices of files that threw a 0
    listing=files(list_ind);
    listing(strncmp('.',listing,1)==1)=[]; %Does the same thing as what
%is below, but easier to understand.
    output_args=listing;
end
```

Appendix C

Supplemental Assessment Documents

This portion of the appendix provides a sample selection of the documents created and used during my research project with the Assessment in Pedagogy and Planning Group and the Instructional Internship Program through the Center for Engaged Teaching and Learning.

C.1 Expectations

The course goals with the respective teaching objectives and learning outcomes for Physics 08 are as follows:

1. Learn the basic principles and mathematical tools of Newtonian mechanics.
    (a) We will present the definitions, language, and mathematical tools of classical mechanics through examples, demonstrations, and discussions of physical phenomena.
        i. You should be able to demonstrate your expertise in this subject by utilizing the definitions, language, and mathematical tools (geometry, algebra, and calculus) to discuss classical mechanics problems verbally, in writing, and mathematically.
        ii. You will most likely discover some misconceptions you have about

the physical world and will be able to reconcile them with a correct understanding in classical mechanics.

2. Learn applications of physics to real-world problems.
   (a) We will demonstrate the processes physicists use to solve problems, and coach you in applying those processes to solve problems in classical mechanics.
      i. You should be able to analyze a written problem or observed phenomena, simplify it, identify the key known and unknown features, make predictions, and evaluate those predictions based on the principles of physics.
3. Develop the problem-solving perseverance required to succeed in the physical sciences and engineering.
   (a) We will reinforce the tools, methods, and material throughout the semester to prepare you for the second course in the series -Physics 009- and beyond.
      i. By learning the basic techniques of problem solving and conscientiously expressing physical problems mathematically you will be well-prepared to study more advanced topics in physics.
4. Connect textbook and lecture material to contemporary research topics.
   (a) We will share our enthusiasm for physics -especially topics in classical mechanics- by connecting course material with realworld problems, demonstrations, and ongoing research.
      i. At the level of an introductory physics student, you will practice analyzing physical phenomena and reading research.
      ii. Your interest in and appreciation for physics will hopefully increase throughout the course, regardless of your major.

C.2 Entrance Survey

The entrance survey that was administered on the first day of discussion.

Entrance Survey

NOTE: *This survey will NOT be graded. Please answer each question to the best of your ability.*

Name: _____

For the following, please indicate:

1. What is your school and major?
   - ☐ Engineering ☐ Undeclared
   - ☐ SNS
   - ☐ SSHA Major: _____
2. What class year are you?
   - ☐ First year ☐ Third year
   - ☐ Second year ☐ Fourth year (or higher)
3. What is the last math class you completed?
   - ☐ Trigonometry ☐ Calculus I
   - ☐ Pre-Calculus ☐ Other: _____
4. What is your enjoyment level of math?
   - ☐ Love ☐ Dislike
   - ☐ Like ☐ Hate
5. Have you taken physics before?
   - ☐ Yes If yes, how long ago? _____
   - ☐ No
6. What are your future plans after graduation?
   - ☐ Graduate school ☐ Other: _____
   - ☐ Work
7. What kind of classroom experiences help you learn best?
   - ☐ Auditory (ex. listening to lecture or communication with other students)
   - ☐ Visual (ex. seeing problems written down or reading)
   - ☐ Kinesthetic (ex. taking notes or doing experiments)
8. How do you prefer to work?
   - ☐ Individually ☐ In groups
9. What does "physics" mean?

10. What part of this class you are most excited AND most nervous about?

11. Rate your opinion about each statement, where 1 = strongly disagree and 5 = strongly agree. [1]

"Problem solving" in physics basically means matching problems with facts or equations and then substituting values to get a number.	1	2	3	4	5
In this course, I do not expect to understand equations in an intuitive sense; they must just be taken as givens.	1	2	3	4	5
Learning physics is a matter of acquiring knowledge that is specifically located in the laws, principles, and equations given in class and/or in the textbook	1	2	3	4	5
When I solve problems I usually look for numbers in a problem and then search for the equation that will give me the right answer	1	2	3	4	5
If I don't remember a particular equation needed for a problem in an exam there's nothing much I can do (legally!) to come up with it.	1	2	3	4	5
The most crucial thing in solving a physics problem is finding the right equation to use.	1	2	3	4	5
Knowledge in physics consists of many pieces of information each of which applies primarily to a specific situation	1	2	3	4	5
"Understanding" physics basically means being able to recall something you have read or been shown.	1	2	3	4	5
A significant problem in this course is being able to memorize all the information I need to know.	1	2	3	4	5
If I came up with two different approaches to a problem and they gave different answers, I would not worry about it; I would just choose the answer that seemed most reasonable. (Assume the answer is not in the back of the book.)	1	2	3	4	5
Only very few specially qualified people are capable of really understanding physics.	1	2	3	4	5
I use the mistakes I make on homework and on exam problems as clues to what I need to do to understand the material better.	1	2	3	4	5

[1] Taken from the Maryland Physics Expectations Survey

12. Using the triangle below, define sine, cosine, and tangent.

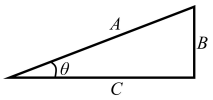

☐ $\sin\theta = {}^{B}/_{A}$, $\cos\theta = {}^{C}/_{A}$, $\tan\theta = {}^{B}/_{C}$

☐ $\sin\theta = {}^{A}/_{C}$, $\cos\theta = {}^{B}/_{C}$, $\tan\theta = {}^{A}/_{B}$

☐ $\sin\theta = {}^{A}/_{B}$, $\cos\theta = {}^{A}/_{C}$, $\tan\theta = {}^{C}/_{B}$

13. How would you find the derivative and integral of a function on a graph?
    - ☐ The derivative is the slope, the integral is where is crosses the y-axis
    - ☐ The derivative is where is crosses the x-axis, the integral is the area
    - ☐ The derivative is the area, the integral is the slope
    - ☐ The derivative is the slope, the integral is the area
14. What is the difference between "speed" and "velocity"?
    - ☐ They are interchangeable
    - ☐ Speed is a vector, velocity is a number
    - ☐ Velocity is a number, speed is a scalar
15. What is negative acceleration?
    - ☐ Something that causes an object to slow down
    - ☐ Something that causes an object to slow down or speed up, depending on the object's motion
    - ☐ Something that causes an object to speed up
16. If a fly collides into a car's windshield, which experiences a greater force?
    - ☐ The fly
    - ☐ The car
    - ☐ The same

C.3 Sample Pre-Presentation Lesson Plan

A lesson plan used during the third week of classes, before the presentations were implemented.

Weekly Teaching Outline, 2015.09.17

PRIOR LEARNING

Related Required Reading:

From *Physics for Scientists and Engineers: A Strategic Approach with Modern Physics* (textbook), Part I: Newton's Laws → Chapter 2: Kinematics in One Dimension and Chapter 3: Vectors and Coordinate Systems.

Worksheet for today (Discussion #3)

Related Lecture Material:

From lecture: Position and velocity vectors, acceleration vectors, uniform motion, motion diagrams with graphs, instantaneous velocity, constant acceleration and free fall, vectors and coordinate systems.

From lab: Kinematics Lab I

TEACHING GOALS

Intended Outcomes for the Class Meeting:

At the end of this lesson, my students will be able to

1. Accurately interpret and draw position, velocity, and acceleration graphs for common situations and explain their reasoning.
2. Become familiar with taking simple integrals and derivatives.

Related Student Assessment:

During the time the students work in groups, I will walk around to listen in on the dialog, ask for questions from students, and test their understanding using Socratic questioning (regardless whether the answer was correct or incorrect). During the first half of the review, I will have the students summarize the relationships among the three key terms. During the second half, I will have them present their conclusions and summarize it on the white board while addressing any misconceptions, such that they have a source they can refer back to at any point.

Related Course Learning Outcomes:

1. You should be able to demonstrate your expertise in this subject by utilizing the definitions, language, and mathematical tools (geometry, algebra, and calculus) to discuss classical mechanics problems verbally, in writing, and mathematically.

2. You should be able to analyze a written problem or observed phenomena, simplify it, identify the key known and unknown features, make predictions, and evaluate those predictions based on the principles of physics.
3. At the level of an introductory physics student, you will practice analyzing physical phenomena and reading research.

LESSON PLAN

5 min: Collect HWNB; explain how to use the PHET program *Moving Man*.
15 min: Allow students to become familiar with the program by playing and inputting numbers of their choice.
60 min: Students working in pairs on worksheet.
10 min: Quick review of observed relationship between position, velocity, and acceleration.
15 min: Students work on calculus worksheet in groups.

C.4 Homework Notebook Rubric

The rubric (developed by Dr. Carrie Menke) provided to the students on how their homework notebooks are graded. The examples for each score have been removed.

Physics Homework Notebook

The homework notebook trains (1) trains you to use a robust problem-solving process, (2) trains you to write up your problems legibly while doing the problem–good for maximum partial credit on exams–and (3) creates a powerful study guide for you to use in this course and beyond. MasteringPhysics just scores your answer.

Students that spend the time writing up their homework legibly (as they work on it), explaining their reasoning, and working through each step of the problem-solving process typically earn higher scores on exams and in the course. Why? Because it helps them learn the material.

Requirements:

1. **Notebook**: The homework must be **bound** and **completely separate from notes and any other course material**. (Using completely separate sections of a multi-subject notebook or 3-ring binder for notes and homework is OK.)
2. **Writing up**: use a robust problem-solving strategy to solve the homework problems.

Table C.1: **Problem-Solving Strategies:** See specific course texts for more detail.

Knight, Chapter 1	Wolfson, Chapter 1	Polya's: How to Solve It
1. Model	1. Interpret	1. Understand the problem
2. Visualize	2. Develop	2. Plan a solution
3. Solve	3. Evaluate	3. Carry out your plan
4. Assess	4. Assess	4. Examine the solution

Recommended:

- **Formatting**:
  - Fold each sheet long-ways, solve the problem on the left-hand side, and *explain the physical reasoning* on the right-hand side.
  - Use arrows, stars, or other ways to *highlight physical reasoning* within the solution.
- **Include Feedback**: Write corrections, hints, and helpful notes after entering your answers into MP. By doing this, you'll see if you make the same mistake over and over; then you can correct it once and for all.

- **Timing**: Write up your work in your homework notebook *while* doing your homework! Legibility is important, but this is not a beauty contest!

Table C.2: **Grading:** Only ***one*** problem from the homework set will be checked.

Score	**Rating**	**Description of Work**
0	Failing	Student did not turn notebook in or soln. copied from a soln. manual.
0.1	Failing	Student did not do the problem, but turned the notebook in.
1	Poor	Student put pencil to paper, but incomplete or only bare-bones solution.
2	Passing	Student solved the problem, but did not use a robust problem-solving method.
2.5	Very Good	Student used a robust problem-solving method, but the work would not make a useful study guide.
3	Excellent	Student used a robust problem-solving method used *and* the work would be a useful study guide.

C.5 Sample Presentation Lesson Plan

A lesson plan used during the eighth week of classes, after the presentations were implemented.

Weekly Teaching Outline, 2015.10.22

PRIOR LEARNING

Related Required Reading:

From *Physics for Scientists and Engineers: A Strategic Approach with Modern Physics* (textbook), Part I: Newton's Laws → Chapter 5: Force and Motion, Chapter 6: Dynamics I: Motion Along a Line, and Chapter 7: Newton's Third Law; Part II: Conservation Laws → Chapter 11: Work.

Related Lecture Material:

From lecture: Newton's Laws and Work

From lab: Dynamics

TEACHING GOALS

Intended Outcomes for the Class Meeting:

At the end of this lesson, my students will be able to

1. Use free body diagrams to visualize the relationship between forces and motion (displacement).
2. Calculate the work done by each force (not dependent on displacement) in the free body diagram described above.

Related Student Assessment:

The students now understand the importance to work efficiently to be able to develop a robust solution in a short time frame; by using this, they can discuss what potential questions may arise with any problem associated with work. From the Q & A sessions, I will be able to find what types of questions groups have difficulty answering, and address them during the recap portion of the discussion session.

Related Course Learning Outcomes:

1. You should be able to demonstrate your expertise in this subject by utilizing the definitions, language, and mathematical tools (geometry, algebra, and calculus) to discuss classical mechanics problems verbally, in writing, and mathematically.
2. You should be able to analyze a written problem or observed phenomena, simplify it, identify the key known and unknown features, make predictions, and evaluate those predictions based on the principles of physics.

3. At the level of an introductory physics student, you will practice analyzing physical phenomena and reading research.

LESSON PLAN

15 min: Describe the general method for determining work with free body diagrams through an example; assign groups and problems.
40 min: Have students determine roles, develop a detailed solution.
20 min: Presentation of a problem by the first group.
5 min: Q & A session for the first group.
20 min: Presentation of another problem by the second group.
5 min: Q & A session for the second group.
5 min: Recap with misconceptions.

C.6 Presentation Rubric

The presentation rubric is shown below. Each group member was given a separate role and graded.

Scribe

Point Details	Points Possible
Modeling	1 for picture of problem 1 for clarity and additional visualization
Identification	1 for knowns and unknowns
Setup	1 for starting equation(s) 1 for filling in equation(s) with specifics
Solution	1 for majority of work shown 1 for final solution with significant figures, units
Organization	1 for legibility and organization
TOTAL	8

Orator

Point Details	Points Possible
Problem	1 for summary of system and identifying main question(s)
Concept	1 for identifying physical principles 1 for using key vocabulary
Reasoning	1 for explaining equation choice 1 for explaining diagram
Solution	1 for explaining work progression 1 for assessment of final answer
Communication	1 for clarity and flow
TOTAL	8

Moderator/Interviewee

Point Details	**Points Possible**
Moderating	1 for introducing group 1 for keeping track of time 1 for opening up for questions 1 for concluding presentation
Q & A	1 for addressing/summarizing question 1 for answering question 1 for reasoning 1 for clarity
TOTAL	8

C.7 Mid-semester Survey

The mid-semester survey administered to my students during the ninth week of the semester.

Mid-Semester Survey

NOTE: *This survey will NOT be graded, nor will your grade be affected by your answers. Please answer each question truthfully, and to the best of your ability. Doing so will help you AND your classmates.*

Name: _____

1. On average, how many hours do you spend studying physics *outside* of class?

2. What aspects of the course have you found most affirming or helpful to your learning?

3. What aspects of the course have you found potentially puzzling or confusing?

4. What surprised you most, so far, about your learning experiences in this course?

5. What aspects of the course do you enjoy?

6. What aspects of the course would you like to see changed?

7. What constructive criticism do you have for the instructor?

8. What constructive criticism do you have for your TA?

9. Rate your opinion about each statement, where 1 = strongly disagree and 5 = strongly agree. [2]

"Problem solving" in physics basically means matching problems with facts or equations and then substituting values to get a number.	1	2	3	4	5
My grade in this course is primarily determined by how familiar I am with the material. Insight or creativity has little to do with it.	1	2	3	4	5
If I don't remember a particular equation needed for a problem in an exam there's nothing much I can do (legally!) to come up with it.	1	2	3	4	5
The best way for me to learn physics is by solving many problems rather than by carefully analyzing a few in detail.	1	2	3	4	5
I read the text in detail and work through many of the examples given there.	1	2	3	4	5
"Understanding" physics basically means being able to recall something you have read or been shown.	1	2	3	4	5
Learning physics made me change some of my ideas about how the physical world works.	1	2	3	4	5
Learning physics is a matter of acquiring knowledge that is specifically located in the laws, principles, and equations given in class and/or in the textbook	1	2	3	4	5
I go over my class notes carefully to prepare for tests in this course.	1	2	3	4	5
All I need to do to understand most of the basic ideas in this course is just read the text, work most of the problems, and/or pay close attention in class.	1	2	3	4	5
The main skill I get out of this course is learning how to solve physics problems.	1	2	3	4	5
In this course, I do not expect to understand equations in an intuitive sense; they must just be taken as givens.	1	2	3	4	5
Spending a lot of time (half an hour or more) working on a problem is a waste of time. If I don't make progress quickly, I'd be better off asking someone who knows more than I do.	1	2	3	4	5

[2] Taken from the Maryland Physics Expectations Survey

Bibliography

[1] A. Ashkin. Acceleration and trapping of particle by radiation pressure. *Phys. Rev. Lett.*, 24(4):156–159, 1970.

[2] D. V. Petrov. Raman spectroscopy of optically trapped particles. *J. Opt. A: Pure Appl. Opt.*, 9(8):S139–S156, 2007.

[3] D. Petrov. Raman spectroscopy of optically trapped particles. *J. Opt. A: Pure Appl. Opt.*, 9(8):S139–S156, 2007.

[4] T. M. Piñón, A. R. Castelli, L. S. Hirst, and J. E. Sharping. Fiber-optic trap-on-a-chip platform for probing low refractive index contrast biomaterials. *Appl. Opt.*, 52(11):2340–2345, 2013.

[5] K. C. Neuman and S. M. Block. Optical trapping. *Rev. Sci. Instrum.*, 75(9):2787–2809, 2004.

[6] M. Faraday. Xvii. on a peculiar class of acoustial figures; and on certain forms assumed by groups of particles upon vibrating elastic surfaces. *Phil. Trans. R. Soc. Lond.*, 121:299–340, 1831.

[7] L. Kiani, T. Lu, and J. E. Sharping. Comparison of amplitude noise of a fiber-optical parametric oscillator and a supercontinuum source. *J. Opt. Soc. Am. B.*, 31(8):1986–1990, 2014.

[8] W. B. Case. The pumping of a swing from the standing position. *Am. J. Phys.*, 64(3):215–220, 1996.

[9] J. Jass, S. Schedin, E. Fällman, J. Ohlsson, U. J. Nilsson, B. E. Uhlin, and O. Axner. Physical properties of *Escherichia coli* P Pili measured by optical tweezers. *Biophys. J.*, 87(6):4271–4283, 2004.

[10] K. Gibble and S. Chu. Laser-cooled Cs frequency standard and a measurement of the frequency shift due to ultracold collision. *Phys. Rev. Lett.*, 70(12):1771–1774, 1993.

[11] M. E. Solmaz, R. Biswas, S. Sankhagowit, J. R. Thompson, C. A. Mejia, N. Malmstadt, and M. L. Povinelli. Optical stretching of giant unilamellar vesicles with an integrated dual-beam optical trap. *Biomed. Opt. Express*, 3(10):2419–2427, 2012.

[12] S. Sankhagowit, S. H. Wu, R. Biswas, C. T. Riche, M. L. Povinelli, and N. Malmstadt. The dynamics of giant unilamellar vesicle oxidation probed by morphological transitions. *Biochim. Biophys. Acta*, 1838(10):2615–2624, 2014.

[13] J. Guck, R. Ananthakrishnan, H. Mahmood, T. J. Moon, C. C. Cunningham, and J. Käs. The optical stretcher: a novel laser tool to micromanipulate cells. *Biophys. J.*, 81(2):767–784, 2001.

[14] J. Guck, R. Ananthakrishnan, T. J. Moon, C. C. Cunningham, and J. Käs. Optical deformability of soft biological dielectrics. *Phys. Rev. Lett.*, 84(23):5451–5454, 2000.

[15] P. B. Bareil, Y. Sheng, Y. Chen, and A. Chiou. Calculation of spherical red blood cell deformation in a dual-beam optical stretcher. *Opt. Express*, 15(24):16029–16034, 2007.

[16] E. A. Evans. New membrane concept applied to the analysis of fluid shear-and micropipette-deformed red blood cells. *Biophys. J.*, 13(9):941–954, 1973.

[17] E. Sidick, S. D. Collins, and A. Knoesen. Trapping forces in a multiple-beam fiber-optic trap. *Appl. Opt.*, 36(25):6423–6432, 1997.

[18] A Huff, C. N. Melton, L. S. Hirst, and J. E. Sharping. Stability and instability for low refractive-index-contrast particle trapping in a dual-beam optical trap. *Biomed. Opt. Express*, 6(10):3812–3819, 2015.

[19] U. Delabre, K. Feld, E. Crespo, G. Whyte, C. Sykes, U. Seifert, and J. Guck. Deformation of phospholipid vesicles in an optical stretcher. *Soft Matter*, 11(30):6075–6088, 2015.

[20] E. J. G. Peterman, F. Gittes, and C. F. Schmidt. Laser-induced heating in optical traps. *Biophys. J.*, 84(2):1308–1316, 2003.

[21] S. M. Barnett. Resolution of the Abraham-Minkowski dilemma. *Phys. Rev. Lett.*, 104(7):070401, 2010.

[22] A. H. Gill and H. S. Simms. Microanalytical methods in oil analysis. *Ind. Eng. Chem.*, 13(6):547–552, 1921.

[23] J.G. Lyubovitsky. *Mapping the cytochrome c folding landscape*. PhD thesis, California Institute of Technology, 2003.

[24] K.P. Bohannon, R.W. Holz, and D. Axelrod. Unknown title. *Biophys. J.*, 110(3), 2016.

[25] M. Habaza, M. Kischbaum, C. Guernth-Marschner, G. Dardikman, I. Barnea, R. Korenstein, C. Duschl, and N.T. Shaked. Rapid 3d refractive-index imaging of live cells in suspension without labeling using dielectrophoretic cell rotation. *Adv. Sci.*, 4(2), 2017.

[26] D. Wang, H. Xia, Z. Liu, and Q. Yang. Study of the mechanism of polymer solution with visco-elastic behavior increasing microscopic oil displacement efficiency and the forming of steady "oil thread" flow channels. In *SPE Asia Pacific Oil and Gas Conference and Exhibition, 17-19 April, Jakarta, Indonesia*. Society of Petroleum Engineers, 2001.

[27] W. C. Griffin. Classification of surface-active agents by "HLB". *J. Soc. Cosmet. Chem.*, 1(5):311–326, 1949.

[28] N. H. Scott. An area modulus of elasticity: Definition and properties. *J. Elast.*, 58(3):269–275, 2000.

[29] R. D. Knight. *Physics for Scientists and Engineers: A Strategic Approach*. Pearson, 3 edition, 2013.

[30] L. Picas, F. Rico, and S. Scheuring. Direct measurement of the mechanical properties of lipid phases in supported bilayers. *Biophys J.*, 102(1):L01–L03, 2012.

[31] W. Rawicz, K. C. Olbrich, and E. Evans. Effect of chain length and unsaturation on elasticity of lipid bilayers. *Biophys J.*, 79(1):328–339, 2000.

[32] T. M. Piñón. *Fiber-based dual-beam optical trapping playform for strtching lipid vesicles*. PhD thesis, University of California, Merced, 2013.

[33] A. Diz-Muñoz, D. A. Fletcher, and O. D. Weiner. Use the force: membrane tension as an organizer of cell shape and motility. *Trends Cell Biol.*, 23:47–53, 2 2013.

[34] R. M. Hochmuth, N. Mohandas, and P. L. Blackshear Jr. Measurement of the elastic modulus for red cell membrane using a fluid mechanical technique. *Biophys. J.*, 13(8):747–762, 1973.

[35] R. M. Hochmuth and R. E. Waugh. Erythrocyte membrane elasticity and viscosity. *Ann. Rev. Physiol.*, 49:209–219, 1987.

[36] R. Kiss, H. Bock, S. Pells, E. Canetta, A. K. Adya, A. J. Moore, P. DeSousa, and N. A. Willoughby. Elastiacity of human embryonic stem cells as determined by atomic force microscopy. *J. Biomech Eng*, 133(10):101009–1–101009–9, 2011.

[37] S. Hénon, G. Lenormand, A. Richert, and F. Gallet. A new determination of the shear modulus of the human erythrocyte membrane using optical tweezers. *Biophys. J*, 76(2):1145–1151, 1999.

[38] G. Lenormand, S. Hénon, A. Richert, J. Siméon, and F. Gallet. Direct measurement of the area expansion and shear moduli of the human red blood cell membrane skeleton. *Biophys. J*, 81(1):43–56, 2001.

[39] O. Brzobohatý, A. V. Arzola nad M. Šiler, L. Chvátal, P. Jákl, S. Simpson, and P. Zemánek. Complex rotational dynamics of multiple spheroidal particles in a circularly polarized, dual beam trap. *Opt. Express*, 23(6):7273–7287, 2015.

[40] G. Xiao, K. Yang, H. Luo, X. Chen, and W. Xiong. Orbital rotation of trapped particle in a transversely misaligned dual-fiber optical trap. *IEEE Photon. J*, 8(1):6100108, 2016.

[41] L Jauffred, S. M. Taheri, R. Schmitt, H. Linke, and L. B. Oddershede. Optical trapping of gold nanoparticles in air. *Nano Lett.*, 15(7):4713–4719, 2015.

[42] P. D. Nation, J. R. Johansson, M. P. Blencowe, and F. Nori. Colloquium: Stimulating uncertainty: Amplifying the quantum vacuum with superconducting circuits. *Rev. Mod. Phys.*, 84(1):1–24, 2012.

[43] M. Aspelmeyer, P. Meystre, and K. Schwab. Quantum optomechanics. *Phys. Today*, 65(7):29–35, 2012.

[44] E. E. Wollman, C. U. Lei, A. J. Weinstein, J. Suh, A. Kronwald, F. Marquardt, A. A. Clerk, and K. C. Schwab. Qunatum squeezing of motion in a mechanical resonator. *Science*, 349(6251):952–955, 2015.

[45] F. Lecocq, J. B. Clark, R. W. Simmonds, J. Aumentado, and J. D. Teufel. Quantum nondemolition measurement of a nonclassical state of a massive object. *Phys. Rev. X*, 5(4):041037–041045, 2015.

[46] J. M. Pirkkalainen, E. Damskägg, M. Brandt, F. Massel, and M. A. Sillanpää. Squeezing of quantum noise of motion in a micromechanical resonator. *Phys. Rev. Lett.*, 115(24):243601–243606, 2015.

[47] W. E. Lamb and R. C. Retherford. Fine structure of the hydrogen atom by a microwave method. *Phys. Rev.*, 72(3):241–243, 1947.

[48] V. Springel, C. S. Frenk, and S. D. M. White. The large-scale structure of the universe. *Nature*, 440(7088):1137–1144, 2006.

[49] S. Weinberg. The cosmological constant problem. *Rev. Mod. Phys.*, 61(1):1–23, 1989.

[50] H. B. G. Casimir. On the attraction between two perfectly conducting plates. *Proc. K. Ned. Akad. Wet.*, 51(793–795), 1948.

[51] S. K. Lamoreaux. Casimir forces: Still surprising after 60 years. *Phys. Today*, 60(2):40–45, 2007.

[52] R. Y. Chiao, R. W. Haun, N. A. Inan, B. Kang, L. A. Martinez, S. J. Minter, G. A. Muñoz, and D. A. Singleton. *Quantum theory: a two-time success story*, chapter 13: A Gravitational Aharonov-Bohm Effect, and Its Connection to Parametric Oscillators and Gravitational Radiation, pages 213–246. Springer-Verlag Mailand, 2014 edition, 2013.

[53] G. L. Baker and J. A. Blackburn. *The Pendulum: a case study in physics*, chapter 3: Pendulums less simple, page 27. Oxford University Press, 2005.

[54] J. R. Taylor. *Classical Mechanics*, chapter 5: Oscillations, pages 161–214. University Science Books, 2005.

[55] W. Case. Parametric instability: An elementary demonstration and discussion. *Am. J. Phys.*, 48(3):218–221, 1980.

[56] A. O. Belyakov, A. P. Syranian, and A. Luongo. Dynamics of the pendulum with periodically varying length. *Physica D*, 238(16):1589–1597, 2009.

[57] E. I. Butikov. Parametric excitation of a linear oscillator. *Eur. J. Phys*, 25(4):535–554, 2004.

[58] Š. Kubínová and J. Šlégr. Physics demonstrations with the arduino board. *Phys. Educ.*, 50(4):472–474, 2015.

[59] C. Galeriu, C. Letson, and G. Esper. An arduino investigation of the rc circuit. *Phys. Teach.*, 53(5):285–288, 2015.

[60] P. A. Tipler and R. A. Llewellyn. *Modern Physics*. W. H. Freeman and Company, 6th edition, 2012.

[61] D. J. Griffiths. *Introduction to Quantum Mechanics*. Prentice Hall, 1995.

[62] J. R. Taylor. *Classical Mechanics*, chapter 12: Nonlinear Mechanics and Chaos, pages 457–466. University Science Books, 2005.

[63] L. W. Anderson and D. R. Krathwohl. *A Taxonomy for Learning, Teaching, and Assessing: A Revision of Bloom's Taxonomy of Educational Objectives*. Pearson, 2001.

[64] S. V. Franklin, E. C. Sayre, and J. W. Clark. Traditionally taught students learn; actively engaged students remember. *Am. J. Phys.*, 82(8):798–801, 2014.

[65] L. Kober. *Reaching Students: What Research Says About Effective Instruction in Undergraduate Science and Engineering*. The National Academies Press, 2014.

[66] L. Springer, M. E. Stanne, and S. S. Donovan. Effects of small-group learning on undergraduates in science, mathematics, engineering, and technology: A meta-analysis. *Rev. Educ. Res.*, 69(1):21–51, 1999.

[67] University of Maryland Physics Education Research Group. Student Expectations in University Physics: MPEX. `https://www.physics.umd.edu/perg/expects/mpex.htm`, Obtained August 2015.

[68] A. Chenciner. *Henri Poincaré, 1912-2012*, chapter Poincaré and the Three- Body Problem, pages 45–133. Birkhäuser, Basel, 2015.

[69] T. McAlpine and A. Huff. Simulation of the dynamics of a plane pendulum with positional dependent torque. In *APS March Meeting Abstracts*, 2009.